FATIGUE RESPONSE OF THIN STIFFENED ALUMINUM CRACKED PANELS REPAIRED WITH BONDED COMPOSITE PATCHES

THESIS

Jason B. Avram, Captain, USAF

AFIT/GMS/ENY/01M-01

DEPARTMENT OF THE AIR FORCE
AIR UNIVERSITY

AIR FORCE INSTITUTE OF TECHNOLOGY

Wright-Patterson Air Force Base, Ohio

20010523 015

The views expressed in this thesis are those of the author and do not reflect the official policy or position of the United States Air Force, Department of Defense, or the U. S. Government.

REPORT DOCUMENTATION PAGE

Form Approved
OMB No. 074-0188

The public reporting burden for this collection of information is estimated to average 1 hour per response, including the time for reviewing instructions, searching existing data sources, gathering and maintaining the data needed, and completing and reviewing the collection of information. Send comments regarding this burden estimate or any other aspect of the collection of information, including suggestions for reducing this burden to Department of Defense, Washington Headquarters Services, Directorate for Information Operations and Reports (0704-0188), 1215 Jefferson Davis Highway, Suite 1204, Arlington, VA 22202-4302. Respondents should be aware that notwithstanding any other provision of law, no person shall be subject to an penalty for failing to comply with a collection of information if it does not display a currently valid OMB control number. **PLEASE DO NOT RETURN YOUR FORM TO THE ABOVE ADDRESS.**

1. REPORT DATE *(DD-MM-YYYY)*	2. REPORT TYPE	3. DATES COVERED *(From – To)*
01-03-2001	Master's Thesis	June 2000-January 2001

4. TITLE AND SUBTITLE

FATIGUE RESPONSE OF THIN STIFFENED ALUMINUM CRACKED PANELS REPAIRED WITH BONDED COMPOSITE PATCHES

5a. CONTRACT NUMBER

5b. GRANT NUMBER

5c. PROGRAM ELEMENT NUMBER

6. AUTHOR(S)

Jason B. Avram, Captain, USAF

5d. PROJECT NUMBER

5e. TASK NUMBER

5f. WORK UNIT NUMBER

7. PERFORMING ORGANIZATION NAMES(S) AND ADDRESS(S)
Air Force Institute of Technology
Graduate School of Engineering and Management (AFIT/ENY)
2950 P Street, Building 640
WPAFB OH 45433-7765

8. PERFORMING ORGANIZATION REPORT NUMBER

AFIT/GMS/ENY/01M-01

9. SPONSORING/MONITORING AGENCY NAME(S) AND ADDRESS(ES)
Mr. Jim Mazza and Mr. Mark Derriso
AFRL/MLSA and AFRL/VASE
Wright-Patterson AFB, OH 45433

10. SPONSOR/MONITOR'S ACRONYM(S)

11. SPONSOR/MONITOR'S REPORT NUMBER(S)

12. DISTRIBUTION/AVAILABILITY STATEMENT

APPROVED FOR PUBLIC RELEASE; DISTRIBUTION UNLIMITED.

13. SUPPLEMENTARY NOTES

Dr. Shankar Mall (937)255-3636 x4587

14. ABSTRACT

This research investigated the fatigue response of precracked and patched 2024-T3 Aluminum panels with stiffeners. Patches were single-sided, unidirectional three ply boron/epoxy. Stiffeners were 2024-T3 aluminum and were riveted and bonded on. Disbonds were introduced into the repair bondline by inserting teflon strips. Three disbond configurations were investigated—crack tip disbond (CTD) located at the edge of the patch in the path of crack propagation, full-width disbond (FWD) covering the entire crack, and end disbond (ED) located at each end of the patch and covering the full width. Each repaired panel was subjected to tension/tension cyclic fatigue with a maximum stress of 120 MPa. The effects disbonds had on fatigue life was studied by comparing disbonded repair fatigue life with that of perfectly bonded repairs. Results showed that disbonds closer to the crack that took up more bondline area had a larger negative impact on fatigue life. While disbonds did have some detrimental effects on repaired panel fatigue life, the disbonded repair cases still performed considerably better than an unrepaired panel. Results also showed that intentional disbonds did not experience significant growth during cyclic fatigue, and cyclic disbonding around the crack only occurred in the wake of the crack tip.

15. SUBJECT TERMS
Bonded Composite Repairs, Disbonds, Cracked Aluminum Panels, Stress Intensity Factor, Boron/Epoxy, Cyclic Fatigue

16. SECURITY CLASSIFICATION OF:			17. LIMITATION OF ABSTRACT	18. NUMBER OF PAGES	19a. NAME OF RESPONSIBLE PERSON
a. REPORT	**b. ABSTRACT**	**c. THIS PAGE**	UU		Dr. Shankar Mall
U	U	U		161	**19b. TELEPHONE NUMBER** *(Include area code)* (937)255-3636 x4587

Standard Form 298 (Rev. 8-98)
Prescribed by ANSI Std. Z39-18

AFIT/GMS/ENY/01M-01

FATIGUE RESPONSE OF THIN STIFFENED ALUMINUM CRACKED PANELS REPAIRED WITH BONDED COMPOSITE PATCHES

THESIS

Presented to the Faculty

Department of Aeronautics and Astronautics

Graduate School of Engineering and Management

Air Force Institute of Technology

Air University

Air Education and Training Command

In Partial Fulfillment of the Requirements for the

Degree of Master of Science in Material Science

Jason B. Avram, B.S.

Captain, USAF

March 2001

AFIT/GMS/ENY/01M-01

FATIGUE RESPONSE OF THIN STIFFENED ALUMINUM CRACKED PANELS REPAIRED WITH BONDED COMPOSITE PATCHES
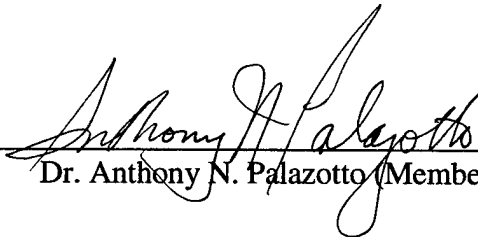
Jason B. Avram, B.S.
Captain, USAF

Approved:
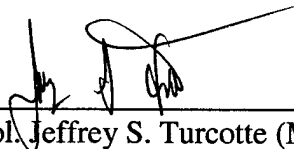
_____
Dr. Shankar Mall (Chairman)

_____
1/8/01
date

_____
Dr. Anthony N. Palazotto (Member)

_____
1/8/01
date

_____
LtCol. Jeffrey S. Turcotte (Member)

_____
08 Jan 2001
date

Acknowledgments

There is a long list of people I would like to thank for their help and understanding over the course of this thesis project. Without their help, I quite possibly would have gone crazy long before I completed the work. Firstly, I would like to thank my advisor, Dr. Shankar Mall, for giving me this topic and guiding me to successful completion of the research. I would also like to thank my boss, Mr. Jim Mazza, for supporting the research and for his understanding over the many months that work sometimes took a back burner to my thesis. I would like to give a special thanks to Jim Huff for turning me into a riveting guru. I guess all that time in the military did you some good after all, Jim (that is, of course, when you weren't drowning helpless sheep). I wouldn't have been able to complete the research without the help of all of the guys and girls in AFRL/MLSA, including Dan McCray, Brian Milligan, Lt Heather Crooks, Dr. Brett Bolan, and Dr. Mark Forte. Their technical expertise was invaluable, as was their advice in the wake of all of my frustrated ramblings. Mark Derriso and the technicians in AFRL/VASE, especially Richard Wiggins and Brian Smyers, were key to my getting this research done on time. Mark allowed me the use of a testing frame for many months and Richard taught me the fine art of infrared imaging. In short, this work was a culmination of many people's effort, not just my own. I'm very grateful to all of them. Lastly, I'd like to thank my wife and editor-in-chief, for her loving support through this whole ordeal. Her smiling face and dedication to our son made this project a lot easier.

Jason Avram

Table of Contents

vi

List of Figures

List of Tables

Abstract

This research investigated the fatigue response of precracked and patched 2024-T3 Aluminum panels with stiffeners. The patches were single-sided, partially bonded, unidirectional three ply boron/epoxy. Stiffeners were 2024-T3 aluminum and were riveted as well as bonded on. Stiffeners were oriented in the direction of loading and were separated by a certain distance, with the crack centered between two stiffeners. Two stiffener separation distances, or spacings, were used—one to simulate transport aircraft fuselage stiffeners and one to simulate transport aircraft wing stiffeners. Disbonds were introduced into the adhesive bondline by inserting teflon strips. Three disbond configurations were investigated—a crack tip disbond (CTD) located at the edge of the patch in the path of crack propagation, a full-width disbond (FWD) covering the entire crack, and an end disbond (ED) located at each end of the patch and covering the full width. Each repaired panel was subjected to tension/tension cyclic fatigue with an R ratio of 0.05 and a maximum stress of 120 MPa.

Fatigue life data for each disbond configuration was compared to fatigue life data for a perfectly bonded repair with the same stiffener configuration. Results showed that disbonds closer to the crack that took up more bondline area had a larger negative impact on fatigue life. ED's, which were located away from the crack, had a negligible effect on the fatigue life of a repaired panel. CTD's, however, which were located in the path of the crack, increased the fatigue crack propagation rate of a repaired panel an average of 27%. FWD's were the worst disbond case, increasing the fatigue crack propagation rate

of a repaired panel an average of 84%. However, since a perfectly bonded patch increased the fatigue life of a stiffened panel by approximately of 470%, the disbonded repair cases still performed considerably better than an unrepaired panel. Repaired panels with intentional CTD's had a fatigue life an average of 360% longer than the unrepaired panel, while repaired panels with intentional FWD's had an average life of 212% longer than the unrepaired panel. Results also showed that intentional disbonds did not experience significant growth during cyclic fatigue, and cyclic disbonding around the crack only occurred in the wake of the crack tip.

FATIGUE RESPONSE OF THIN STIFFENED ALUMINUM CRACKED PANELS

REPAIRED WITH BONDED COMPOSITE PATCHES

Chapter 1   Introduction

The average age of military and civilian aircraft is growing older at a fast pace, and shows no sign of slowing down. For civilian and military aircraft, an expected service life of twenty years is typical, but because of military budget cuts and civilian industry requirements to make a profit, aircraft have service lives that are much longer. According to Table 1 (1), the average service life of six key Air Force airframes is already over 25 years, and the expected retirement age is over 52 years.

Table 1   Air Force Aircraft Average Age Comparison

Aircraft	Year Fielded	Average Age	Proposed Retirement	Retirement Age
C/KC-135	1956	35.0	2040	79
B-52H	1961	34.3	2030	68
T-38	1961	28.5	2020	52
C-141	1965	29.5	2003	36
E-3	1977	16.3	2025	45
F-16	1979	7.6	2025	36

As aircraft become older and accumulate more flight hours, the tendency they have to develop corrosion problems, fatigue cracking, overload cracking, etc. increases. This problem was never more evident than after an incident involving Aloha Airlines Flight 243 (2). During the flight, part of the fuselage ripped off, causing the death of a

female flight attendant. The cause was linked to stress corrosion cracking caused by the aircraft's flight environment and high number of flight hours. As a direct result of this tragedy, the U.S. government established the National Aging Aircraft Research Program under the direction of the Federal Aviation Administration (FAA) and the Airframe Structural Integrity Program under the direction of the National Aeronautics and Space Administration (NASA) (3). The Air Force, aware of its aging aircraft fleet, established its own Aging Aircraft Program.

There are three basic ways to address aging aircraft problems as they arise: 1) aircraft replacement, 2) part replacement, 3) part repair. The first, aircraft replacement, is not much of an option because of the high cost of modern day aircraft. As seen in Table 2 (4), the approximate cost of some common modern day military and commercial aircraft can be from $18 million to $1 billion. Government budget cuts and the demand for industry to make a profit creates a need to continue to use current aircraft for as long as possible.

Table 2 Military and Commercial Aircraft Costs

Aircraft Type	Cost
Lockheed Martin F-16 Fighting Falcon	$24 Million (1999)
Boeing F-15 Eagle	$35 Million
Lockheed Martin F-22 Raptor	$100 Million
Northrup Grumman B-2 Spirit	$1 Billion (1996)
Boeing C-17 Globemaster III	$175 Million (1996)
Boeing F/A18 Hornet	$25 Million (1991)
Boeing AH-64 Apache	$18 Million (1996)
Boeing Sikorsky RAH-66 Comanche	$20 Million
Boeing 737	$40 Million (1997)
Boeing 747	$170 Million (1996)
Boeing 777	$128-$170 Million (dependent on model)

The second option, part replacement, can create many problems. For older aircraft, such as the KC-135 and B-52, parts can be very difficult to obtain because they may not be in production anymore. Parts may have to be specially manufactured, leading to very high costs and long waiting periods. Also, replacing an entire aircraft part, depending on how substantial it is, can take a very long time, creating problems with training and mission sortie rates, especially in the case of fleet-wide problems. The third option, part repair, is the easiest and cheapest way to address the problem. By focusing on fixing individual part damage, as opposed to replacing the entire part or airframe, the time and money needed to get the airframe up and running again is reduced.

The are two main options for repair of aircraft: bolted or riveted mechanically fastened repair and adhesively bonded repair with either metal or composite patches. Both have their advantages and disadvantages, which will be discussed in greater detail in Section 2.3, but while mechanically fastened repairs have been widely used for years and tend to be simpler than bonded repairs, they introduce numerous additional stress concentrations into the damaged area. Adhesively bonded patches repair aircraft damage without introducing additional damage. While they are less well known in the maintenance arena than mechanically fastened repairs, the ability to repair aircraft without introducing new damage is very desirable.

Adhesively bonded repair technology was first researched by the U.S. Air Force in the early 1970's on the General Dynamics F-111 (5). A boron doubler modification was installed on the left wing, which had been placed in a test jig at Convair Aerospace Division Structures Test Facility, San Diego, California. The boron doubler lasted for 100 test blocks, the equivalent of 40,000 test hours, and for an additional 10,000 cycles at

75% design limit load. Adhesively bonded repair technology began to emerge as a viable alternative to aircraft and part replacement.

The Air Force had not performed much research into bonded repair technology in the early 1970's, which created a lack of faith in the ability of the technology to perform over a long period of time in harsh environments. Combined with the fact that the United States Department of Defense had a large budget in the 1970's and 80's, leading to a casual view toward aging aircraft concerns, the U.S. did not heavily pursue bonded repairs. Australia, however, had a smaller defense budget and relied heavily on maintaining their current aircraft. They took an aggressive attitude toward adhesively bonded repairs as a means to keep their aircraft flying longer. Australian F-111's purchased from the U.S. were fitted with bonded boron doublers prior to delivery. This helped Australia's Aeronautical Research Laboratory (ARL) (now called the Aeronautical and Maritime Research Laboratory (AMRL)) move in the direction of adhesively bonded repair technology.

Once introduced to the potential advantages of bonded repair technology, ARL moved quickly towards becoming proficient in making the repairs. ARL made most of the initial advancements in bonded repair technology, including inventing the first successful grit blast/silane surface preparation technique used to create a better and more durable bond between the patch and aircraft skin (surface preparations will be discussed in greater detail in Section 2.4.3). Australia was by far the most aggressive in performing actual adhesively bonded aircraft repairs, with a great deal of success. Table 3 (6) lists some of the different aircraft repairs performed by ARL since 1975 and comments on the success of those repairs.

4

Table 3 Australian Bonded Repair Applications

Cracking	Material	Component	Aircraft	Comments
Stress-corrosion	7075-T6	Wing plank	Hercules	Over 300 repairs since 1975
Fatigue	Mg Alloy MSR	Landing wheel	Macchi	Life doubled, at least
Fatigue	AU4SG	Fin skin	Mirage	In service since 1978
Fatigue	AU4SG	Lower wing skin	Mirage	Over 150 repairs since 1979
Fatigue	2024-T3	Upper wing skin	Nomad (fatigue test)	Over 105,900 simulated flying hours
Fatigue	2024-T3	Door frame	Nomad (fatigue tests)	Over 106,619 simulated flying hours
Stress-corrosion	7075-T6	Console truss	F-111	In service since 1980
Lightning burn	2024-T3	Fuselage skin	Orion	In service since 1980

With the United States decreasing defense spending in the 1990's, along with attention gained from aircraft failures such as Aloha Airlines' Flight 243, aging aircraft concerns became more of a priority, and the U. S. started to follow Australia's lead in bonded repair research and application. Both the Air Force and Navy have been major contributors in the area of adhesively bonded repair technology. Both have performed numerous research projects in the area of adhesives, surface preparations, and fatigue crack propagation to help the success of bonded composite repairs on aircraft. The Air Force and Navy have also put numerous repairs on operational aircraft, including the C-141, F-18, and F-16. Table 4 (7) details the different bonded repairs performed on U. S. aircraft.

Table 4 U. S. Bonded Repair Applications

Aircraft	User	Application	Patch Material
F-16	USAF	Fatigue Cracking-Fuel Vent Hole	Boron/Epoxy
L-1011	Delta Airlines	Enhancement-Door Corner	Boron/Epoxy
B-52	USAF	Enhancement-Crown Skin Fuel Access Panel	Boron/Epoxy
C-5A	USAF	Fatigue Cracking-Crown Skin	GLARE
T-38	USAF	Fatigue Cracking-Leading Edge Spar	
C-141	USAF	Wet-wing Fuel Weep Hole	Boron/Epoxy
C-130	USAF	Corrosion Pitting in Lower Wing Skin	Boron/Epoxy

Bonded Repair technology is becoming more and more advanced and accepted, but additional research is always needed to help predict how well bonded composite patches can perform their job. Both Australian (8) and U. S. Air Force research (9; 10; 11; 3) showed the benefits of utilizing this technology on thin and thick structures. Denney (11) investigated the effects of debonds in the adhesive bondline of boron/epoxy composite patch repairs on thin (1mm) aluminum. The study of thin aluminum was furthered by Mills and Ryan (10) (1mm $\leq$ t $\leq$ 3.175mm). Shubbe (9) studied the performance of fully bonded repairs on thick structures (t = 6.35mm) and Conley (3) furthered the work by studying partially bonded composite repairs on thick structures (t = 6.35mm).

All of the research done prior was on unstiffened aluminum panels with varying thicknesses. Actual aircraft are not simply aluminum panels, they are stiffened structures. As seen in Figure 1 (12:A20.2), aircraft consist of skin, stringers, webs, and spars. All of this underlying structure stiffens the aluminum panel that makes up the skin and significantly impacts the fatigue characteristics of the aircraft. Performing fatigue

6

testing on unstiffened aluminum panels and using the data to make judgements on how stiffened aircraft structure will perform is not the most or best that can be done. A better approximation of the real-world environment involves stiffened structure. The current study was performed to characterize the effect of debonds on the fatigue life of thin aluminum panels (t = 1 mm) reinforced with aluminum stiffeners (t = 1.6 mm).
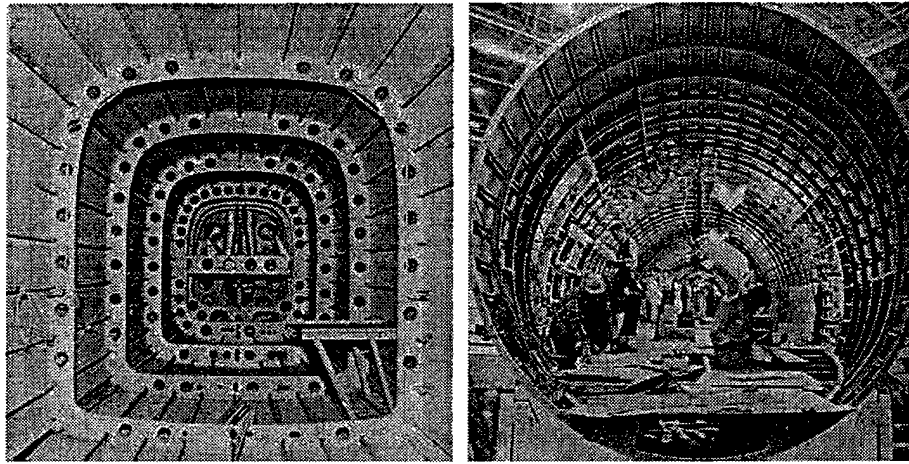
Figure 1 Stiffened Aircraft Structure

Thin aluminum panels were machined to a dog-bone configuration, pre-cracked, fitted with stiffeners, repaired with an adhesively bonded composite patch, and then fatigued under constant-amplitude stress fatigue cycling until the crack either reached the stiffeners and stopped, or failure occurred. Disbonds were placed in different areas in the bondline to investigate the effect of debonds on fatigue life. Crack tip disbonds (CTD), full-width disbonds (FWD), and end disbonds (ED) were all investigated. Two different stiffener configurations were looked at, as well. The disbond configurations are shown in Figure 2, while the two stiffener configurations, as well as complete dimensions of the

7

aluminum panel, are shown in Figure 3. The aluminum panels were AL2024-T3 with dimensions of 558.8x254x1.016mm (width given is at crack location). Stiffeners were AL2024-T3 with nominal dimension of 403.225x25.4x1.6mm. The patch used was a 3 ply boron/epoxy laminate with dimensions of 102x69x0.381mm.

This thesis has been separated into five distinct chapters, each summarizing a different area of the study. This first chapter outlined the motivation behind the research. The second chapter discusses background information and past research efforts in bonded repair technology. The third chapter discusses experimental setup and testing procedures. Chapter four details the results of the study and discusses exactly what impact the results have on the technology. The fifth chapter provides a brief summary of the report and closing remarks, including future areas of research that should be performed.
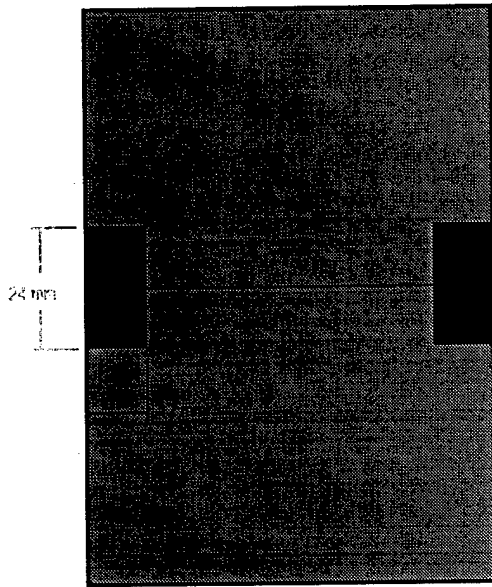
a) Crack Tip Disbond
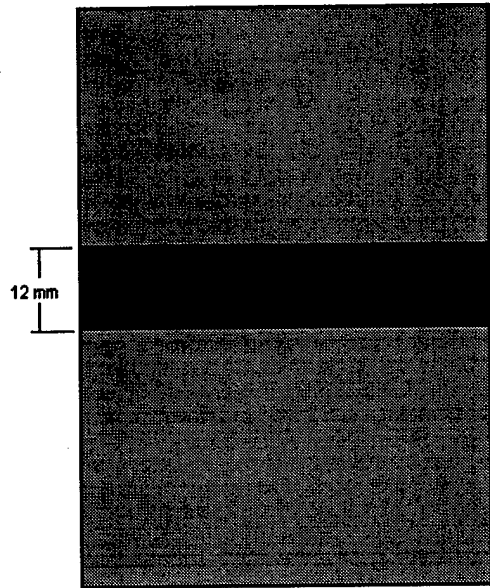
b) Full-Width Disbond
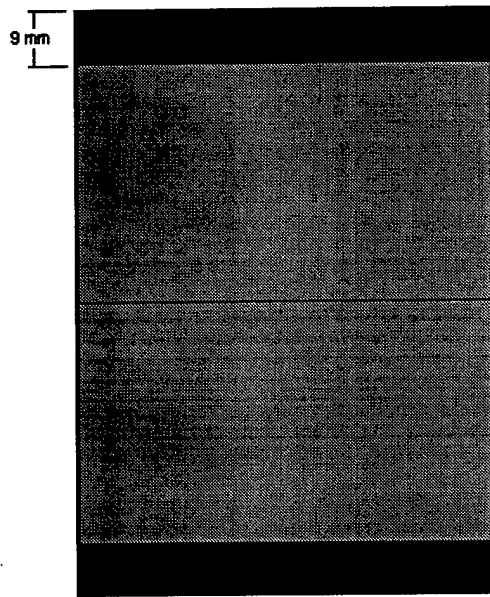
c) End Disbond

Figure 2 Disbond Configurations
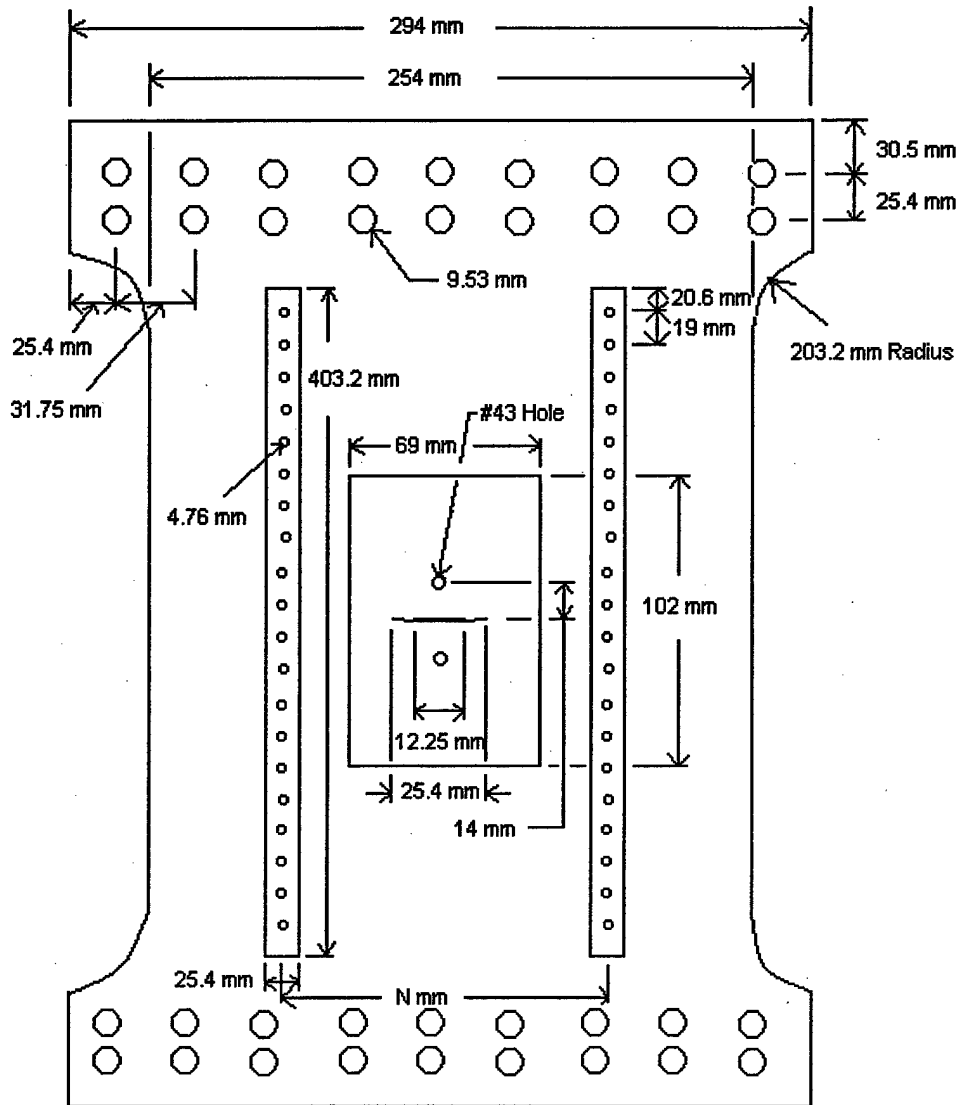
Figure 3 Panel Configuration
(N = 102 mm and 152 mm)
Aluminum Panel Thickness = 1 mm
Stiffener Thickness = 1.6 mm (stiffeners on both sides of panel)

Chapter 2   Background

2.1   History

In the early 1970's, the United States Air Force began initial research in the area of adhesively bonded composite repairs, with testing being undertaken at Convair Aerospace Division Structures Test Facility, San Diego, California. "On 29 April 1970, the F-111 full-scale right hand fatigue test wing experienced a catastrophic failure. The failure was initiated from a fatigue crack in the lower plate of the high strength steel wing pivot fitting during the 31st block of a planned 40 block test." (5) Because the wing failed prematurely in testing, a retrofit had to be designed to ensure that the F-111 could meet its life span requirements. Testing on the left wing of the F-111A full-scale fatigue test article began in September 1970. A boron doubler modification was applied to the left wing and the wing successfully survived 100 total blocks of testing (40,000 test hours). To accelerate fatigue damage, the wing then underwent constant amplitude fatigue cycling at the highest load in the test spectrum (75% of design limit load). "The wing survived 10,151 cycles of this load, when, on 22 Feb 72, it failed catastrophically from a fatigue crack in the aluminum wing skin in the WPF (wing pivot fitting) splice area (5)." From the success of this program was born the modern day adhesively bonded composite repair technology, or "crack patching."

The United States did not have a lot of confidence in adhesively bonded crack patching because of a lack of experience and subsequent test data to support the technology. That, when combined with the fact that the Department of Defense had a nonchalant view toward aging aircraft concerns in the 70's and 80's because of the

enormous defense budget, led to the U.S. not embracing bonded repairs. Australia, however, had a much smaller defense budget and therefore relied heavily on maintaining their current aircraft. Australia received their first exposure to crack patching in the early 1970's after purchasing F-111A's from the U.S. Air Force which were retrofitted with bonded boron doublers prior to delivery. After seeing the possible advantages that bonded repairs had over bolted or riveted repairs (discussed in detail later in this chapter) for inexpensively prolonging aircraft life, ARL aggressively pursued utilizing the technology for their other aging aircraft concerns.

ARL performed much of the early bonded repair research, including patch material selection, adhesive system analysis, surface preparation development, and patch design. By 1984, Australia had performed hundreds of bonded repairs on six different aircraft, including the F-111, C-130 Hercules, Mirage, Nomad, and Orion, all with great success (6). The United States re-entered the bonded repair picture in the 1990's when defense spending was reduced and accidents such as Aloha Airlines' Flight 243 (2), caused the Air Force and Navy to turn their eyes toward aging aircraft concerns. The United States has since performed numerous successful bonded composite repairs to aircraft such as the F-16, B-52, C-5A, and C-141 (7).

2.2 Theory of Linear Elastic Fracture Mechanics

To better understand how an aircraft repair works and the different advantages of mechanically fastened or bonded repairs, it is helpful to understand some of the theory involving cracks in thin metallic structure. This section focuses on some of the

elementary theory of Linear Elastic Fracture Mechanics, since all structures have inherent pre-existing cracks or flaws that cause the failure.

Consider a crack in an infinite plate, Figure 4 (13; 3). The stress intensity factor for an opening mode, K_I, must first be defined, since it is the driving force for crack growth. The stress intensity factor is the linear elastic fracture mechanics parameter relating remote load, crack size, and structural geometry and may be expressed in the following form (13):

$$K_I = \sigma\sqrt{\pi a}F(a) \tag{1}$$

where

σ = remote stress
a = half the crack length
$F(a)$ = dimensionless geometric factor

The stress intensity factor characterizes the magnitude of the crack tip stress field.

13
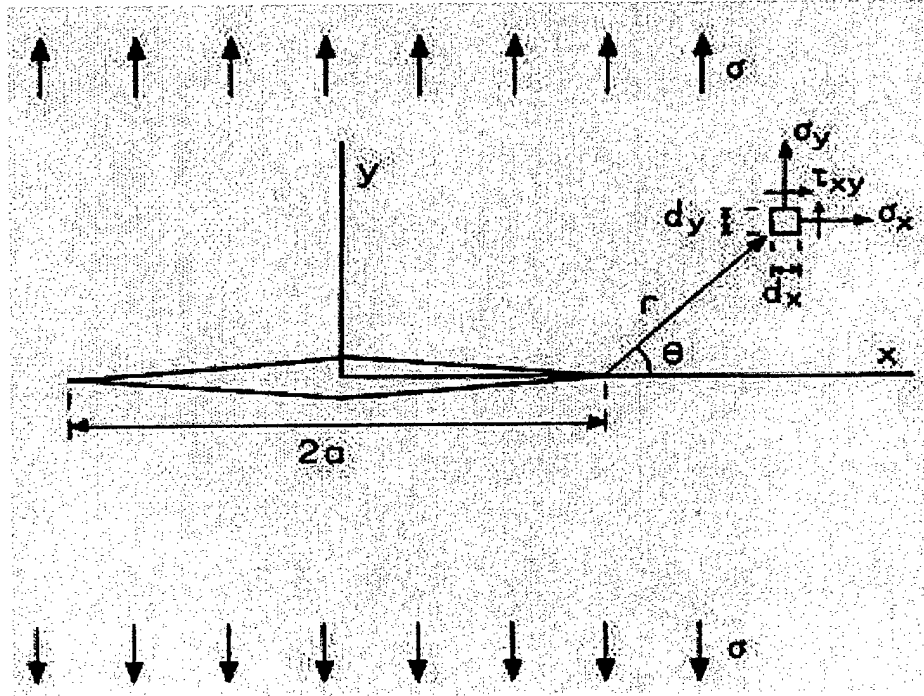
Figure 4 Crack in an Infinite Plate

For the crack geometry shown in Figure 4 (center crack in an infinite plate), K is given by

$$K_I = \sigma\sqrt{\pi a} \qquad (2)$$

This is due to the fact that no geometry effects, such as thickness, proximity to an edge,

or closeness to another crack, have to be factored in. Near the crack tip (r/a < 0.05), the

stress field is given by (14:12)

$$\sigma_y = \frac{K_I}{\sqrt{2\pi r}}\cos\frac{\theta}{2}\left[1 + \sin\frac{\theta}{2}\sin\frac{3\theta}{2}\right] \tag{3}$$

$$\sigma_x = \frac{K_I}{\sqrt{2\pi r}}\cos\frac{\theta}{2}\left[1 - \sin\frac{\theta}{2}\sin\frac{3\theta}{2}\right] \tag{4}$$

$$\tau_{xy} = \frac{K_I}{\sqrt{2\pi r}}\left[\sin\frac{\theta}{2}\cos\frac{\theta}{2}\cos\frac{3\theta}{2}\right] \tag{5}$$

There are three different loading modes that can be applied to cracks. Each one affects the crack in different ways, and therefore creates a different K solution, either K_I, K_{II}, or K_{III}. Normal stresses create mode I crack opening, which is known as the "opening mode." "The displacements of the crack surfaces are perpendicular to the plane of the crack (14:8)." Mode II is referred to as the "sliding mode" and is caused by in-plane shear stresses. Crack tip displacements are in the plane of the crack and perpendicular to the crack leading edge. The "tearing mode," or mode III occurs as a result of out of plane shear. Crack surface displacements are in the plane and parallel to the crack leading edge. Figure 5 (13) illustrates the three different modes of crack loading. Almost all cracks in aircraft skin are the result of mode I loading.

Figure 5 Crack Loading Modes

15
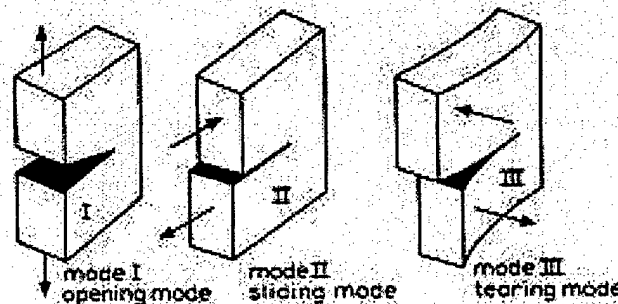
Figure 5 Crack Loading Modes

Now that the mode I stress intensity factor, K_I, has been defined, it must be correlated with crack growth due to fatigue. One of the simplest and most useful equations to accomplish this is the Paris Law, shown below.

$$\frac{da}{dN} = c\Delta K^m \qquad (6)$$

where

da = change in crack length
dN = change in the number of loading cycles
c,m = material constants

This relationship shows that the larger the stress intensity factor, the higher the crack growth rate. Therefore reducing the stress intensity factor is the key to accomplishing a successful aircraft repair. Fatiguing of aircraft components, however, directly opposes this task. The longer cracks grow and the smaller the crack tip radius becomes (the crack tip radius is defined as the radius of the circle drawn inside the tip of the crack—the smaller the radius, the sharper the crack tip), the larger the stress intensity factor becomes, which is precisely what the fatigue cracking process produces. This process is shown below in Figure 6. "A sharp crack in a tension field causes a large stress concentration at its tip where slip can occur fairly easily. The material above the crack (stages 1 and 2 in Figure 6) may slip along a favorable slip plane in the direction of maximum shear stress. Due to that slip the crack opens, but it also extends in length. Slip can now occur on another plane (stage 3). Work hardening and increasing stress will

16

(14:60)." This process, because it increases the crack length and cyclically sharpens the

crack tip, creates increasingly larger stress intensity factors. According to the Paris Law,

this creates increasing crack growth rates. Minimizing K_I and slowing down or stopping

its growth is the aim of all crack repair techniques.
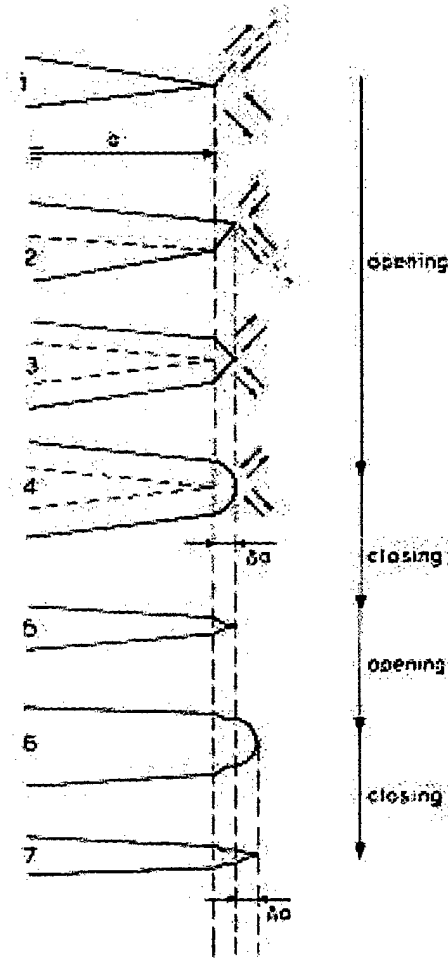
Figure 6 Fatigue Crack Growth Model

2.3 Adhesive Bonding versus Mechanically Fastened

Whether maintainers are using mechanically fastened metallic repairs or adhesively bonded composite repairs, the goal is the same: safely prolong aircraft life inexpensively and easily for as long as possible. To do this, K_I must be reduced at the crack tip, thereby stopping or significantly reducing crack growth. Traditional methods of aircraft repair involve mechanically fastened metallic reinforcements, utilizing either bolts or rivets. The maintenance community has decades of experience applying mechanically fastened metallic repairs to many different types of aircraft that span four major wars. The repairs are mainly aimed at restoring strength back to the damaged area, which is done both simply and inexpensively by bolting or riveting on metallic patches. In recent years, as bonded repair techniques have developed to support an aging aircraft fleet that is the oldest of any time in history, as well as to better repair new, more advanced aircraft, there has not been a lot of confidence in crack patching technology. There is no doubt that composite materials are strong enough (boron fibers are much stronger than steel and three times as stiff as aluminum), but the idea of "gluing" on a patch to fix a multi-million dollar aircraft makes maintainers uneasy. There are distinct advantages and disadvantages of both repair methodologies, and they are discussed in the following paragraphs.

Mechanically fastened repairs have been performed for years and provide many advantages. They are very simple and inexpensive to perform, restoring strength to damaged aircraft components. There is not a lot of specialized training involved with teaching maintainers the process. All of the materials involved with bolted/riveted repairs-bolts, rivets, metal sheet, sealant-are inexpensive and easy to find in industry.

None of the materials have specific shelf lives or difficult storage criteria. This provides for easy in-field repairs to damaged aircraft. Also, designing and applying a mechanically fastened patch doesn't require any specialized equipment. This also aids in battlefield repairs. Materials used to apply mechanically fastened repairs are very compatible with aircraft components, therefore, there are no concerns such as coefficient of thermal expansion (CTE) mismatch and galvanic corrosion.

While mechanically fastened repairs offer some advantages, they also have several disadvantages. For one, in order to repair damage to an aircraft structure, maintainers have to inflict more damage, in the form of bolt holes or rivet holes. This provides a very inefficient repair with unneeded stress concentrations. Also, stress is transferred to mechanically fastened repairs as concentrations at each bolt/rivet. By inducing numerous stress concentrations, a badly designed repair can actually cause the aircraft component to be worse off after the repair. Also, holes that must be drilled for mechanical fasteners increase the possibility of damaging internal components, such as hydraulic lines or electrical wiring, during the repair (6). There is also a threat of fretting with a bad mechanical repair. Lastly, loss of rivets or bolts during flight creates the possibility for foreign object damage (FOD), as these parts could get sucked into an engine.

"Compared to mechanical methods, such as riveting or bolting, for attaching the patch, adhesive bonding provides very efficient load transfer into the patch from the cracked component and introduces minimum stress concentrations into the structure (6)." While mechanically fastened patches transfer stress with concentrated loads (bolts or rivets), bonded composite repairs transfer stress along the entire surface area of the patch,

19

providing much more efficient load transfer. A well designed and bonded patch causes the stress intensity at the crack tip to reach a limiting factor, K_{∞}, no matter how long the crack length becomes. This is shown schematically in Figure 7 (15; 11). Further, a well designed patch, because it efficiently carries the stress of the aircraft part, significantly reduces the need for short inspection intervals. This can be seen in Figure 8 (16; 11). Also, adhesive
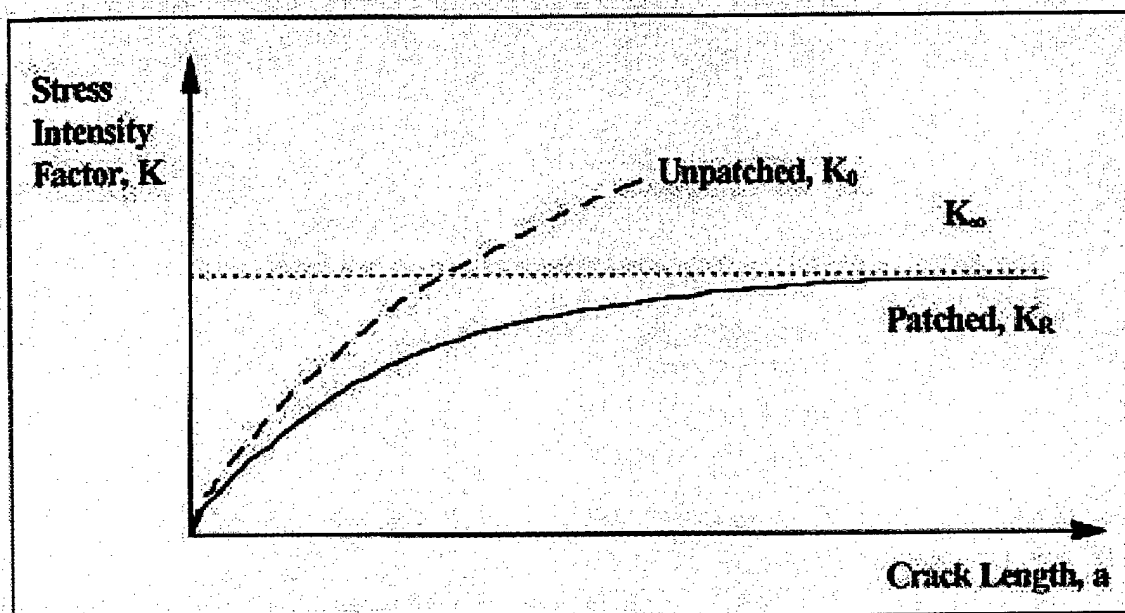
Figure 7 Reduction in the Stress Intensity Factor with Repair
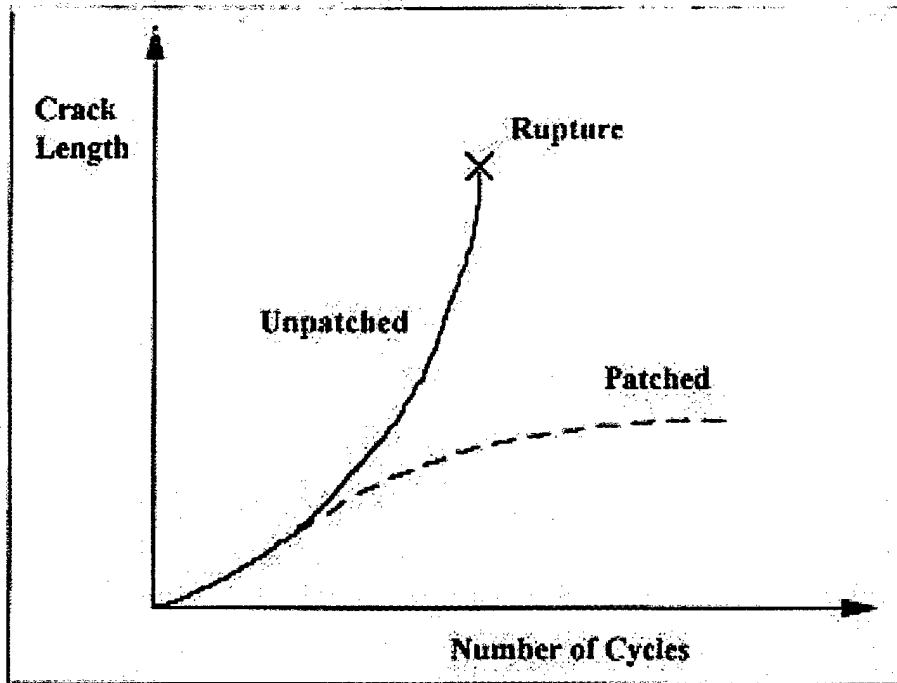
Figure 8 Effect of Patching on the Lifetime of a Cracked Structure

bonding provides a sealed interface, protecting the damaged area from corrosion and

reducing the threat of stress corrosion cracking. Because composite materials are much

stronger and stiffer than metallic materials, patches can be made approximately three

times thinner. This provides not only a weight savings, but the air stream is not affected

nearly as much with composite patches. Lastly, the biggest advantage gained by

performing bonded repairs is the lack of additional damage in the repair area. No bolts or

rivets are needed, allowing maintainers to simply fix the area without further weakening

of the structure.

While crack patching is a technology with a lot of advantages, it has its share of

disadvantages. For one, performing a bonded repair is more complicated than performing

a bolted or riveted repair. Some technical equipment is involved which requires

specialized training. Also, field repairs are more difficult to perform because a lot of the materials, such as the adhesives and composites, need to be refrigerated and have short shelf lives, usually about six months. Besides the repair process, there are also some concerns with material compatibility. Composite materials, such as boron/epoxy and graphite/epoxy, have lower coefficients of thermal expansion (CTE) than aluminum. This creates residual stresses in the repair that could possibly lead to stress corrosion cracking. As a last note, some composites, particularly graphite, can create galvanic corrosion problems when in direct contact with aluminum.

2.4   Design of Repairs

The goal of a properly designed bonded repair is to restore the damaged structure's ultimate load carrying capability. Damage growth should either be arrested or significantly retarded. The repair must be carried out without causing further damage or creating a weak link in the structure. In short, the repair allows the structure to fulfill its original intended function (17).

2.4.1   Patch Design

The *Guidelines for Composite Repair of Metallic Structures* handbook (7) lists the following guidelines on how a final composite patch design is achieved.

- Perform a thorough Damage Tolerance Analysis

- Use guidelines and analytical tools to size the repair

- Analytical methods can be used to optimize the repair design (Patch material, lay-up, dimensions, adhesive, etc.)

- The results of linear analysis can only be used if the strains remain in the elastic region, else it can only be used for sizing/optimizing of the design

- If extensive modeling (3D-FEM, linear/non-linear) is not performed, extensive testing with actual spectrum loads and realistic (or conservative) specimens must determine if the repair will perform as expected

- Extensive modeling can reduce the need for extensive testing, however, the model must be checked, at least using static test coupons

- In all cases, knowing the loads in the repaired area is a key issue to make a successful repair

As the above list states, there is a lot of thought and work that goes into designing a composite repair, but the first place to start is in knowing what loads exist in the repair area that the patch will be applied to. This study investigates a patched aluminum panel undergoing mode I loading, as seen in Figure 9.
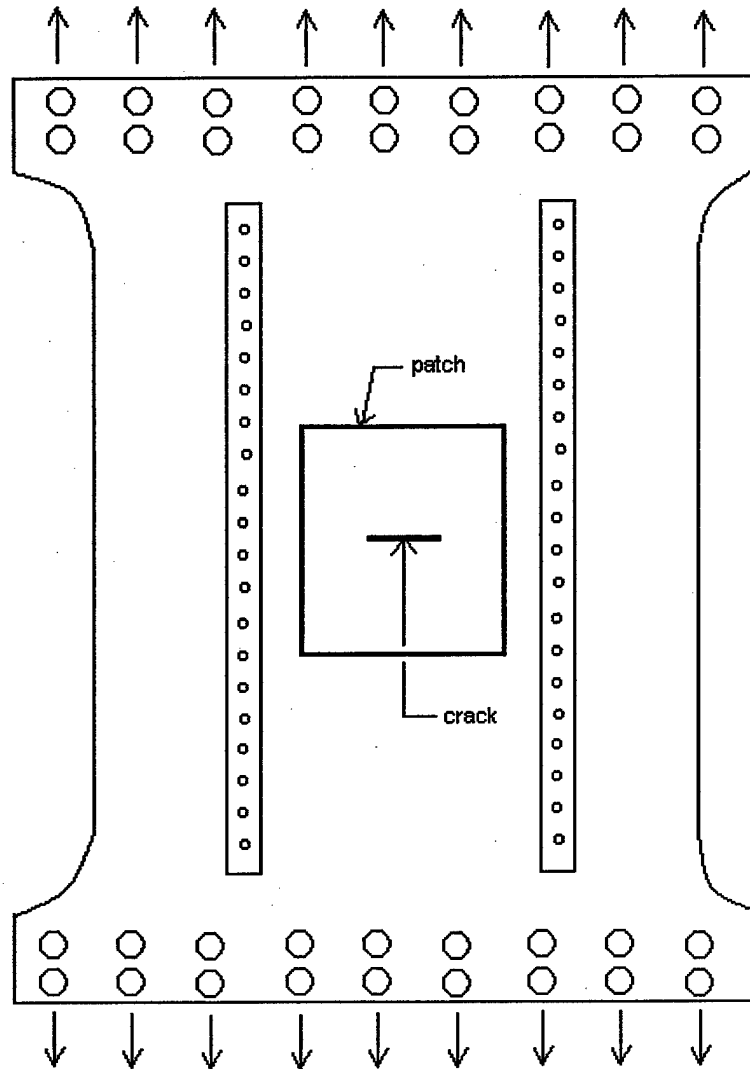
Figure 9 Patched Aluminum Panel in Tension
(Panel has a thickness of 1 mm; Stiffeners have a thickness of 1.6 mm)

Tension on an aluminum panel/patch system creates shear stress in the bondline.

Also, because the patch is bonded to the surface of the panel and picks up stress, a neutral

axis shift occurs. This neutral axis shift creates normal stresses in the form of out of

plane bending that acts at the tips of the patch. This is shown in Figure 10 (3). Normal

and shear stresses are the main drivers for patch failure and, when referring to bonded

repairs can lead to possible peel and cleavage stress. These four loading states are shown

schematically in Figure 11 (11; 17).
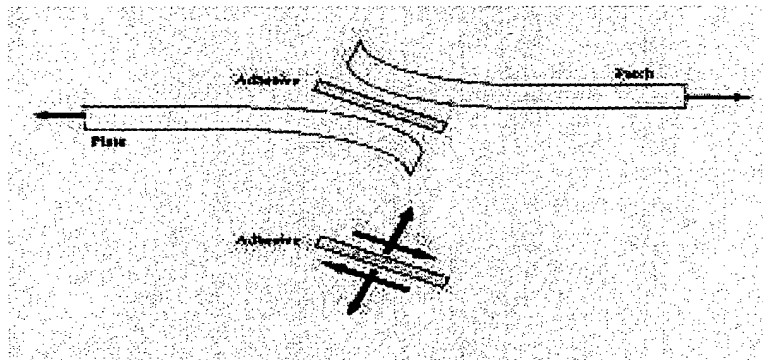
Figure 10 Bending Caused by Neutral Axis Shift in Single Sided Repair
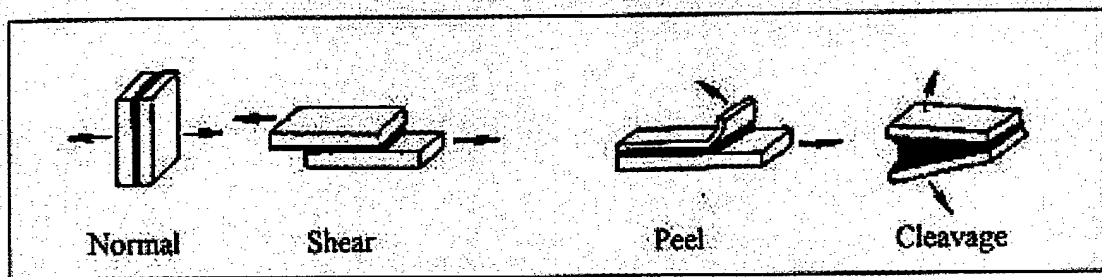
Figure 11 Loading on Adhesive Bonds

While designing adhesively bonded composite repairs is very technical, there are

a few "rules of thumb" that have been established to aid maintainers. They include (3):

- Choose repair materials (composites, adhesives) that have load-carrying capability greater than or equal to that of the parent material.

- Use a double lap arrangement whenever practical to eliminate the bending problems associated with a neutral axis shift.

- Use overlap distances of roughly 30 times the thickness of the parent structure for double lap repairs and 80 times for single lap repairs.

- Taper the thickness of the repair patch tips to relieve adhesive peel stresses. The taper slope should be approximately 1:10.

- Ensure a smooth fillet is produced in the bonding process to reduce stress concentrations.

- Maintain a stiffness ratio (S) of $1 \leq E_r t_r / E_p t_p \leq 1.5$ (7), where E_r and E_p are the Young's modulus of the repair and panel respectively and t_r and t_p are the thicknesses of the repair and panel (9; 17).

The actual patch design process detailed in the *Guidelines for Composite Repair of Metallic Structures (7)* handbook will be briefly summarized in Section 2.6.

2.4.2 Repair Material Selection

When performing a bonded repair, the two most important materials are the patch material-boron, graphite, fiberglass, etc.-and the adhesive-paste, film, or foam. A brief discussion of the selection criteria for each of these materials follows below.

When selecting composite patch materials, the two most important physical properties are strength (uniaxial ultimate strength-σ_{ult}) and stiffness (Young's Modulus, E). It is these two properties that allow the patch to be manufactured much thinner than metallic patches, providing a lighter, more aerodynamic and desirable repair. Having a strong, thin patch is desirable since it reduces the out of plane bending due to the neutral axis shift, in turn reducing the patch tip peel stresses and increasing the durability of the repair. While this is very desirable, maintainers have to be careful not to make the patch too much stronger than the parent material being repaired. The stronger the patch is, the more quickly load will be transferred from the cracked panel, possibly creating high load attraction stresses in the panel outside of the patch tips. For this reason, there are criteria

26

for the stiffness ratio, S, between the patch and the repaired structure, as shown below (7).

$$S = \frac{E_p t_p}{E_s t_s}$$ (7)

where

E_p = Young's modulus of the patch
t_p = Thickness of the patch
E_s = Young's modulus of the structure
T_s = Thickness of the structure

Table 5 (17; 18) contains material properties for some of the more common composite materials used for bonded aircraft repairs (subscript L designates longitudinal properties and subscript T designates transverse properties).

Table 5   Cured Patch Material Properties

Patch Material	E_L/E_T (Gpa)	Poisson Ratio	CTE, α_L ($10^{-6}/°C$)	Strength (MPa)
2024-T3	72.4/72.4	.33	22.7	324
Boron/Epoxy	210/25	.168	4.5	1590
GLARE 2	65.6/50.7	.33	17.9	390
Graphite/Epoxy	138/14.5	.20	-1	1447
Glass/Epoxy	50/14.5	.3	6.1	1130

When selecting adhesives for bonded repair applications, there are several properties to consider. An adhesive with a high shear modulus is the best. High shear modulus adhesives transfer the stress from the cracked component to the patch more efficiently and are thus better in reducing the stress intensity at the crack tip in the damaged part. This reduces crack growth and leads to a successful repair that increases the aircraft life. The adhesive should also have good peel strength to offset the loads

27

caused by secondary (out of plane) bending. Adhesive cure temperature must also be considered. While low temperature cures are easier to perform (less equipment needed and easier to control on the aircraft), those adhesives will not perform as well at higher temperatures, as often experienced by aircraft. While higher temperature curing adhesives create some unwanted problems, such as concerns over residual thermal stresses and CTE mismatch, they are more desired, especially for high performance aircraft. Lastly, an adhesive that is more environmentally durable is desired.

Adhesives for bonded repair applications are available in three different forms: foam, paste, and film. Foam adhesives expand during cure and are used to fill large cracks or holes. Paste adhesives usually come in two part mixtures. Each part must be carefully measured out and mixed. They are then spread with a flat tool, such as a spatula. An advantage of paste adhesives is that they are easy to use, since they can normally be cured at room temperature. They also do not necessarily need to be refrigerated, so they have a pretty long shelf life with easy storage. There is a lot of room for human error in the mixing of paste adhesives. Directions must be followed carefully. Also, paste adhesives tend to induce a lot of porosity in the bondline because of trapped air remaining from the mixing procedure. The third type of adhesive, film adhesive, is the best adhesive to use for long term repairs. They exhibit the best strength and durability properties since they provide good bondline thickness control and do not inherently cause a lot of bondline porosity. They do, however, require refrigerated storage and usually have recommended shelf lives of 6 months. This makes field repairs with film adhesive harder. Also, they have to be cured at elevated temperatures, which

can be complicated to perform on aircraft in the field. Table 6 (11) below gives examples

of each type of adhesive and some of their properties.

Table 6 Structural Adhesive Properties

Adhesive	Adhesive Type	Cure Time/Temp	Storage	Supplier
FM-39	Foam	1 hr/121°C	6 months @ -18°C	American Cyanamid
EC-1386	Paste (one part)	1 hr/177°C	4.5°C or below	3M
EA-9309	Paste (two part)	3 days/room temp or 1 hr/66°C	12 months @ room temp	Dextor Corp/Hysol
FM-73	Film	1hr/121°C	6 months @ -18°C	American Cyanamid
AF163-2M	Film	1hr/121°C	6 months @ -18°C	3M

2.4.3 Surface Preparation

Surface preparation of the damaged parent structure is the most critical step in the

bonded repair process. One expert writes, "Surface preparation of the metal adherend is

the keystone upon which the structural adhesive bond is formed. If not done correctly, all

else is for naught (19)." It is well known in the bonded repair community that almost all

bonded repairs fail as a result of environmental attack at the adhesive/parent structure

interface. A good surface preparation technique will prevent this and ensure the success

of the bonded repair. There are two main successful surface preparation techniques-

phosphoric acid anodizing (PAA) and grit blast/silane (GBS). This section will discuss

those processes, as well as variations and new technology on the horizon.

PAA was developed by Boeing and is known to be the best surface preparation

technique for ensuring durable and long-lasting bonds that withstand environmental

attack. The process consists of degreasing the surface of the damaged part and then "dipping" the part in a series of acid etch baths. This process is not always feasible, since the damaged structure must be removed from the aircraft for the process. The USAF developed a variation of the process, known as PACS, or phosphoric acid containment system. This allowed the process to be performed on aircraft. The main disadvantage of this process is the need to use a corrosive substance on the aircraft. Unless extreme caution is taken, the corrosive substance can effect other parts of the aircraft and cause eventual stress corrosion cracking problems.

GBS is a completely different process that involves degreasing, deoxidizing, "roughing-up" the damaged surface by grit blasting, and applying a silane solution. This provides a physical and chemical bond between the adhesive and metal. This process is widely used because it can be performed on aircraft and provides a bond comparable to PAA. The major disadvantage of this procedure is the hassle associated with containing the grit on the aircraft. If not contained, the aluminum oxide grit would get into the aircraft components, possibly causing damage. To defeat this problem, the USAF designed a grit containment box, shown in Figure 12. The entire process will be discussed in detail in Section 3.2.

Figure 12 Grit Containment Box

The newest surface preparation technique is known as Solgel and shows the most promise. It has not yet been cleared for mass applications and is still undergoing testing, but the process offers many advantages. The most notable advantage is the fact that it does not need to be cured. While the GBS procedure requires silane to be baked for an hour at 104°C, Solgel only requires a 3 minute application period, no bake, and then primer can be applied.

2.5 Past Efforts

Because of the importance of addressing aging aircraft concerns and the potential advantages of bonded composite repairs, much research has gone into characterizing bonded repairs, both experimental and theoretical. This section details past efforts to better understand bonded composite repairs.

31

Some of the first research performed in this area was done by Baker at the Australian Aeronautical and Maritime research laboratory (20; 8; 6; 19). Baker characterized crack growth in aluminum panels utilizing edge cracked panels bonded together over a honeycomb core. He obtained constant crack growth rates while the crack was underneath the patch. Every crack tip has an associated stress intensity factor, K. When a patch is applied to a crack, the stress in the panel is lowered, resulting in a new repaired stress intensity factor, ΔK_r. Baker showed that ΔK_r remains approximately constant and stable within the composite patch bondline. Denney (11) later confirmed this same mechanism for the repair of thin aluminum panels (t = 1mm). Baker also research the effect of debonds and elevated temperature on bond strength and durability. His research showed that as disbond size increased, bondline life decreased. His elevated temperature testing showed that as temperature increased, life decreased. This effect is due to an increase in ΔK_r with elevated temperature as a result of increased adhesive plasticity and decreased adhesive shear stiffness. This initial work was used to validate bonded repairs as a viable alternative to mechanically fastened repairs.

One of the United States' first efforts in bonded repair research was the Primary Adhesively Bonded Structure Technology (PABST) program of 1978. "One of the primary objectives of the Air Force multidisciplined Primary Adhesively Bonded Structure Technology (PABST) Development Program was to achieve significant improvement in the durability of primary fuselage structure through 'the development and validation – ultimately by full-scale test – of adhesively bonded structures technology (21).'" This program, which involved testing a fuselage manufactured completely by adhesive bonding, showed that adhesive bonds were very damage tolerant and durable.

Adhesive bonds were found to have higher shear strength than the aluminum adherends. The bondline was very tolerant of damage in the form of small debonds as long as they did not decrease the shear strength of the adhesive below that of the aluminum. The PABST program also monitored three disbonds located in various fuselage splice joints. The disbonds did not decrease joint strength over the life of the program. This testing concluded that most disbonds, except those at the edges of the patch, could go unrepaired. As a result of this program, confidence in bonded repairs was substantially increased.

Fredell (17) performed tests using both boron/epoxy and Glare (aluminum/fiberglass laminate) to characterize the effects of coefficient of thermal expansion (CTE) mismatch on the life of bonded repairs. His research showed that residual stresses in the metal/patch system can be significantly reduced by using patch materials with CTE's close to that of the damaged part. Fredell's research led to a demonstrator program where two Glare patches were applied to stress corrosion cracks on the aft upper crown of a C-5A (22; 3).

Denney (11) attempted to characterize the effect of disbond size and location on thin aluminum panels (t = 1mm) repaired with boron/epoxy patches. He also investigated two different adhesive systems, high-temperature curing film adhesive and room temperature curing paste adhesive, to determine how they affected repair life. Disbonds were placed in the repair bondline using thin teflon tape and the repaired aluminum panel was then fatigued under constant amplitude loading. His research showed a decreased repair life with the presence of disbonds, although it was in most cases a minimal reduction. His research supported the conclusions of Baker concerning ΔK_r and debond

33

growth. Denney recorded constant crack growth rates while the crack was in the repair bondline. C-scans of the bondline after testing showed no significant increase in debond size. Even with worst case debonds present, his work showed significant increases in life of repaired panels over unrepaired panels. His research also showed that film adhesives performed better than paste adhesives because of less porosity in the bondline.

Denney's work was carried on by Mills and Ryan (10), who considered repairs to thicker structures ($1mm \leq t \leq 3.15mm$). They used the same processes as Denney and found decreased life of the repair with increased debond size (still with significant increases in life over the unrepaired case).

The bonded repair problems were approached from an entirely analytical method by Ratwani (23; 24). He used an empirically weighted analytical method that used experimental results from thick and thin plates to formulate his weighting factor. "He used a semi-analytical method involving through-the-thickness stress-distribution and strip model of the plate to determine different back face stress intensity factors for plates of different thicknesses with a single sided repair (3)." The results compared fairly well with experimental data for thin plates, but lost accuracy with increasing plate thickness.

Stub (9) investigated repair geometry and stiffness ratios on single sided repair of thick plates ($3.15mm \leq t \leq 6.35mm$). His research showed that, due to reduced thermal stresses and bending, a stiffness ratio for thicker plates of 1, as opposed to the 1.4 used for most thin cases, improved bonded repair life the most. He also developed a finite element model known as the 3-Layer technique and used it in conjunction with empirical data to come up with a weighting factor for prediction of ΔK_r and bonded repair life.

Lastly, Conley attempted to increase the knowledge base of bonded repair to thick structures by "1) experimentally investigating the fatigue response of repaired thick aluminum panels with bondline flaws and , 2) investigating the accuracy of current finite element modeling techniques in predicting the life of repaired thick aluminum panels (3)." His research involved fatigue testing thick (t = 6.35mm) aluminum panels repaired with partially bonded boron/epoxy unidirectional patches. Debonds were inserted using thin teflon tape and ranged in size from 5% to 20% of the total bond area. Debonds away from the crack showed little or no effect on life of the repair, however, life was significantly influenced by how much of the crack was "bridged" by the adhesive/patch system. C-scans showed little or no debond growth during fatigue testing. Conley performed numerical analysis using finite element modeling to support his research. He used a three layer model, with separate layers modeling the panel, adhesive, and patch. Results from the finite element model matched very closely the experimental data.

2.6   Composite Patch Design Process

When possible, it is always better to perform a double-sided repair. This removes the neutral axis shift, hence removing out-of-plane bending stresses and reducing peel stresses at the patch ends. This study utilized a single-sided repair, since most aircraft repairs are single-sided, therefore this section will focus on the design process for a single-sided composite repair. This process comes from the *Guidelines for Composite Repair to Metallic Structures* handbook (7) which uses equations taken from Royal Australian Air Force standards (RAAF C5033) (25) and research performed by Rose. The details related to the development of the equations are outlined in references 29-31,

but they are not included here. Careful inspection of the following equations shows that Rose carried out approximations of the stress fields in the patch and structure based on stiffness averaging techniques. The goal of the patch in repairing damaged structure is to "bridge" the crack and provide an alternate load path, thereby reducing the stress intensity at the crack tips. The following equations detail the methods used to approximate the best patch size and the stresses encountered in the patch and skin.

2.6.1 Patch Stiffness

When dealing with cracks and cutouts, as this study does, the stiffness ratio, S, between a composite patch and the damaged structure, as previously defined in equation (7) is:

$$S = \frac{E_p t_p}{E_s t_s} \qquad (7)$$

where

E_p = Young's modulus of the patch
t_p = Thickness of the patch
E_s = Young's modulus of the structure
t_s = Thickness of the structure

The stiffness ratio should be $1.0 \leq S \leq 1.5$.

2.6.2 Coefficient of Thermal Expansion

CTE mismatch between the composite patch and repaired structure plays an important role in the success of the repair. The closer the CTE's match, the greater the repair life because of less residual thermal stresses in the repair. In general, composite materials have lower CTE's than metal structures. The effective CTE of the restrained metal structure, α_{eff}, will be much lower than that of the unrestrained structure

36

surrounding the repair. This is because 1) only a small area of the structure (the repaired area) is being heated, and 2) the unheated, cold substructure prevents free thermal expansion. The following rule of thumb is used: if less than 30% of a panel/structure is heated, an effective CTE of the repair must be calculated as shown below:

$$\alpha_{eff} = \frac{\alpha_s(1+v_s)}{2} \tag{8}$$

where

α_{eff} = Effective CTE of the repaired structure
α_s = CTE of the structure's material
v_s = Poisson's ratio of the structure's material

In all other cases, the CTE of the structure can be used. "The more sub-structure is present, which prevents thermal buckling and free expansion, and the smaller the heat blanket, the lower the effective CTE of the structure will be, and the lower the resulting $K_{repaired}$ (7)."

2.6.3 Patch Length

Initial patch length (P_l) in the Royal Australian Air Force (RAAF)-standard is defined as:

$$P_l = 4(l_p + l_e) + l_w \tag{9}$$

where

l_p = Plastic transfer length in the adhesive
l_e = Elastic transfer length in the adhesive
l_w = Defect width (l_w is zero for a crack)

Plastic transfer length is defined as "the minimum plastic and elastic zone size where the $d\tau/dl$ is zero or almost zero (i.e. the shear-overlap length curve reaches a minimum in shear stress) (7)." If the plastic zone of the adhesive can transfer the entire load in the joint, then the plastic zone length is defined as:

$$l_p = \frac{UTS_s * t_s}{N\tau_p} \qquad (10)$$

where

l_p = Length of the plastic zone
t_s = Thickness of the repaired structure
τ_p = Plastic shear stress of the adhesive
N = Number of transfer zones (2 for single-sided; 4 for double sided)

Elastic transfer length is defined as:

$$l_e = \frac{3}{\lambda} \qquad (11)$$

with

$$\lambda = \sqrt{\frac{G}{t_a}\left(\frac{2}{E_s t_s} + \frac{1}{E_p t_p}\right)} \qquad (12)$$

for a double-lap joint, and

$$\lambda = \sqrt{\frac{G}{t_a}\left(\frac{1}{E_s t_s} + \frac{1}{E_p t_p}\right)} \qquad (13)$$

for a single-lap joint, where

G = Adhesive shear modulus
t_a = Adhesive thickness

2.6.4 Patch Width

The minimum recommended patch with is:

$$P_w \geq 2 \times l_c \text{ and } P_w \geq l_c + 1"$$ (14)

where

$$l_c = \text{crack length}$$

An aspect ratio (P_l/P_w) of 1 is preferred in order to reduce the skin stress near the patch-tip.

2.6.5 Patch Termination on the Structure

To reduce patch-tip stresses, there are several guidelines to follow with regards to patch termination. Patch termination is defined as the edge of the patch with the taper.

- Terminate at a stiffening element to make the joint more balanced

- Terminate at least at a distance of l, with l/t_s of 50-100, beyond a stiffening element, to allow for enough flexibility to prevent high bending-stresses

- If countersunk fasteners are present, terminate on top of the fastener covering the complete fastener head, or at least 3 diameters away from the fastener head.

2.6.6 Patch-Tip Stress and Patch Shape

Due to load attraction and bending at the patch-tip, there will be increased stress in the skin. The following equation defines the patch-tip stress in the structure:

$$\sigma_{tip} = \Omega \sigma_{applied} + \left[E_s \left((\alpha_s - \alpha_{eff})(RT - T_{eff}) + (\alpha_p - \alpha_s)(T_{oper} - RT) \right) \right]$$ (15)

where

σ_{tip} = Skin stress at the patch tip
Ω = Load inclusion factor
E_s = Young's modulus of the repaired structure
$\sigma_{applied}$ = Applied/far-field stress
α_s = CTE of the repaired material
α_p = CTE of the patch material
$T_{eff} = (T_{cure} + T_g)/2$
T_{oper} = Operating temperature of the repair
RT = Room temperature
α_{eff} = Effective CTE of the repaired structure

The load inclusion factor, Ω, depends on both the shape and stiffness of the patch. Thicker bondlines may reduce patch-tip stresses.

Based on finite element modeling, the aspect ratio of the patch is more important than its shape (rectangular, circular, elliptical, octagonal). Table 7 shows the effect of both the aspect ratio (P_l/P_w) and the stiffness ratio for typical patch configurations.

Table 7 Example Values for Load Inclusion Factors in an Infinite Panel (Franc2D-L) (7)

S	1	3/2	3/1	4/1
1	1.18	1.2	1.22	1.23
1.2	1.2	1.22	1.25	1.26
1.4	1.22	1.24	1.27	1.28
1.6	1.24	1.27	1.29	1.30

2.6.7 Stress Under the Patch

With the patch-tip stress known, the following equation gives the stress under the patch:

$$\sigma_{under} = \frac{E_s t_s}{\left(E_p t_p + E_s t_s\right)}\sigma_{tip} \qquad (16)$$

For a double-sided patch over cracked structure, t_p is the total thickness of the two patches.

2.6.8 Shear Strain in the Adhesive

With the stress under the patch known, the adhesive shear strain can be calculated with the following equations:

$$\lambda_{under} = \frac{\sigma_{under} t_s \lambda}{G} \tag{17}$$

for elastic cases, and

$$\lambda_{under} = \frac{\tau_p}{2G}\left[1 + \left(\frac{\sigma_{under} t_s \lambda}{\tau_p}\right)^2\right] \tag{18}$$

for inelastic cases, with

$$\lambda = \sqrt{\frac{G}{t_a}\left(\frac{1}{E_s t_s} + \frac{1}{E_p t_p}\right)} \tag{19}$$

where

G = Shear modulus of the adhesive
t_a = Thickness of the adhesive

For a double-sided patch, t_p is the total thickness of both patches combined.

2.6.9 Effectiveness of the Repair

The effectiveness of the repair on halting crack growth of the structure can be determined by calculating $K_{repaired}$. The equations are shown below:

$$K_{repaired} = \sigma_{under} \sqrt{\frac{E_s t_s \lambda t_a}{G}} \qquad (20)$$

for elastic cases, and

$$K_{repaired} = \sqrt{\frac{E_s t_a}{G}\left[\sigma_{under}\tau_p\left(1+\left(\frac{\sigma_{under}\lambda t_s}{\tau_p}\right)^2\right) - \frac{\tau_p^2}{3\lambda t_s}\left(1+2\left(\frac{\sigma_{under}\lambda t_s}{\tau_p}\right)^3\right)\right]} \qquad (21)$$

for inelastic cases.

The greater the reduction in stress intensity at the crack tip of the repaired structure over the unrepaired structure, the longer the life of the repair.

2.6.10 Peel Stress

Out-of-plane deformations due to the neutral axis shift of a single sided bonded composite repair can cause high peel stresses at the patch end. These stresses are one of the leading causes of repair failure. The maximum peel load that can be carried by a certain repair is given by the following equation:

$$\sigma_{peel} = \tau_p \left[\frac{3E_t' t_p \left(1-v_a^2\right)}{E_p t_a}\right]^{\frac{1}{4}} \qquad (22)$$

where

$$\frac{1}{E_t'} = \frac{1}{E_t} + \frac{2}{E_s} + \frac{4}{E_p} \qquad (23)$$

for joints with dissimilar adherends, which is usually the case with bonded repairs.

In order to reduce the peel stresses on the patch, tapering of the patch ends is performed. This reduces the effect of the neutral axis shift and also lessens the effect of load attraction into the skin surrounding the repair. For an optimized non-linear taper, the first step length, x_1, is determined from the transfer length, λ, as shown below.

$$x_1 = \frac{5}{\lambda} \tag{24}$$

The length of each consecutive step is given by the following equation and is shown schematically in Figure 13 (7).

$$x_2 = \frac{x_1}{2} \text{ and for the following steps: } x_n = \frac{x_{n-1}}{n} \tag{25}$$
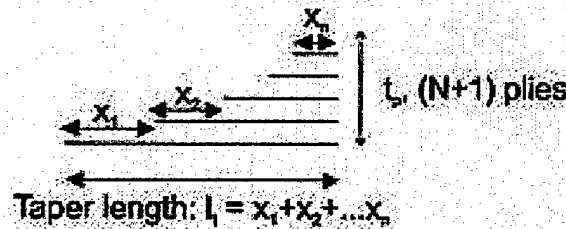
Figure 13 Taper Length Schematic

The longest patch ply will have a length of the calculated patch length plus two times the total taper length.

2.6.11 Patch Stress

The maximum stress in the patch can be calculated with the following equation:

$$\sigma_p = S \cdot \sigma_{tip} \qquad (26)$$

In order to guarantee the integrity of the composite patch, the maximum-allowable stress in the patch should be less than 40% of the ultimate strength of the material under room temperature and dry (RTD) testing conditions. The factor of 0.4 is used to allow for lower composite materials properties at, for example, hot-wet conditions and environmental breakdown over the service life of the patch (7).

2.6.12 Optimization of the Patch Design

Table 8 (7) below shows some possible bonded repair problem areas and different methods to remedy them.

Table 8 Patch Critical Areas and Possible Remedies

Critical Areas	How to reduce stresses in that area
Stress Intensity ($K_{repaired}$) too high	▪ K1: Stiffer patch (either thicker or stiffer material ▪ K2: Shorter patch ▪ K3: For "cold" applications, patch material with a higher CTE
Patch stress too high	▪ P1: Thicker patch ▪ P2: Wider patch ▪ P3: Shorter overlap ▪ P4: Stronger patch material
Skin stress (at patch tip) too high	▪ S1: Thinner patch ▪ S2: Wider patch ▪ S3: Shorter patch ▪ S4: More tapered patch ▪ S5: For "cold" applications, patch material with a lower CTE
Adhesive shear strain too high	▪ A1: Thicker patch ▪ A2: Patch with a higher CTE ▪ A3: Thicker adhesive film ▪ A4: Lower cure temperature
Load transfer length	▪ L1: Longer patch ▪ L2: Thinner patch
Peel stress too high	▪ PL1: More tapered patch ▪ PL2: Thinner patch

Chapter 3   Experimental Setup and Test Procedure

This chapter will discuss the experimental setup and testing procedures involved in this study. Topics such as materials used, patch design processes, testing loads, and specific equipment will be discussed.

3.1   Materials

Test materials utilized in this effort include bare 2024-T3 aluminum panel, a three-ply unidirectional boron/epoxy prepreg composite, and AF-163-2M aerospace adhesive. The aluminum used had two different thicknesses—1mm for the panel and 1.6mm for the stiffeners. The aluminum was provided by the Air Force Research Laboratory Materials Integrity Branch (AFRL/MLSA). Prepreg stands for "pre-impregnated" and simply means that the boron used was already suspended in resin and frozen. The prepreg was provided by AFRL/MLSA. The AF-163-2M is manufactured by 3M corporation and provided by AFRL/MLSA. Material properties for these materials are provided in Table 9 (26; 16).

Table 9 Patch System Material Properties

Material Property	2024-T3	Boron/Epoxy	AF-163-2M
E_L/E_T (GPA)	72.4/72.4	210/25	NA
$\sigma_{ult_L}/\sigma_{ult_T}$ (MPA)	448/448	1590/83	NA
α_L/α_T ($10^{-6}/°C$)	22.7/22.7	4.5/20	NA
G (MPa)	NA	NA	405.8
γ_{yield} (%)	NA	NA	≈ 9
ν_L	0.33	0.168	NA

L-longitudinal; T-transverse

3.2 Specimen Design and Fabrication

The design and fabrication of these test specimens involved eight steps:

1. Machining of the aluminum panels to test configuration dimensions.

2. Pre-cracking of the aluminum panels.

3. Surface preparation of the aluminum panel bonding surfaces.

4. Designing the three-ply boron/epoxy patch.

5. Manufacturing of the three-ply boron/epoxy patch.

6. Bonding on the boron/epoxy patch.

7. Manufacturing the 25.4 mm (1") aluminum stiffeners.

8. Riveting/bonding on the aluminum stiffeners.

3.2.1 Machining the Aluminum Panel

The aluminum panels were first cut down to a rough dimension of 304.8mm x 558.8mm (12" x 22") with a shear press. They were then sent out to a local machine shop to be milled to the exact dimensions of 304.8 mm x 558.8 mm "dog-boned" down to 254 mm (10"). Because this was the first research investigating the fatigue response of repaired, stiffened panels, dimensions were chosen to closely match dimensions of earlier work focusing on unrepaired, stiffened structures performed by Heinimann (27). The width of the panels is slightly wider to accommodate the two different stiffener spacings investigated. The machine shop also performed the electrical discharge machining (EDM) of the panels to create a 12.7mm (0.5") notch in the center of the panel. A schematic of the completed panel is shown below in Figure 14.
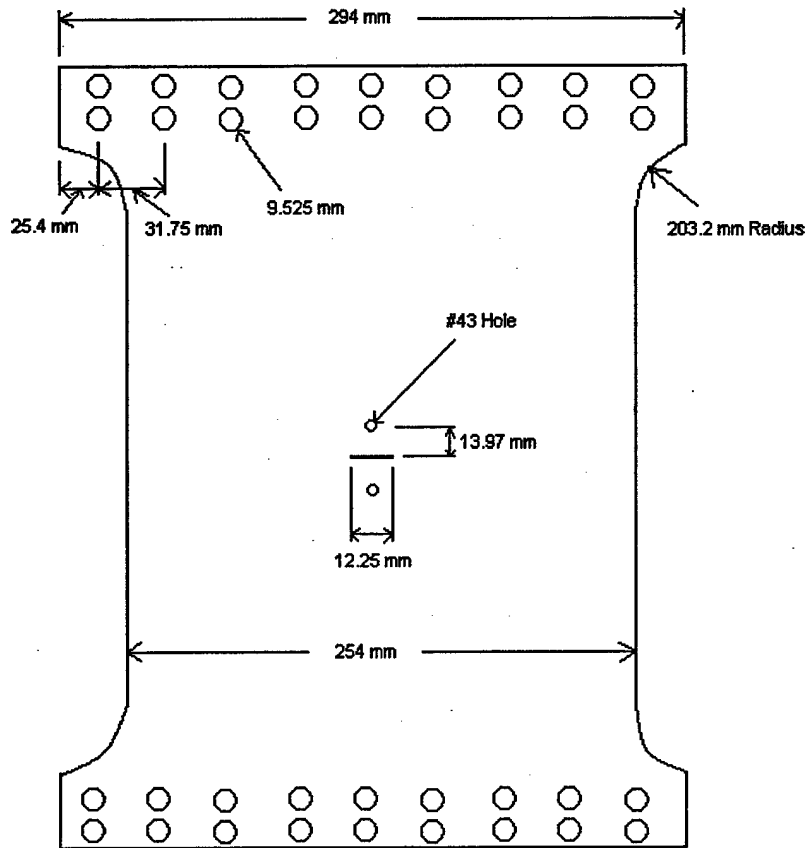
Figure 14 2024-T3 Aluminum Test Panel

3.2.2 Pre-cracking the Aluminum Panels

Once machining of the aluminum test panels was complete, pre-cracking of the panels was accomplished. The panels were placed in MTS (Materials Testing System) tensile test machines, shown in Figure 15. The aluminum panels were then fitted with crack-opening displacement (COD) clip-on gauges to measure the crack growth per cycle. These gauges shut the testing down when the crack length reached a certain point. This is shown in Figure 16. The cracks were grown out to approximately 25.4 mm (1").
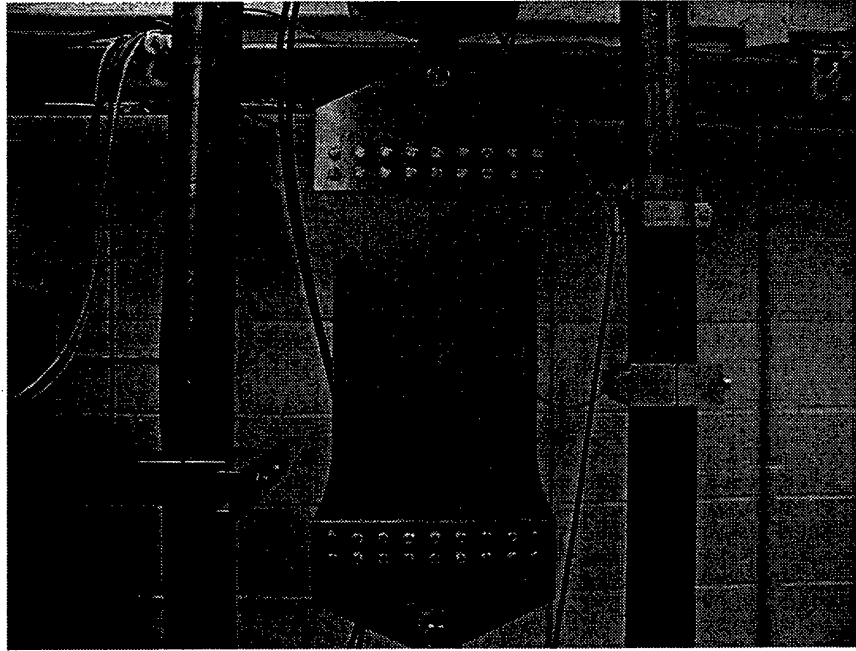
Figure 15 Aluminum Panel in MTS Tensile Test Machine
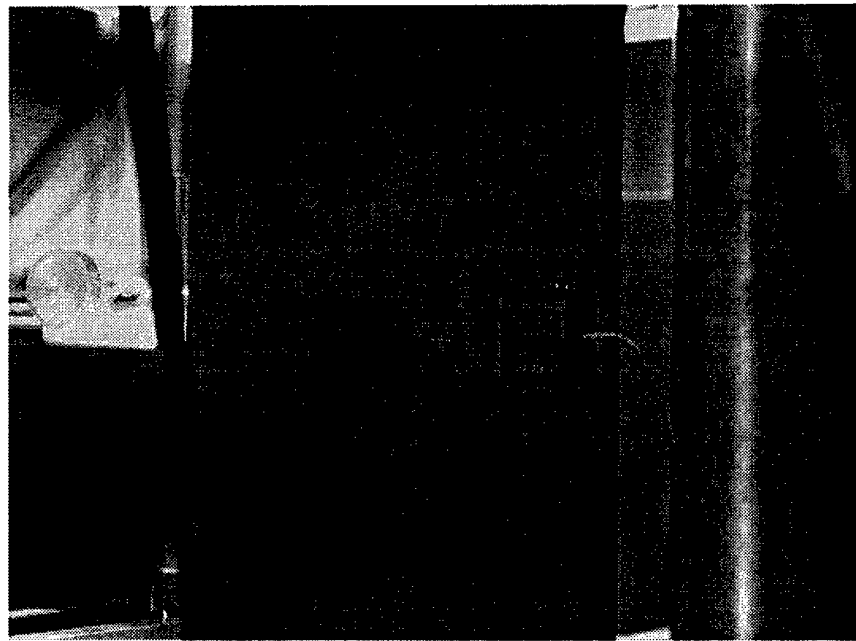
Figure 16 Aluminum Panel Fitted with COD "Clip-Gauge"

Pre-crack lengths for each of the 18 specimens, along with the number of cycles necessary to reach the crack length, are shown below in Table 10. All of the panels were pre-cracked at 5 Hertz at a load of 100 MPa.

Table 10 Specimen Pre-cracking Crack Lengths and Cycles

Specimen Number	Final Crack Length After Pre-cracking (mm/inches)	Number of Cycles Necessary to Reach Crack Length
A-1	24.9174/0.981	38981
A-2	25.1714/0.991	34938
A-3	25.4000/1.000	41063
A-4	27.4828/1.082	43683
A-5	26.7208/1.052	42070
A-6	27.7622/1.093	44220
A-7	26.7716/1.054	41473
A-8	25.4254/1.001	40890
A-9	29.0068/1.142	46584
A-10	25.1714/0.991	36559
A-11	25.7048/1.012	38760
A-12	25.4000/1.000	39902
A-13	25.2730/0.995	42017
A-14	25.6540/1.010	41423
A-15	25.5524/1.006	40528
A-16	26.2890/1.035	41433
A-17	26.8224/1.056	44442
A-18	25.1460/0.990	40819

3.2.3 Surface Preparation of the Aluminum Panels

The bonding surface of the aluminum panels was prepared using the grit blast/silane (GBS) surface preparation technique. The process is detailed below:

- Degrease the bonding surface with lint-free, Duralace aerospace-grade wipes soaked in solvent. Acetone was used for this study.

- De-oxidize the bonding surface using 3M Scotch-Brite™ 7447B general use abrasive pads.

- Degrease the bonding surface again to remove any particles from the surface.

49

- Lightly grit blast the surface using 50 micron aluminum oxide grit using 30-100 psi oil-free nitrogen pressure. 60 psi nitrogen pressure was used in this process.

- Apply a 1%-3% silane solution to the bonding surface with complete coverage for 10 minutes. The silane solution must be hydrolyzed for 1 hour prior to use and should be used within 2 hours. Excess silane solution should be blown off with oil-free nitrogen after 10 minutes.

- The silane was baked for 1 hour at 104°C (220°F).

- Once the silane had cooled to 32°C (90°F), Cytec BR-127 corrosion inhibiting primer was applied with a primer spray gun connected to dry, oil-free nitrogen. Primer was applied until a thickness of 0.0254 mm to .0762 mm (0.001 to 0.003 inches) was reached. After drying for 30 minutes at room temperature (RT), the primer was baked for 1 hour at 121°C (250°F).

This process encourages adhesion between the metal and the adhesive, providing a very strong bond comparable to phosphoric acid anodization (PAA), which is the best surface preparation technique. The primer layer protects the metal/adhesive interface from corrosive environmental attack, which is the leading cause of patch debond.

3.2.4 Design of the Boron/Epoxy Patch

Boron/epoxy was chosen as the material for the composite patches because it is the most common composite used for patching damaged aircraft structure. This is due to several advantages gained by using boron. Firstly, it is stiffer and stronger than other possible materials, such as aluminum, fiberglass, or graphite. This results in thinner, more aerodynamic repairs. While aluminum or aluminum/fiberglass laminate patches would solve CTE mismatch problems in the repair area, which induce bending and residual stresses, these materials are approximately one third as stiff and result in much bulkier repairs. Secondly, boron does not cause galvanic corrosion problems when in

50

contact with aluminum, while graphite does. Lastly, boron/epoxy, as opposed to graphite or aluminum, is non-conductive and allows for easy use of conventional nondestructive evaluation (NDE) techniques, such as Eddy Current, to monitor the damaged area underneath the patch.

The boron/epoxy patches used in this study were designed according to the *Guidelines for Composite Repair of Metallic Structures* handbook (7). The process is described in detail in section 2.6, *Composite Patch Design Process*, and the exact calculations for this patch design are shown in Appendix A: Composite Patch Design. The patch had the following dimensions:

Table 11 Boron/Epoxy Patch Dimensions

Ply Number	Length mm (in)	Width mm (in)
1	102 (4.02)	69 (2.71)
2	80 (3.15)	69 (2.71)
3	69 (2.71)	69 (2.71)

3.2.5 Manufacture of the Boron/Epoxy Patch

It is common practice to use the largest composite ply as a cover ply over the patch, as it provides good environmental protection. This is what was done for six of the fourteen patches bonded on to panels. The other eight panels had a simple "wedding cake" lay-up configuration, with no cover ply utilized. Both patches consisted of three plies with the same dimensions, so the strength of both patch configurations was equivalent. Schematics of each type of patch are shown below in Figure 17 and Figure 18.

51
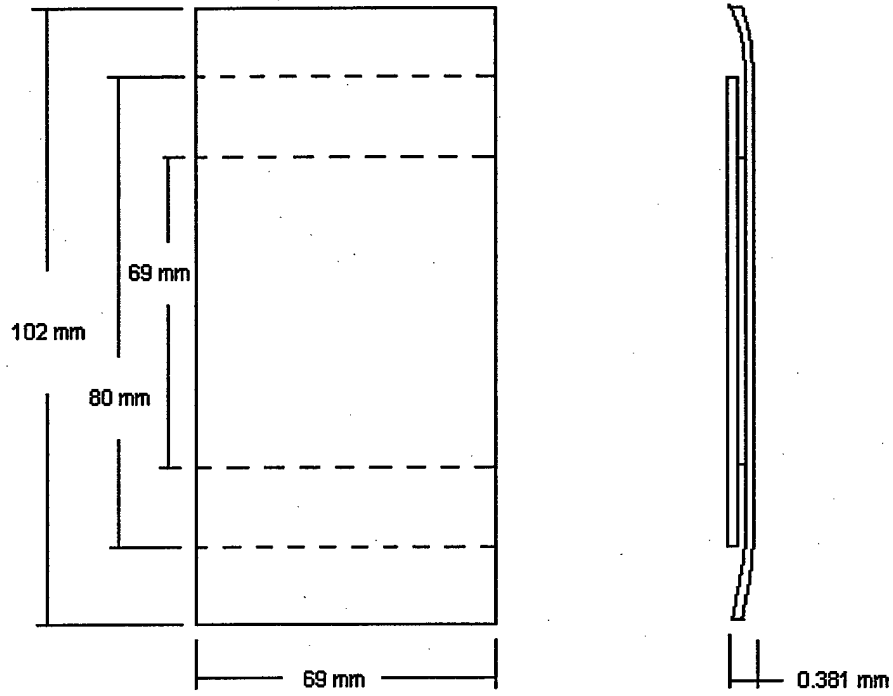
Figure 17 Boron/Epoxy Patch Lay-up with Cover Ply
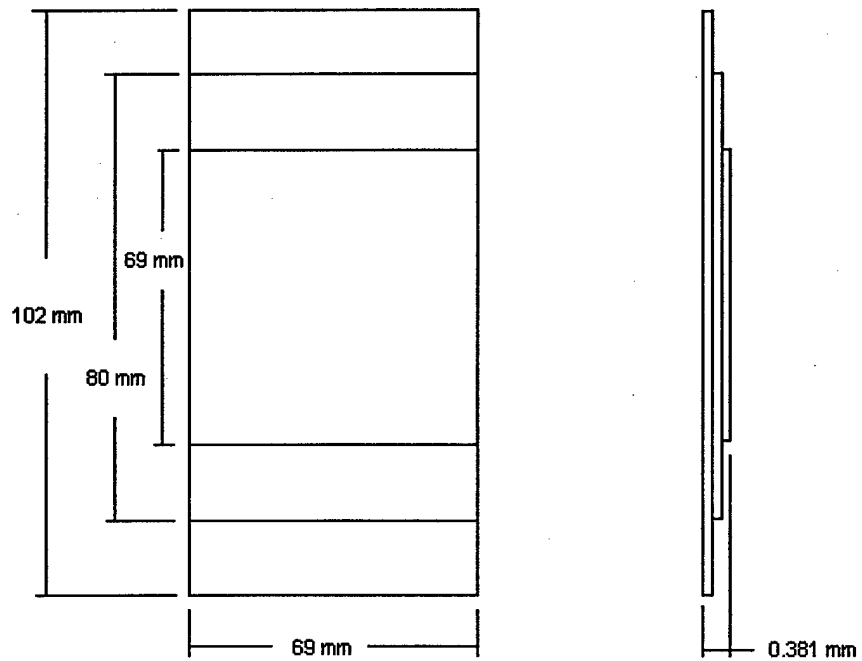
Figure 18 Boron/Epoxy Patch Lay-up with No Cover Ply

Once the patches were cut to size and configured properly, they were cured in a

portaclave that applies both high temperature and pressure to ensure a nicely cured patch.

Figure 19 shows the portaclave/hotbonder used to cure the patches and Figure 20 shows a

C-SCAN of a cured patch. By comparing colors in the C-SCAN with the color chart at

the bottom of the print-out, the C-SCAN shows the patch is well-consolidated with no

delaminations.
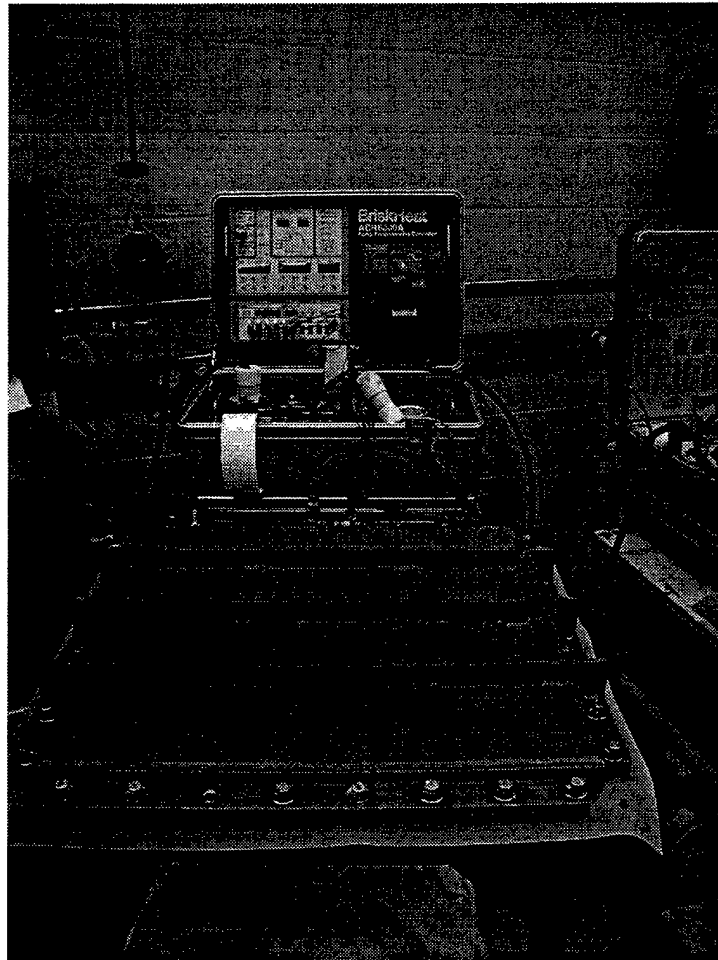
Figure 19 Portaclave and Hotbonder used to Cure Boron/Epoxy Patches

53
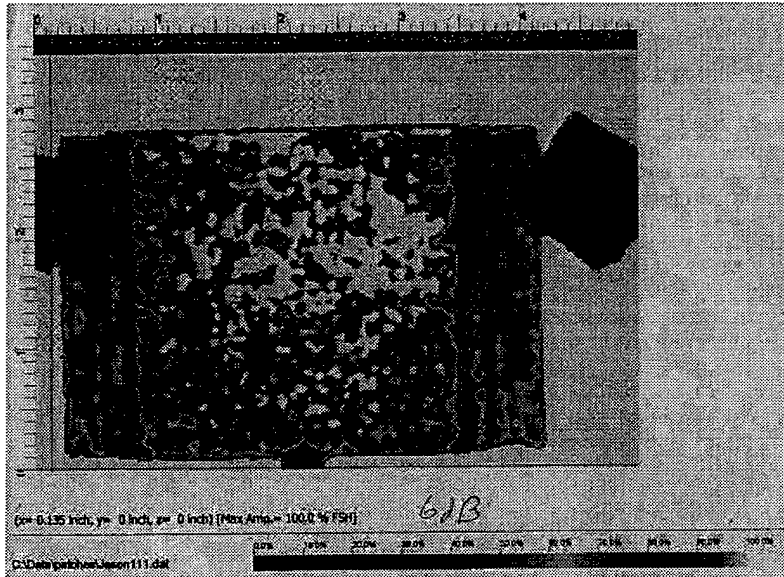
Figure 20 C-Scan of Cured Boron/Epoxy Patch

The patches underwent a 1.67°C (3°F) per minute ramp up to 121°C (250°F) where they were cured under positive pressure (30-35 psi) for 1 hour.

3.2.6 Bonding Boron/Epoxy Patch onto the Aluminum Panel

Once both the aluminum panel was prepared (machined, pre-cracked, and surface preparation applied) and the boron/epoxy patch had been manufactured, the patch had to then be bonded on to the panel. Cross-hairs were marked on the panel (outside of the bonding surface) and the non-bonding surface of the patch. This made for much more accurate placement of the patch in the middle of the panel. The bonding surface of the patch was lightly grit blasted so a physical bond could be formed with the adhesive. AF-163-2M adhesive was then cut out slightly larger than the perimeter of the patch. This was done to create a nice fillet around the perimeter of the patch and reduce stress concentrations at the edges. Using the cross-hairs, the patch, with the adhesive stuck to

54

the bonding surface, was placed in the center of the aluminum panel. To keep the patch from sliding around as the adhesive plasticized at the cure temperature, "flash-breaker" tape with a temperature range up to 400°F was applied (Airtech, Flashbreaker 1).

The aluminum panel/composite patch system was then placed in a portaclave and put through a 2-stage curing cycle. The panel was first ramped up to 82.2°C (180°F) at 1.67°C (3°F) per minute and held for 30 minutes. During this stage, the panel was under full vacuum, or approximately 25" Hg, until it reached 82.2°C (180°F). This is to remove as much porosity (trapped air) from the adhesive bondline as possible. When the panel reached 82.2°C (180°F), the vacuum level was reduced to 13" Hg. If the panel remains at full vacuum while the adhesive starts to cure, large amounts of porosity will develop. By reducing the vacuum level to 13" Hg, the air trapped in the bondline is allowed to "shrink" in size, creating less porosity and a better bondline. It would be best to use positive pressure to bond the patch to the panel, but since maintainers do not have means to apply positive pressure to on-aircraft parts, this study used vacuum in an attempt to give more realistic results. After the initial cure, the panel was ramped to 121°C (250°F) at 2.22°C (4°F) per minute and held for an additional hour.

3.2.7 Manufacture of Aluminum Stiffeners

Aluminum stiffeners were designed in accordance with Heinimann's Ph.D. thesis, "Analysis of Stiffened Panels with Multiple Site Damage (27)." He used 1.6 mm (0.063") thick 2024-T3 aluminum for his panels and 2.29 mm (0.09") thick 2024-T3 aluminum for his stiffeners. He used stiffener widths of 19.05 mm (0.75") and 38.1 mm (1.5"). The skin thickness used for this study was 1 mm (0.04"). Using the same skin to

55

stiffener ratio as Heinimann, $\dfrac{1.6}{2.29} = 0.699$, a stiffener thickness of 1.6 mm (0.063")

was determined. A stiffener width of 24.5 mm (1") was chosen, as it fell in between the

two widths used by Heinimann.

The stiffeners in this study were bonded to the aluminum panels, as well as

riveted. Because of this, certain steps had to be taken to reduce stress concentrations at

the stiffener tips. Just like the boron/epoxy patch, the ends of the stiffeners were

"tapered" by grinding them down. This was performed to reduce the stress

concentrations due to load attraction from the surrounding skin. Also, the ends of the

stiffeners were rounded to reduce the stress concentrations at the corners. This process

helped to ensure that no fatigue crack initiation would occur in the skin outside of the

stiffener tips. A schematic of the stiffeners is shown below in Figure 21.
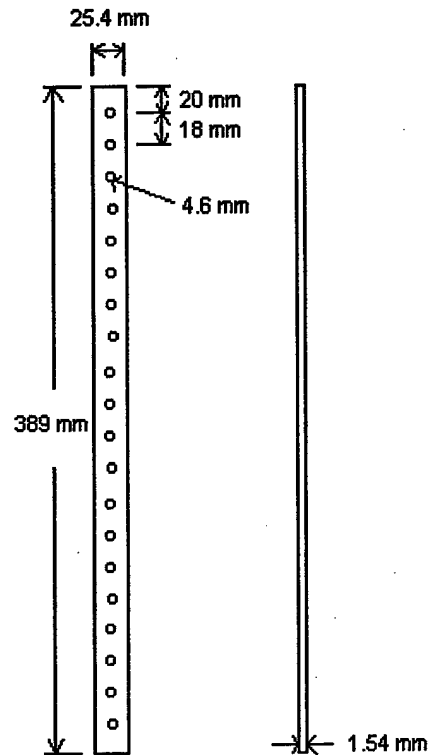
Figure 21 Aluminum Stiffener

3.2.8   Attaching Stiffeners to the Aluminum Panel

Stiffeners were applied to the aluminum panels in five steps:

1. Holes were drilled through the stiffeners and panels using "clicos" to ensure good hole alignment.

2. The panel and stiffener bonding surfaces were prepared with a scuff sand/solvent wipe process.

3. AF-163-2M was cut-out for each stiffener and the stiffener was affixed to the aluminum panel with "clicos."

4. The stiffener was riveted to the aluminum panel.

5. The panel, with the stiffeners now riveted on, was "vacuum-bagged" and the AF-163-2M adhesive was cured. Stiffeners were bonded on *as well as* riveted to prevent fatigue crack initiation in the rivet holes. This problem will be discussed in detail in Section 4.1.2.

57

The first three steps are self-explanatory. The last two steps are further explained in detail below.

3.2.9   Riveting the Stiffener to the Aluminum Panel

The stiffeners were attached to the panels using a pneumatic riveting process. All tools needed (rivets, reemer, bucking bar, and pneumatic rivet gun) are shown in Figure 22. The rivet holes in the stiffeners and panels were first "reemed" to 4.85 mm (0.191") to ensure the proper size for the rivets and to reduce the chances of fatigue crack initiation in the holes. This process is shown in Figure 23. Rivets were then inserted into the holes and installed one at a time. This consisted of placing the rivet gun against the head of the rivet and the bucking bar against the butt. As the gun hit the rivet, the bucking bar deformed the butt and the rivet filled the hole. Because the panel tends to expand slightly as it is riveted, it is best to work from the center of the panel out toward the ends to reduce any deformity in the panel. This process is shown in Figure 24, Figure 25, and Figure 26.

Figure 22 Riveting Tools
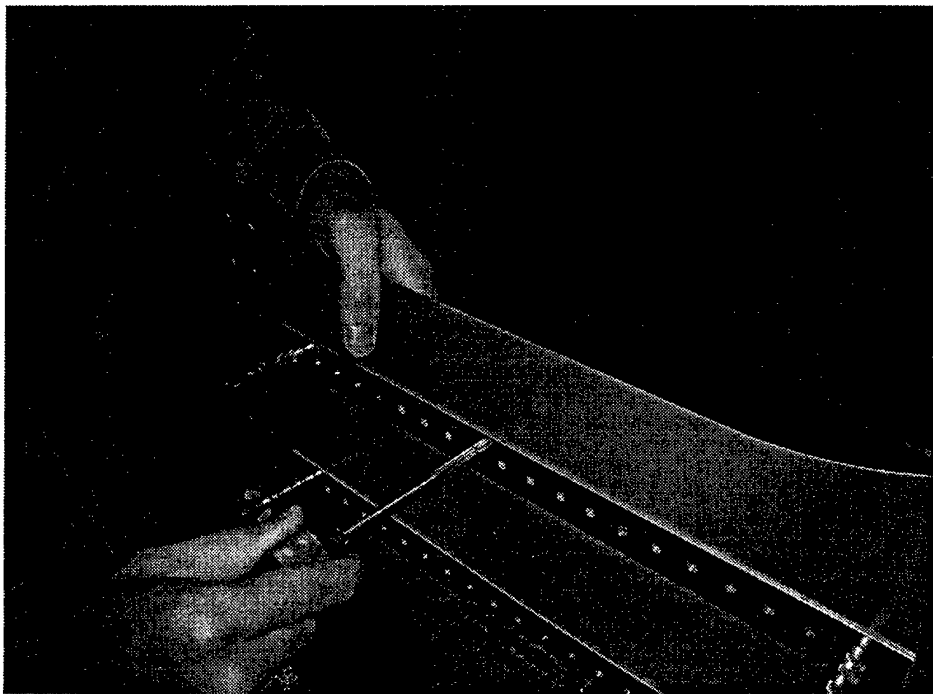
Figure 23 Process for "Reeming" the Rivet Holes
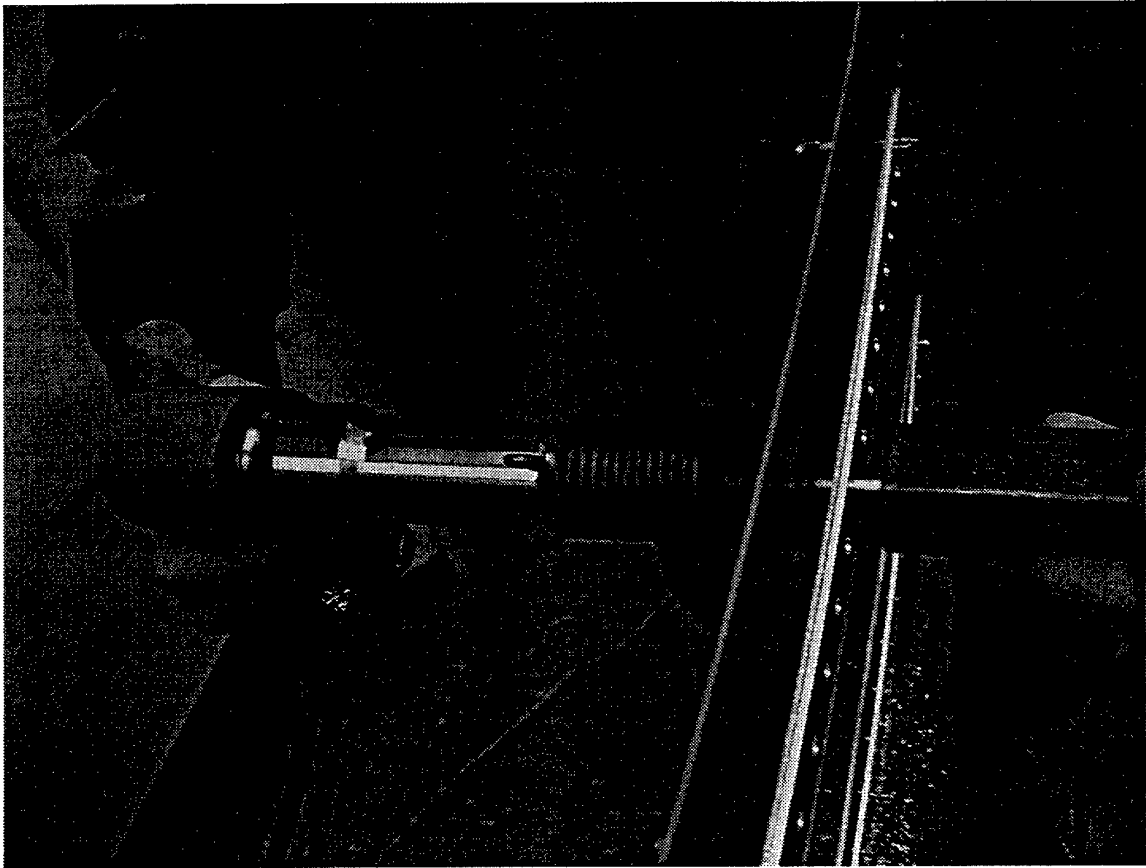
Figure 24 Deforming Rivet with a Pneumatic Gun and Bucking Bar
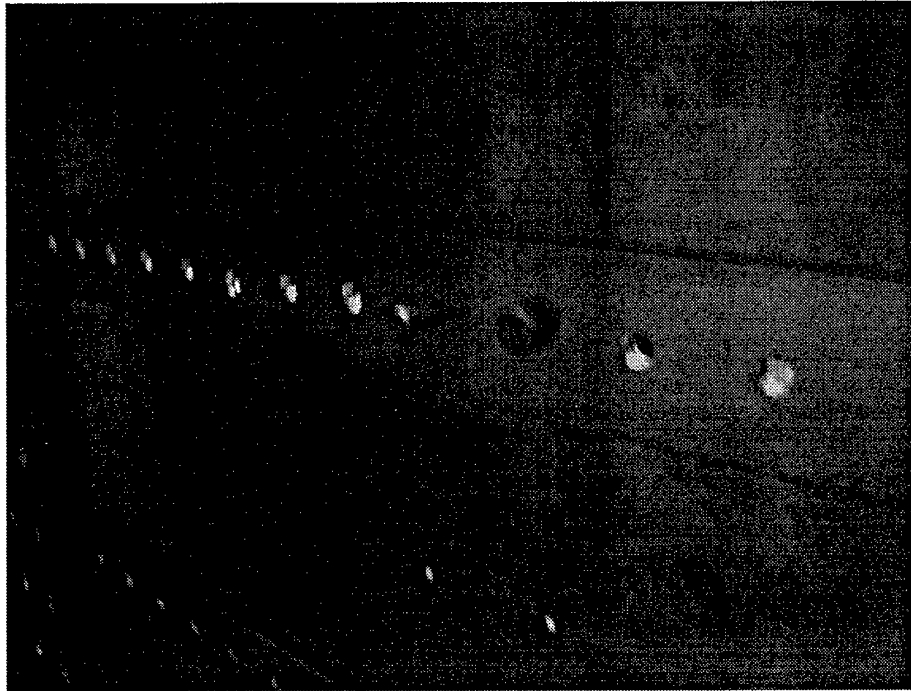
Figure 25 Unfinished and Finished Rivet
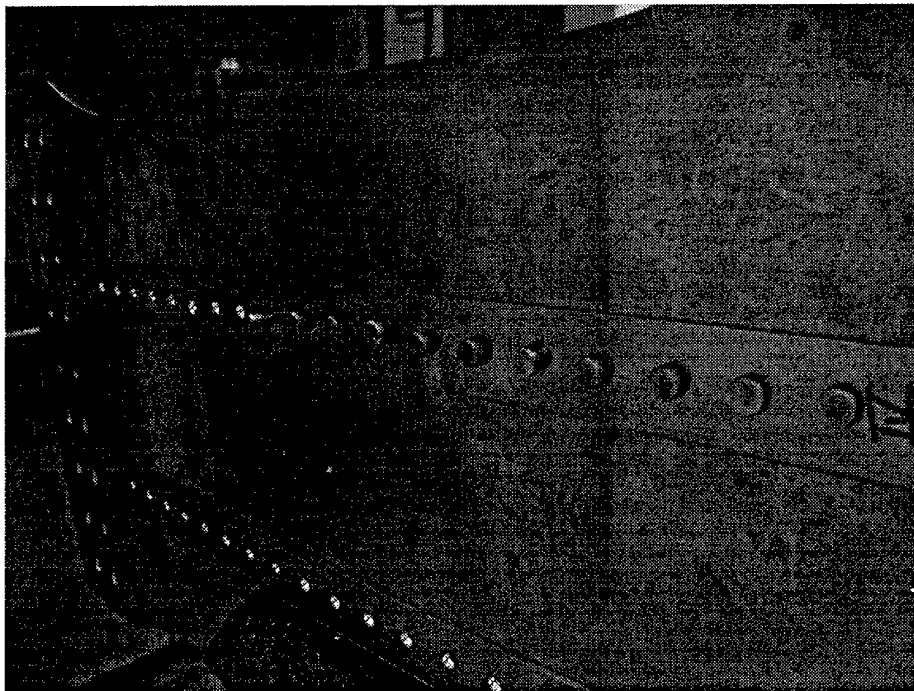
Figure 26 Finished Rivets

3.2.10 Bonding the Riveted Stiffeners to the Aluminum Panels

Bonding the stiffeners to the aluminum panels was performed by curing the AF-163-2M adhesive in an oven under vacuum. To accomplish this, an envelope vacuum bag was manufactured around the panel. Once the bag was complete with full vacuum applied to the panel, it was inserted into the oven. The cure cycle used was a ramp up to 82.2°C (180°F) at 1.67°C (3°F) per minute. This was held for 30 minutes. During this stage, the panel was under full vacuum, or approximately 25" Hg, until it reached 82.2°C (180°F). When the panel reached 82.2°C (180°F), the vacuum level was reduced to 13" Hg. After the initial cure, the panel was ramped to 121°C (250°F) at 2.22°C (4°F) and held for an additional hour. A completed panel, with boron/epoxy patch and stiffeners applied, is shown below in Figure 27.
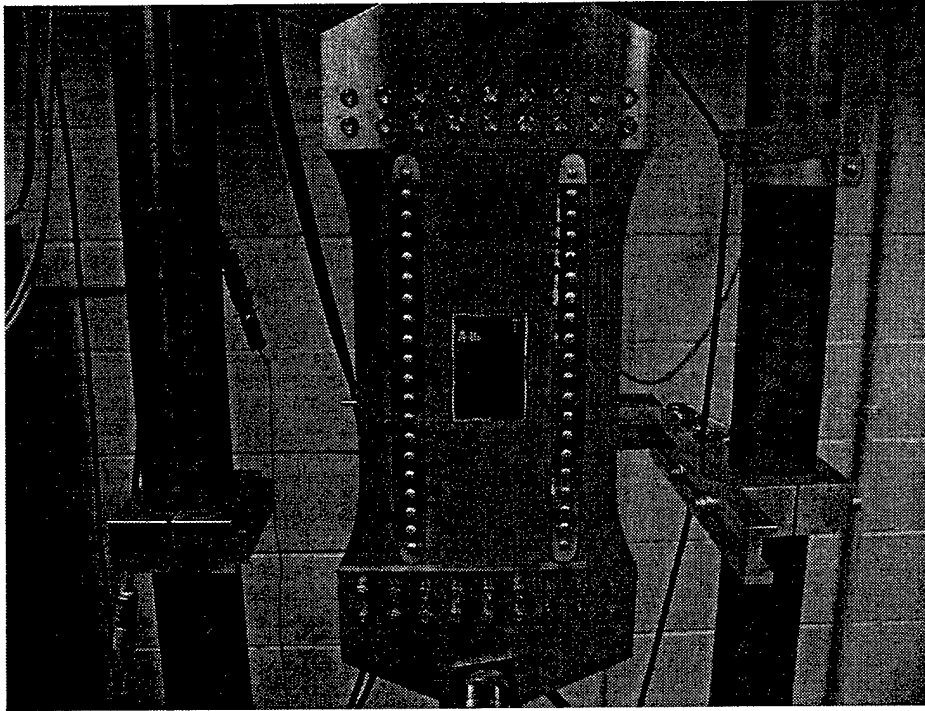
Figure 27 Completed Panel with Boron/Epoxy Patch and Stiffeners

3.3   Testing Procedures

Testing was performed in the Air Force Research Laboratory Air Vehicles

Fatigue and Fracture Lab Laboratory on MTS tensile machines, as was seen in Figure 27.

All fatigue testing was performed at 8 hertz and 120 MPa. Cracks were measured

utilizing a "floating" microscope mounted to the MTS machine, as seen in Figure 28.

Crack length data, as well as cycles to reach the crack lengths, were immediately stored

in a Microsoft Excel 97 spreadsheet. Panels were fatigued until one of three things

happened:

1. In the case of unstiffened specimens, the panels were cycled until catastrophic
    failure of the specimen.

2. In the case of stiffened specimens, the panels were cycled until the crack tips
    reached the stiffeners and crack lengths could no longer be measured.

63

3. Also in the case of stiffened specimens, until the panel ruptured due to fatigue crack initiation at a different location, either a rivet hole or just outside the stiffener tip.
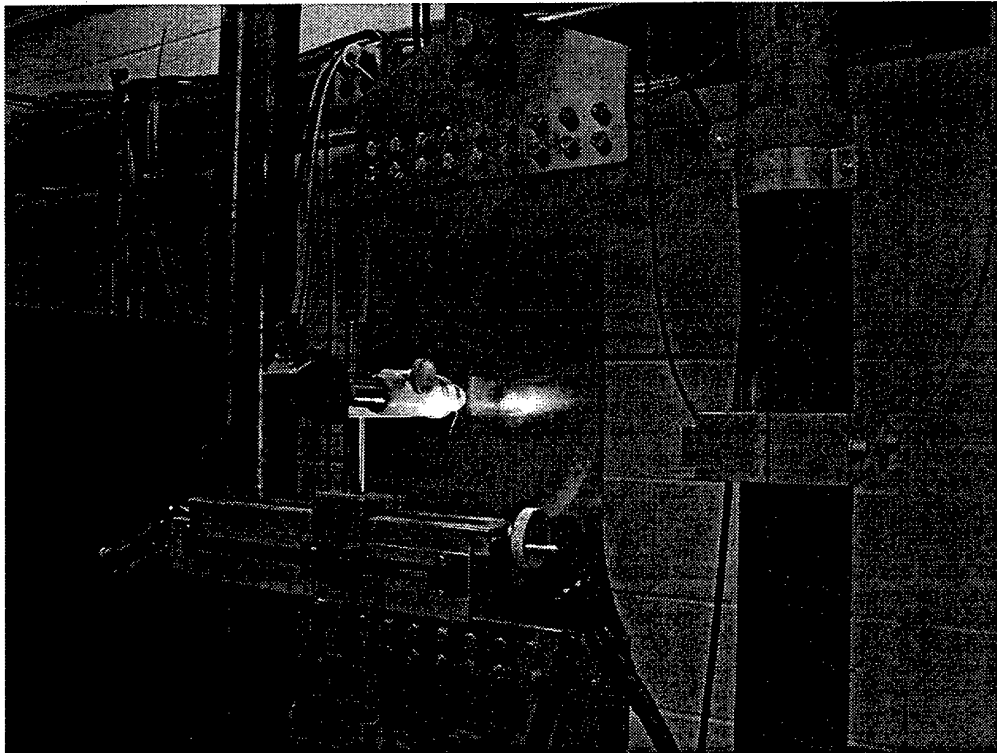
Figure 28 Floating Microscope for Crack Length Measurements

Infrared pictures were periodically taken to record changes in delaminations in the adhesive bondline under the patch. This was accomplished with the Inframetric 760 IR camera system. This equipment is shown in Figure 29 and Figure 30. The patch was first heated up with a standard heat gun, shown in Figure 31, and the infrared camera displayed "hot spots" in the bondline. Delaminations remain hot longer because air acts as an insulator between the patch and the metal panel. This keeps the patch from cooling

down due to contact with the metal. A picture of the IR camera in operation is shown in

Figure 32, and an infrared picture showing disbonds can be seen in Figure 33.
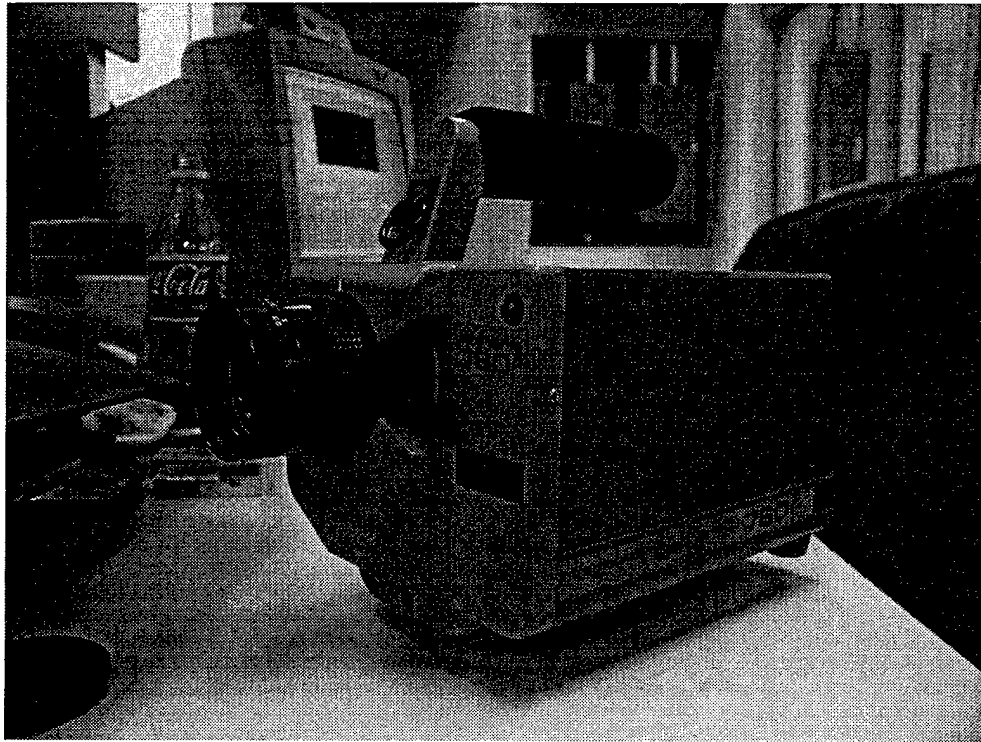
Figure 29 Inframetrics 760 IR Camera

Figure 30 Inframetrics 760 IR Data Acquisition Device
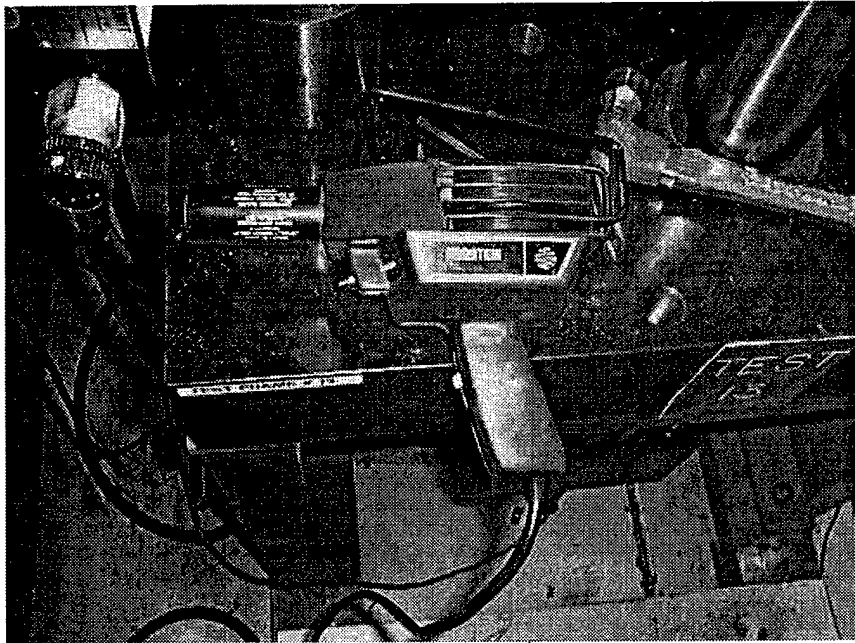
Figure 31 Heat-Gun Used for Infrared Pictures
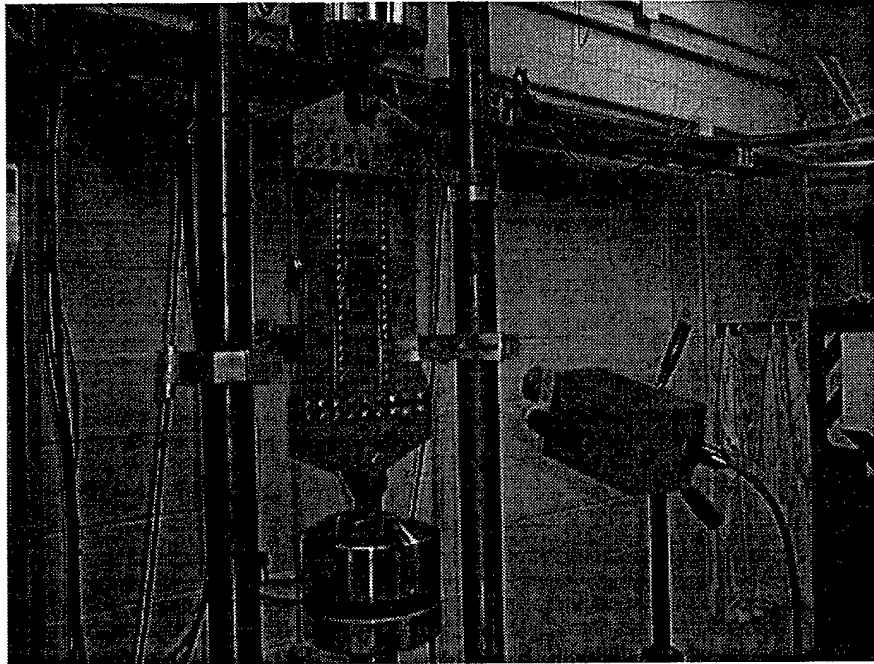
Figure 32 IR Camera in Operation
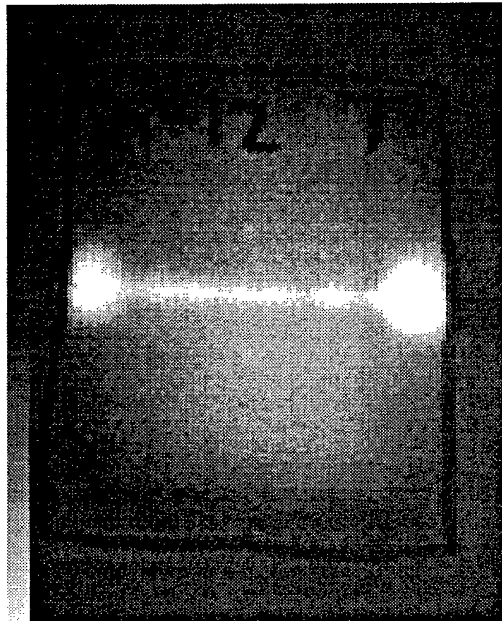
Figure 33 Infrared Picture Showing Disbonding

Chapter 4   Results and Discussion

The purpose of this chapter is to document experimental results obtained from fatigue cycling eighteen panels to failure with twelve different testing configurations incorporating some of the following different design scenarios:

- Stiffeners with 102 mm (4 inch) of centerline separation

- Stiffeners with 152 mm (6 inch) of centerline separation

- Completely bonded (CB) boron/epoxy patches

- Boron/epoxy patches with crack tip disbonds (CTD)

- Boron/epoxy patches with full width disbonds (FWD)

- Boron/epoxy patches with end disbonds (ED)

Disbond and stiffener configurations are as defined in Figure 2 and Figure 3, respectively, in Chapter 1. Table 12 details the exact testing configuration of each specimen, along with cycles to failure.

This chapter is divided into two sections. The first section will discuss the effects of stiffeners and stiffener spacing on the life of a bonded repair and the second section will discuss the effects of disbond size and location on the life of a repair. Both sections will first detail test results and then discuss those results.

Table 12 Experimental Test Matrix

Specimen Number	Stiffener Configuration (mm/in)	Disbond Configuration	Disbond Area (%)	Peak Load (MPa)	R = $\sigma_{min}/\sigma_{max}$	Cycles to Failure
A-1	No stiffener	Baseline (no patch)	NA	120	0.05	8,687
A-2	No stiffener	CB	0	120	0.05	132,558
A-3	152/6	Baseline (no patch)	NA	120	0.05	54,500
A-4	102/4	CB	0	120	0.05	65,576*
A-5	102/4	CB	0	120	0.05	405,010
A-6	152/6	CB	0	120	0.05	95,267*
A-7	152/6	CB	0	120	0.05	55,011*
A-8	102/4	CTD	8.2	120	0.05	351,109*
A-9	152/6	CB	0	120	0.05	401,006
A-10	102/4	CTD	8.2	120	0.05	305,007
A-11	152/6	CTD	8.2	120	0.05	375,010
A-12	152/6	CTD	8.2	120	0.05	375,006
A-13	152/6	FWD	11.7	120	0.05	275,007
A-14	102/4	FWD	11.7	120	0.05	315,011
A-15	102/4	ED	17.6	120	0.05	395,000
A-16	152/6	ED	17.6	120	0.05	212,816*
A-17	102/4	FWD	11.7	120	0.05	235,011
A-18	102/4	Baseline (no patch)	NA	120	0.05	73,988

CB—completely bonded
CTD—crack tip disbond
FWD—full-width disbond
ED—end disbond
* premature failure which is explained in text

4.1 Effects of Stiffeners and Stiffener Spacing on Repair Life

To determine the effect of stiffeners and stiffener spacing on bonded repair life, two baseline panel scenarios will be examined—repaired and unrepaired.

4.1.1 Unrepaired Panel Comparison

In order to determine the effect of stiffeners and their spacing on unrepaired panel life, a baseline unrepaired panel (no stiffener/no patch) was compared to baseline unrepaired stiffened panels (102 mm and 152 mm spaced stiffeners with no patch). 152 mm and 102 mm spaced stiffeners were used to simulate stiffener spacing in transport aircraft fuselage and wings, respectively. Table 13 documents the fatigue lives of the three panels, and Figure 34 shows the comparison. The baseline unstiffened panel fatigue life correlates well with Denny's data (11).

Table 13 Comparison of Fatigue Lives Between Stiffened and Unstiffened Panels

Specimen Number	Configuration	Cycles to Failure
A-1	No stiffeners/No patch	8,687
A-3	152 mm Stiffeners/No patch	54,500
A-18	102 mm Stiffeners/No patch	69,007
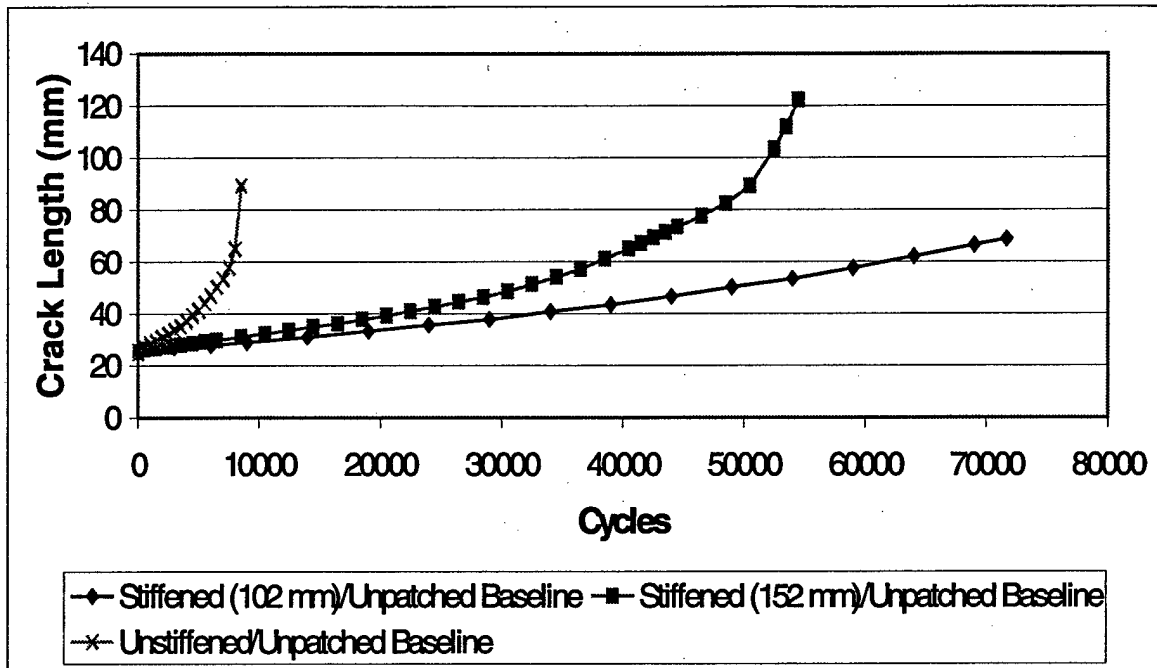
Figure 34 Stiffener Effect on Unrepaired Panel Fatigue Life

In the case of panel A-1, the unstiffened/unrepaired baseline panel, failure was

defined as the moment catastrophic failure occurred. For stiffened panels, failure was

defined in one of two ways. Firstly, failure was defined when at least one of the crack

tips reached the stiffener, making it impossible to monitor the crack growth any longer.

This was the case for panel A-3, the panel with the 152 mm spaced stiffeners. For panel

A-18 with the 102 mm spaced stiffeners, however, the crack tips never reached the

stiffeners because failure occurred prematurely due to fatigue crack initiation at a rivet

hole in the first stiffener rivet row (illustrated in Figure 35). This is the second, less

common mode of failure. The 102 mm spaced stiffeners, with their closer proximity to

the crack tips, retarded the crack growth to such an extent that it became easier for the

71

panel to initiate a new crack at the first rivet row rather than to continue propagating the

initial crack out toward the stiffeners. This failure is shown in Figure 36.
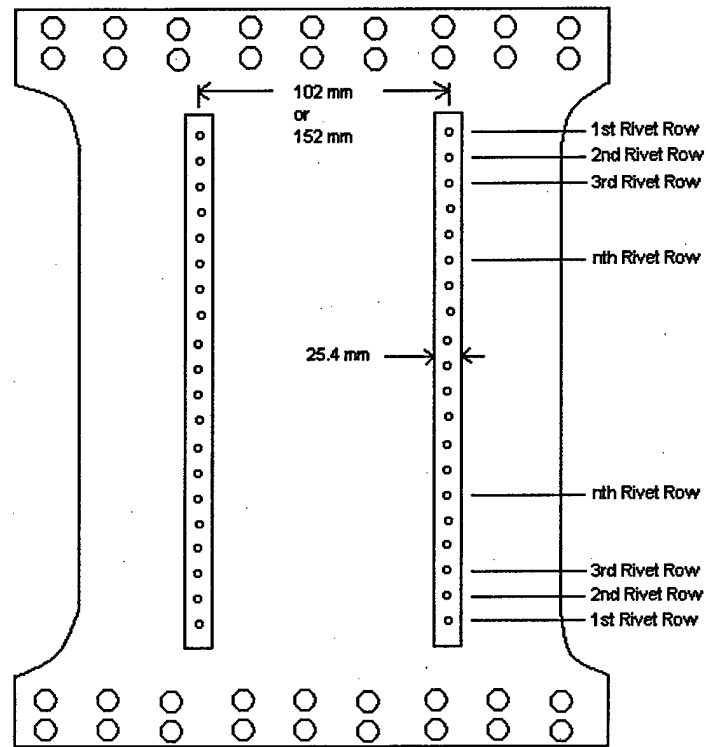
Figure 35 Rivet Row Illustration
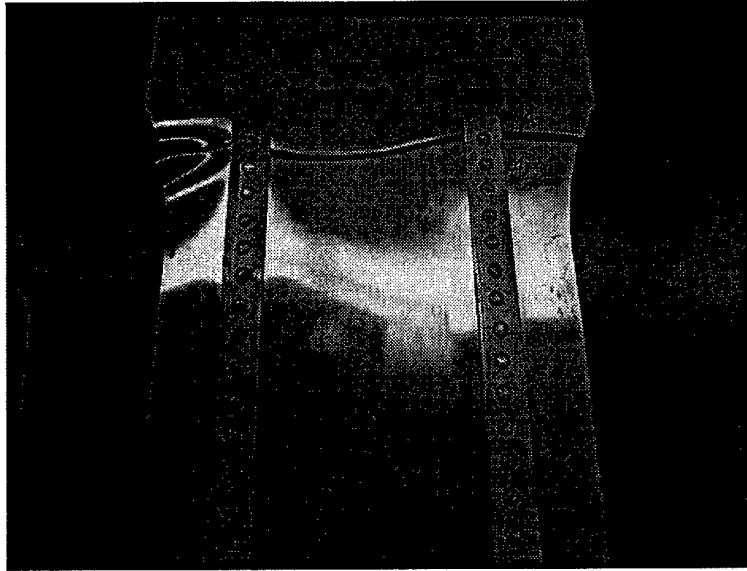
Figure 36 Failure Resulting From Fatigue Crack Initiation/Propagation at First Stiffener Rivet Row

When dealing with riveted structure, stress is transferred from the panel in decreasing percentage by subsequent rivets (28:24). This is why the crack initiated in the first rivet row. The 152 mm spaced stiffeners did not provide enough crack retardation to drive the failure into the rivet row. This phenomenon of "driving" failure into the rivet row was seen in both cases (152 mm and 102 mm spaced stiffeners) of the repaired panels and will be discussed further in latter sections.

Comparing the data from all three panel configurations, it can be seen that stiffened aluminum structure performs much better than unstiffened structure. Table 14 shows a comparison of the cycles needed to reach equivalent crack lengths for all three panel configurations. Since the patch used to repair the panels was 69 mm (2.71 inches) wide, that crack length was used for comparison. Even though these initial panels were unrepaired, comparing all the panels at the same crack length allows for easy data

correlation between different testing configurations. 152 mm centered stiffeners increased the unrepaired panel life by more than 5 times, while 102 mm centered stiffeners increased the unrepaired panel life by more than 8.5 times.

Table 14 Fatigue Life Comparison of Unstiffened and Stiffened Unrepaired Panels

Panel Number	Configuration	Crack Length mm/in	Cycles to Reach Crack Length*
A-1	Unstiffened/Unrepaired	69/2.71	8,077
A-3	6" Stiffeners/Unrepaired	69/2.71	42,238
A-18	4" Stiffeners/Unrepaired	69/2.71	71,664

* Interpolated Results

The increase in fatigue life is due to two things: 1) increased stiffness in the repair area resulting in lower out-of-plane bending stresses and 2) reduced stress in the vicinity of the crack tips due to the stiffeners carrying some of the load. Stiffness can be calculated with the following equations:

$$Stiffness = E * I \qquad (27)$$

with

$$I_{zz} = \frac{bh^3}{12} \qquad (28)$$

where

E = Young's Modulus of the material

I = Moment of Inertia of the cross-section

b = Width of the panel

h = Thickness of the panel

74

Using this equation, the stiffness of an unstiffened/unrepaired aluminum panel is 1.607 Nm^2. By adding the stiffeners to the panel, the stiffness (found using the Parallel Axis Theorem) increases to 24.03 Nm^2, or an increase in stiffness of 15 times. The mode I stress intensity at the crack tip can be calculated with the following equation:

$$K_I = \sigma\sqrt{\pi a} \tag{29}$$

where

K_I = Mode I Stress Intensity Factor
σ = Stress at the crack tip
a = Crack length ÷ 2

In the case of the unstiffened/unrepaired panel, A-1, the far-field stress was 120 MPa and the initial crack length was 24.9 mm (0.981"), creating an initial stress intensity, K_{Ii}, of 23.73 MPa√m. With the addition of stiffeners, the stress at the crack tip was diminished because of load transfer from the panel to the stiffener. This in turn caused a decrease in the initial K_I. This reduction in stress intensity resulted in slower crack propagation. This phenomenon can be seen in Figure 34. As the crack tip approaches the stiffener, the stress it experiences will decrease because the load "pick up" of the stiffener is greater in close proximity. This will be discussed more in the next section.

4.1.2   Repaired Panel Comparison

In order to see the effect that stiffeners had on repaired aluminum panels, both configurations of repaired stiffened panels (152 mm and 102 mm spaced stiffeners) are compared to an unstiffened/repaired baseline panel. Problems were again encountered, however, with fatigue crack initiation at the first rivet row leading to premature

catastrophic failure. This occurred in both stiffened panel configurations because the patch, combined with the stiffeners, even for the case of 152 mm centered stiffeners, strengthened the repaired area to such an extent that it drove the failure into the rivet row. This can be seen in Figure 37, which compares unstiffened/repaired panel fatigue life to that of stiffened/repaired panels. The stiffened panels were performing much better than the unstiffened panel before they failed.
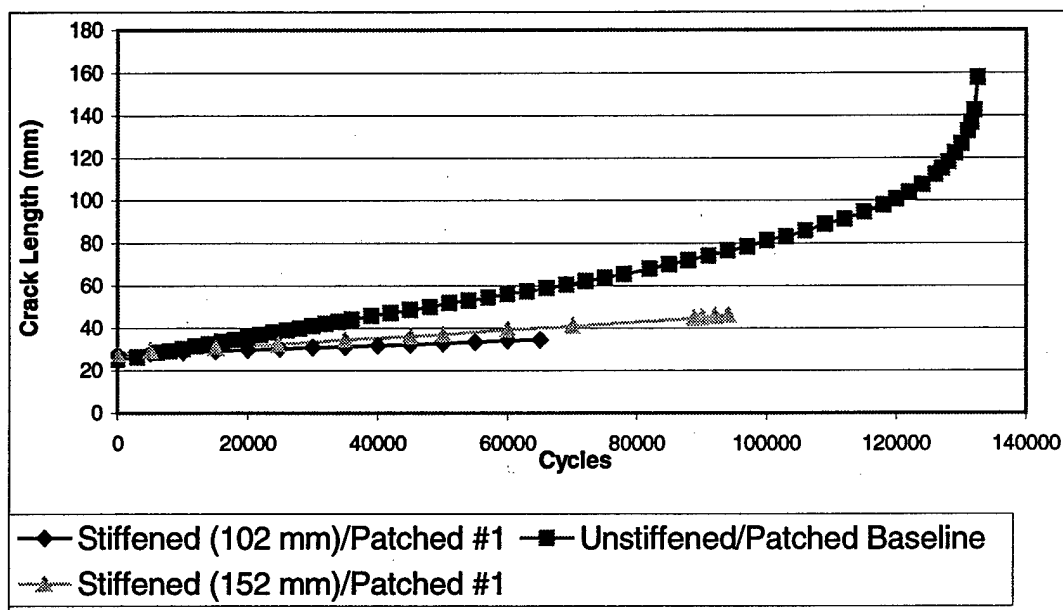
Figure 37 Repaired Fatigue Life of Unstiffened and Stiffened Panels

To remove this failure mode, along with riveting the stiffeners to the panels, they were bonded as well. This reduced the stress concentration at the rivet holes and drove the failure back into the initial crack underneath the patch. Table 15 presents the fatigue life data of each panel and Figure 38 shows the fatigue lives graphically. Fatigue life data for panels with riveted-only stiffeners (not adhesively bonded) is also included in

Figure 38. Comparing this data to the fatigue lives of panels with riveted and bonded stiffeners shows very good correlation, since the curves for unbonded and bonded stiffeners lie on top of each other. Therefore, it can be concluded that bonding the stiffeners does not change the crack growth behavior of the panel, it only ensures that no crack initiation will occur in the rivet holes. Data for the unstiffened/unrepaired baseline panel is also provided in Figure 38 to show the advantages of repaired panels over unrepaired panels.

Table 15 Comparison of Fatigue Life Between Repaired Stiffened and Unstiffened Panels

Specimen Number	Configuration	Cycles to Failure
A-2	Unstiffened/Repaired	132,558
A-9	152 mm Stiffeners/Repaired	401,006
A-5	102 mm Stiffeners/Repaired	405,010
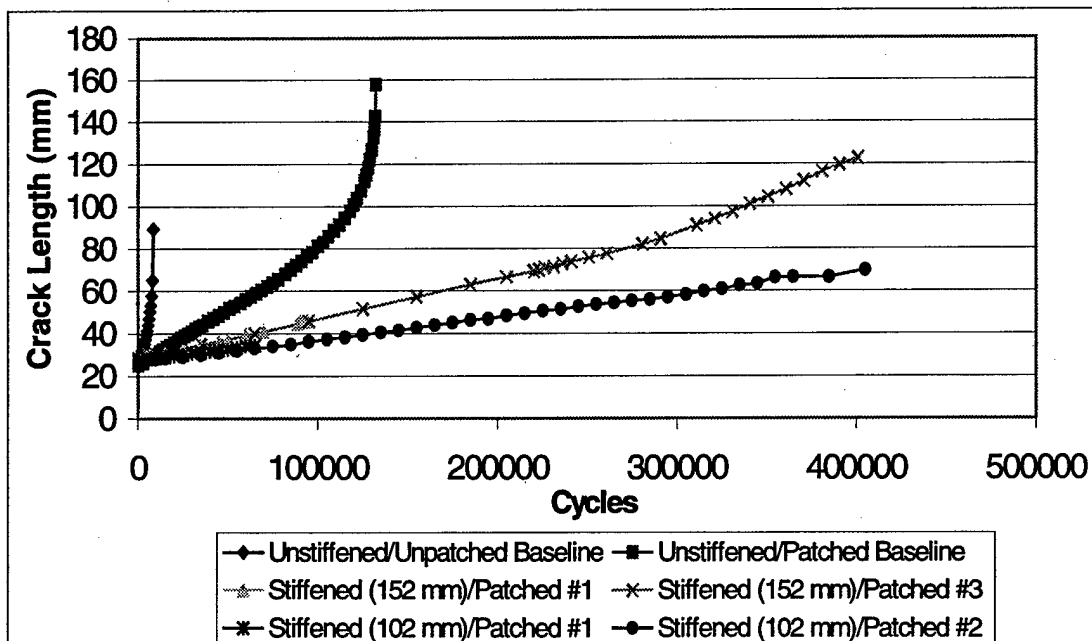
Figure 38 Repaired Fatigue Life of Bonded/Riveted Stiffened Panels vs. Unstiffened Panels

Comparing unstiffened/repaired data to stiffened/repaired data shows a large increase in fatigue life of the repaired panel when stiffeners were present. Table 16 presents a comparison of crack lengths and cycles for each of the three specimens, as well as the unstiffened/unrepaired baseline specimen. 152 mm spaced stiffeners (A-9) increased the fatigue life of the repaired panel by 2.6 times, while the 102 mm spaced stiffeners (A-5) increased the fatigue life by 4.8 times. The increases are less substantial than fatigue life increases obtained by adding stiffeners to unrepaired panels (an increase of 2.6 times compared to an increase of 5 times for 152 mm spaced stiffeners; an increase of 4.8 times compared to an increase of 8.5 times for 102 mm spaced stiffeners). This is probably due to the fact that the unstiffened/unrepaired panel (A-1) performed so poorly in comparison to repaired panels, failing after only 8,687 cycles. By applying just a bonded boron/epoxy patch alone to the panel, without stiffeners, the fatigue life is increased over 10 times. When compared to the stiffened repaired structures, A-9 had a fatigue life over 27 times longer and A-5 had a fatigue life almost 50 times longer than A-1.

Table 16 Fatigue Life Comparison of Unstiffened and Stiffened Repaired Panels

Panel Number	Configuration	Crack Length (mm/in)	Cycles to Reach Crack Length*
A-1	Baseline unstiffened/unrepaired	69/2.71	8,077
A-2	Baseline unstiffened/repaired	69/2.71	83,445
A-5	102 mm stiffeners/repaired	69/2.71	400,580
A-9	152 mm stiffeners/repaired	69/2.71	218,880

* Interpolated Results

The increased performance is again due to increased stiffness in the vicinity of the crack, but is mostly accounted for by decreased stress intensity at the crack tip due to the bonded repair. Using equation (28) as in Section 4.1.1, the stiffness of the stiffened/patched panel is calculated to be 24.1 Nm^2, which is a slight improvement over the 24.03 Nm^2 of the unrepaired/stiffened panel. The factor that accounts for most of the improvement is the decrease in stress intensity factor due to the boron/epoxy patch bridging the crack. To determine the repaired initial stress intensity, K_R, the Rose Model (11; 29; 30; 31) will be utilized. The Rose Model analysis is divided into two stages. Stage I, also known as the inclusion analogy, involves analysis of a bonded reinforcement on an uncracked plate and is performed for the sole purpose of determining the normal stress distribution, σ_0, in the plate in the area of the bonded patch. Stage II analysis deals with the fact that there is a crack in the plate which allows σ_0 to *relax* and become zero at the crack faces. The two stages of analysis, when completed, result in a value for the repaired stress intensity factor, K_R.

The major assumption in Stage I Rose model analysis is that the patch and the plate form a perfect rigid bond which allows no movement between the patch and the plate. The plate and patch are viewed as an *equivalent inclusion* (Figure 39 (17:115)) of higher stiffness than the surrounding plate. To determine the normal stress distribution, σ_0, in the reinforced plate, three calculations must be performed (11):

1. Calculation of the elastic constants of the equivalent inclusion.

2. Calculation of the stress in the equivalent inclusion.

3. Calculation of the load sharing between the plate and the bonded patch.
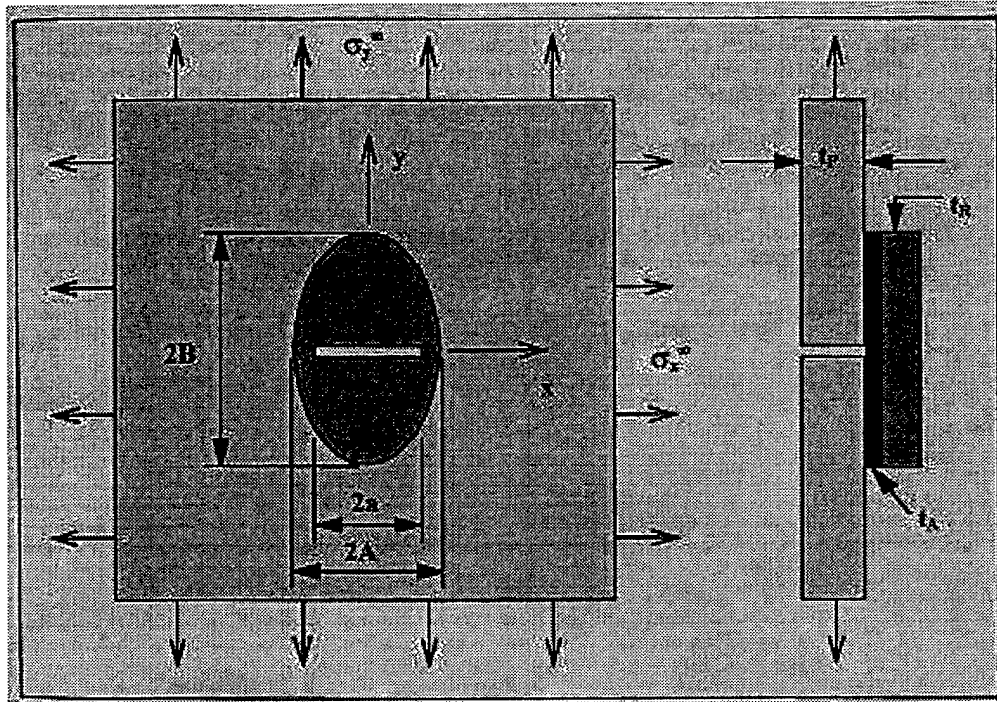
Figure 39 Equivalent Inclusion

To make the analysis more simple, Rose's underlying assumption is that the patch and the plate have the same Poisson ratio. This results in an equivalent inclusion stiffness of $E_p t_p + E_R t_R$. Load carried across y = 0 within the inclusion, |x| < A, is a force per unit length, F, defined below (where 2A = patch width; 2B = patch length):

$$F = \sigma_y^\infty t_p \left\{ 1 + \frac{S}{D} \left[1 + 2(1+S)\frac{B}{A}\left(1 - v\frac{\sigma_x^\infty}{\sigma_y^\infty}\right) + (1 + S - vS)\left(\frac{\sigma_x^\infty}{\sigma_y^\infty} - v\right) \right] \right\} \qquad (30)$$

$$D = 3(1+S)^2 + 2(1+S)\left(\frac{B}{A} + \frac{A}{B} + vS\right) + 1 - v^2 S^2 \qquad (31)$$

$$S = \frac{E_R t_R}{E_P t_P} \qquad (32)$$

80

where

F = Force per unit length
ν = Poisson's Ratio

The normal stress in the plate caused by the shared load between the plate and

reinforcement is given by:

$$\sigma_0 = \sigma_y^P \left(|x| \langle A, y = 0 \right) = \frac{F}{t_P(1+S)} \qquad (33)$$

Once the stress at the crack, σ_0, is known, Stage II Rose Model analysis can be

performed, which assumes a crack in an infinite plate. The stress intensity factor for a

center cracked plate is:

$$K_0 = \sigma_0 [\pi a]^{\frac{1}{2}} \qquad (34)$$

This stress intensity factor is one upper bound of the repaired stress intensity factor, K_R.

"However, in comparison to an unbounded K_0 with crack length for a nominal center

cracked plate, K_R does not exceed a limiting value of K_∞ as shown in Figure 40 (11; 15).

Rose shows that $K_\infty = K_0$ at a characteristic crack length, Λ (11)." The equation for Λ is

shown below:

$$\Lambda = \frac{1}{\pi} \left[E_P t_P \left(\frac{t_A}{G_A} \right) \beta \right] = \frac{1}{\pi} \left(1 + \frac{1}{S} \right) \beta^{-1} \qquad (35)$$

where

$$1/\beta = \text{load transfer length}$$
$$t_A = \text{adhesive layer thickness}$$
$$G_A = \text{adhesive shear modulus}$$
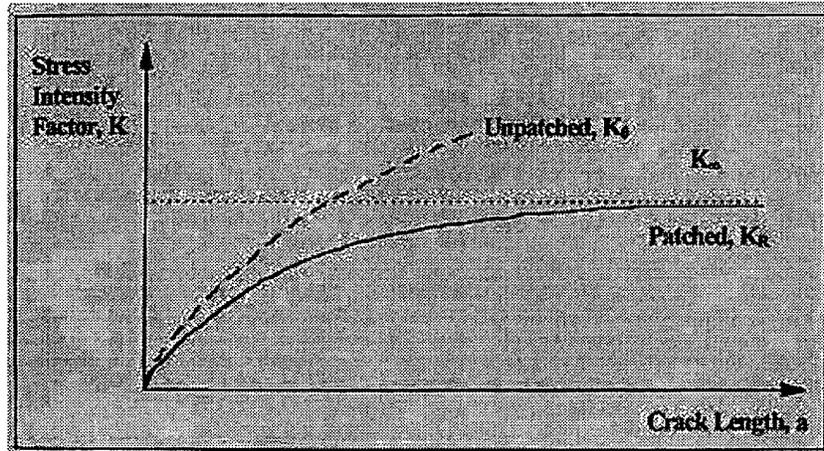
Figure 40 Reduction in Stress Intensity Factor with Repair

Therefore $K_\infty = \sigma_0 [\pi\Lambda]^{\frac{1}{2}}$ is also an upper bound for K_R. "K_0 and K_∞ are the first terms in the asymptotic expansions of K_R in the limits $a/\Lambda \ll 1$ and $a/\Lambda \gg 1$ (11)." Interpolating between the asymptotes, K_R is defined as:

$$K_R = \sigma_0 \left[\frac{\pi a \Lambda}{a + \Lambda} \right]^{\frac{1}{2}} \tag{36}$$

Using the above equations for the case of panel A-3 results in a repaired stress intensity factor, K_R, of 11.5 MPa√m as opposed to an unrepaired stress intensity factor for the same panel of 23.86 MPa√m. In other words, the bonded repair reduced the stress intensity at the crack tips by 51.8%.

82

4.2   Effect of Disbond Location on Bonded Repair Fatigue Life

As has already been noted, the unstiffened/repaired panel (A-2) had a fatigue life over 10 times longer than the baseline unstiffened/unrepaired panel. Adding stiffeners to the repair extended the fatigue life even more, increasing the life over 27 times for the 152 mm (6") centered stiffeners and almost 50 times for the 102 mm (4") centered stiffeners. This data is shown in Table 16. This section will address the effect that disbond location had on the repaired fatigue life of stiffened panels by comparing the fatigue lives of three different disbond configurations—crack tip disbond (CTD), full-width disbond (FWD), and end disbond (ED)—with the fatigue lives of perfectly bonded repaired panels with the same testing configurations. The exact dimensions and configuration for each disbond type is shown in Figure 2 of Chapter 1.

4.2.1   Effect of Crack Tip Disbond (CTD) on Fatigue Life of the Repair

Four fatigue panels with CTD's were tested—two with 152 mm spaced stiffeners (panels A-11 and A-12) and two with 102 mm spaced stiffeners (panels A-8 and A-10). Disbonds accounted for approximately 8% of the bondline area of the patch and are shown schematically in Figure 41. The fatigue life data of the disbonded panels, along with the fatigue life data of different baseline panels used for comparison, are shown in Table 17. The data is broken up into two sections—cycles to reach 45 mm of crack length and cycles to reach 69 mm of crack length—for easier comparison. Initial crack propagation occurred under the completely bonded section of the patch, which makes up the first 45 mm of total crack length. The final 24 mm (12 mm for each crack tip) of crack tip propagation underneath the patch occurred in a completely disbonded region of

83

the patch. By comparing the data separately, the effect of the disbond can be better understood. The results are shown schematically in Figure 42, Figure 46, and Figure 51. Figure 42 shows the effect of the CTD on panels with 152 mm spaced stiffeners and how the fatigue life of those panels compared to the baseline data. Figure 46 shows the same for panels with 102 mm spaced stiffeners. Figure 51 shows a direct comparison between CTD effects when dealing with 152 mm spaced stiffeners and 102 mm spaced stiffeners.
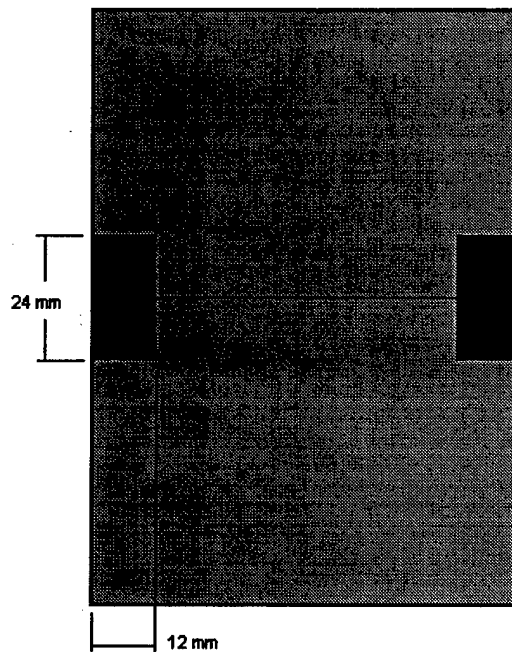
Figure 41 Schematic of CTD

Table 17 Effect of CTD on Fatigue Life

Specimen	Configuration	Crack Length (mm/inch)	Cycles*	Crack Length (mm/inch)	Additional Cycles*
A-1	Baseline (unstiff/unrep.)	45/1.77	5,656	69/2.71	2,421
A-2	Baseline (unstiff/CB patch)	45/1.77	37,695	69/2.71	45,750
A-3	152 mm stiff/unrep.	45/1.77	27,057	69/2.71	15,181
A-18	102 mm stiff/unrep.	45/1.77	41,608	69/2.71	30,056
A-5	102 mm stiff/CB	45/1.77	174,212	69/2.71	226,368
A-9	152 mm stiff/CB	45/1.77	90,418	69/2.71	128,462
A-8	102 mm stiff/CTD	45/1.77	273,400	69/2.71	222,875**
A-10	102 mm stiff/CTD	45/1.77	141,411	69/2.71	140,330
A-11	152 mm stiff/CTD	45/1.77	120,630	69/2.71	102,494
A-12	152 mm stiff/CTD	45/1.77	124,951	69/2.71	96,004

* Interpolated results
** Panel failed early due to fatigue crack initiation in the first rivet row

4.2.1.1 CTD Effects in the 152 mm Spaced Stiffener Panel

The overall fatigue life of the repaired panels with 152 mm spaced stiffeners with CTD's decreased slightly when compared to the perfectly bonded case, as seen in Figure 42. By comparing the data within the two regions defined in Table 17 (2a = 45 mm and 2a = 69 mm), the panels with CTD's present actually initially performed slightly better than the completely bonded baseline panel—about 10%. Once the crack tips reached the disbonds, crack propagation increased slightly. Within the disbonded region spanning a 45 mm total crack length and a 69 mm total crack length (the width of the patch), the CTD panels had 29% faster average crack propagation rate than the completely bonded panels. While the completely bonded panel maintained linear crack growth underneath the patch (Figure 42), the CTD panels show a slight curve upward, indicating that the disbond does adversely affect crack growth rates. This data supports

Baker's (32) observation that disbonds in front of the crack tip have little or no effect on crack tip propagation. It is only when disbonds appear in the crack tip wake that they make a difference. From the edge of the patch out to the stiffeners, the CTD panels' average crack growth rate was approximately 18% faster than that of the completely bonded repaired patch and the overall fatigue life of the repaired panels containing CTD's was approximately 7% shorter. Table 18 shows the crack growth per cycle (da/dN) for each of the three panels broken out by region and Figure 43 shows the same data in graphical form. The figure shows that the CTD panels had a consistently higher crack propagation rate than the CB panel. All three panel's crack propagation rates decreased as the crack tips approached the stiffeners. Figure 43 also displays the crack propagation rate of the baseline unrepaired panel with 152 mm spaced stiffeners for comparison. The benefits of bonded composite repairs can easily be seen in the reduced crack propagation rates.
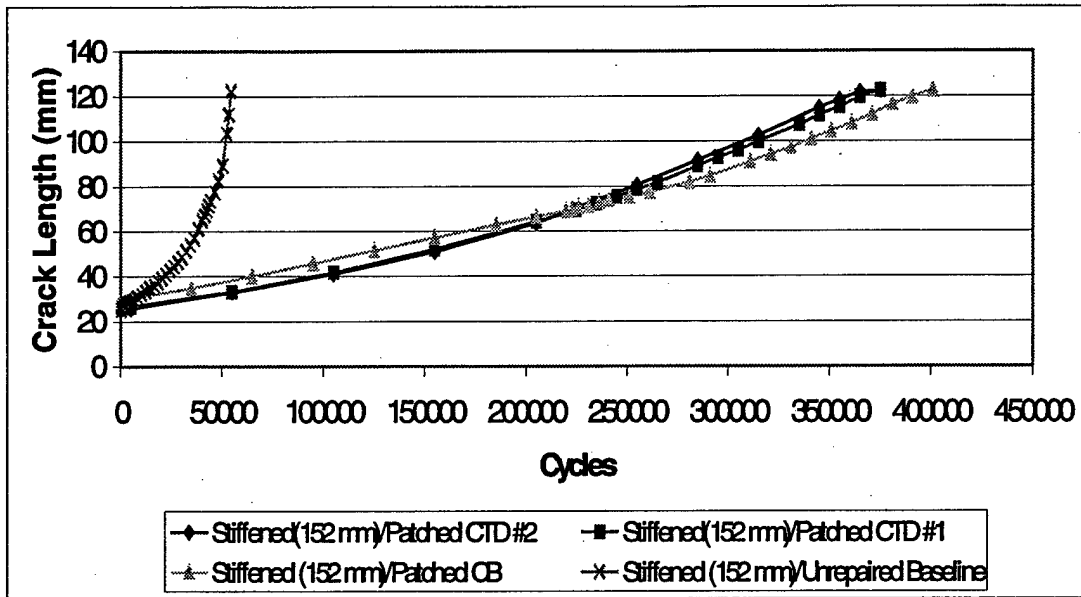
Figure 42 CTD Effects on Fatigue Life of 152 mm Centered Stiffened Panels

Table 18 Average Crack Growth per Cycle for 152 mm Spaced Stiffener Panel with CTD

Specimen Number	Configuration	da/dN Section I (mm/cycle)*	da/dN Section II (mm/cycle)*	da/dN Sections III (mm/cycle)*
A-9	152 mm stiff/CB	0.000089	0.000094	0.000148
A-11	152 mm stiff/CTD	0.000080	0.000117	0.000176
A-12	152 mm stiff/CTD	0.000079	0.000125	0.000174

Section 1 – crack growth between end of precrack and start of disbond
Section 2 – crack growth within disbond
Section 3 – crack growth between edge of patch and beginning of stiffener
* Interpolated data
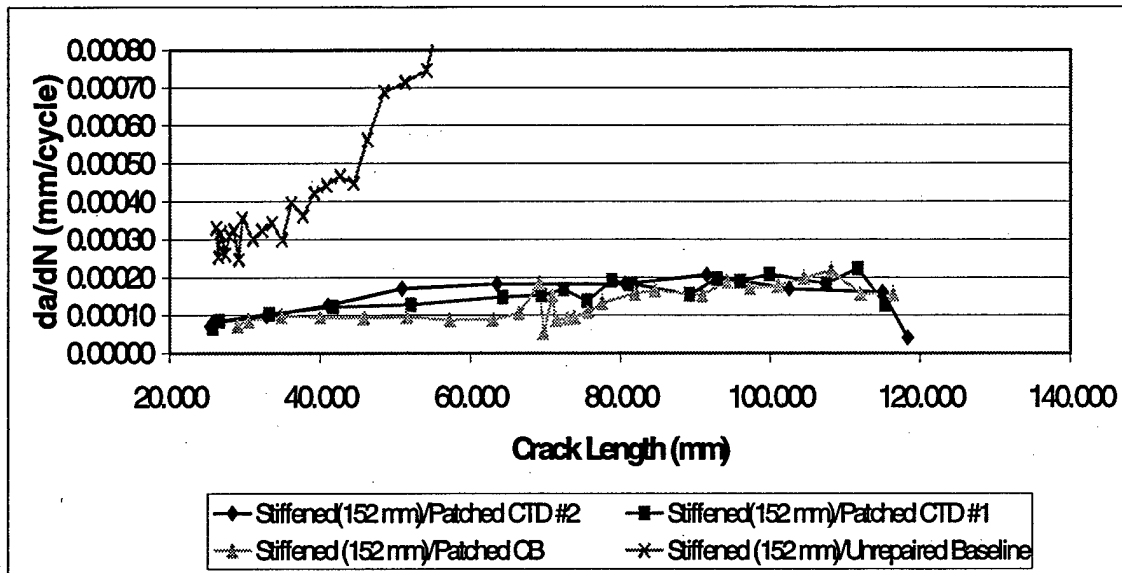
Figure 43 Crack Growth per Cycle for 152 mm Spaced Stiffener Panel

The testing showed excellent correlation, since both panels with CTD's present,

panels A-11 and A-12, had fatigue life curves that fell right on top of each other. While

there was a minor reduction in fatigue life with the disbond present, the repaired structure

still performed considerably better than the unrepaired structure. Panels A-11 and A-12,

even with disbonds present, had a fatigue life on average of 688% longer than the

unrepaired stiffened panel. This result supports the idea that bonded repairs are very

durable. Also, by comparing infrared (IR) pictures of the repair (Figure 44) taken at

different cycle counts during testing with a C-SCAN of the repair (Figure 45) performed

after failure, no substantial disbond growth occurred over the life of the repair. The

figures, especially the end-of-life C-SCAN, do show that there was minimal disbonding

around the crack, but the initial intentional disbonds did not grow larger. The three IR

pictures were taken at 5,009, 205,007, and 345,006 cycles and corresponded to 26.581

mm (1.046 inches), 64.364 mm (2.534 inches), and 111.646 mm (4.396 inches). The C-

SCAN was taken after 375,010 cycles, corresponding to a crack length of 122.339 mm

(4.816 inches).
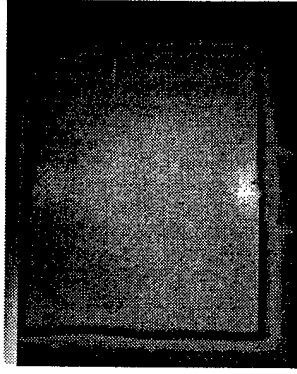
5009 Cycles
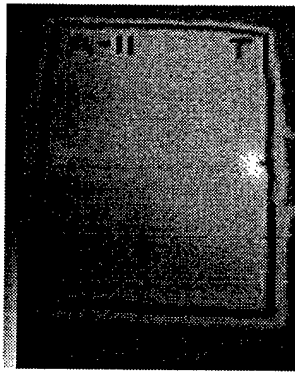
205,007 Cycles
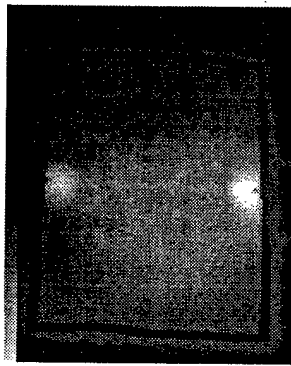
345,006 Cycles

Figure 44 Infrared Pictures of Panel A-11 with CTD
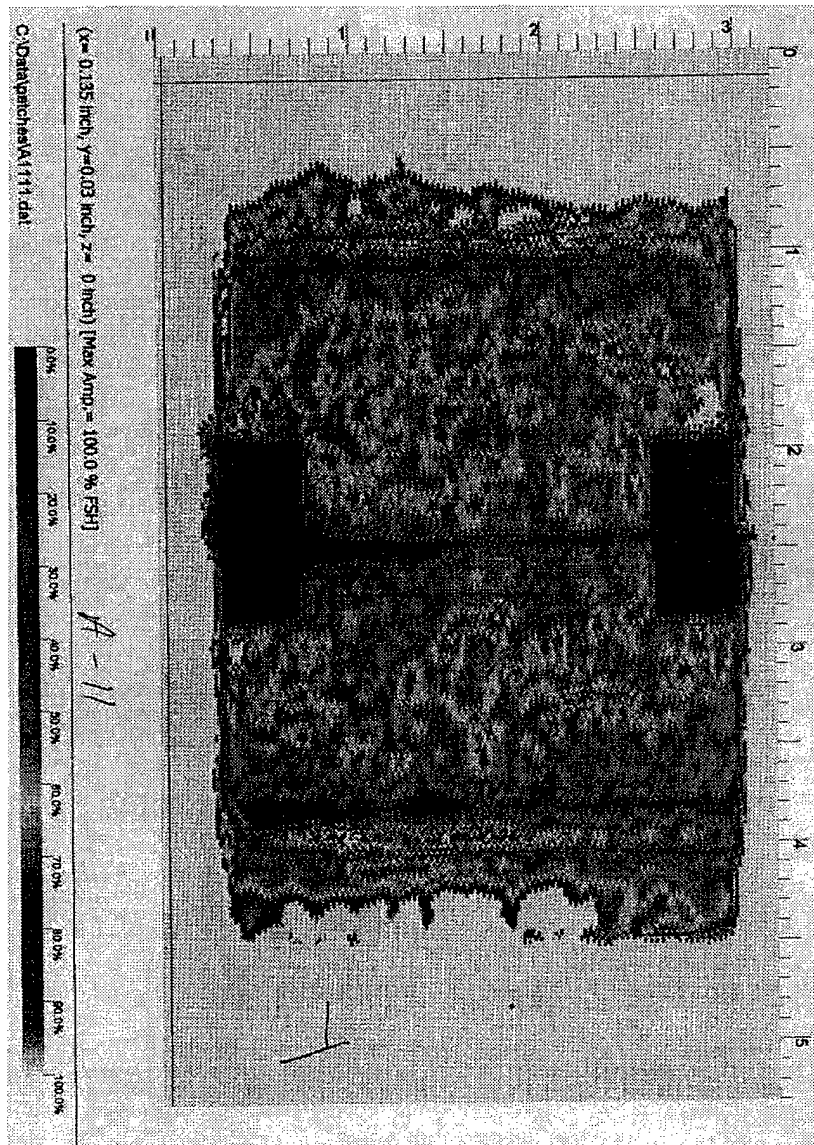
Figure 45 End-of-Life C-Scan of Panel A-11 with CTD

4.2.1.2 CTD Effects in the 102 mm Spaced Stiffener Panel

This testing showed the same trends as that of A-11 and A-12 for one of the panels, A-10, but showed an entirely different result for the other panel, A-8. The fatigue life of the repaired 102 mm spaced stiffener panel, A-10, decreased by approximately 16% when compared to the perfectly bonded case. However, the fatigue life of panel A-8 showed an increase of almost 43% when compared to the perfectly bonded panel. The fatigue life curves of each panel, along with the perfectly bonded case and unrepaired case, are shown in Figure 46.
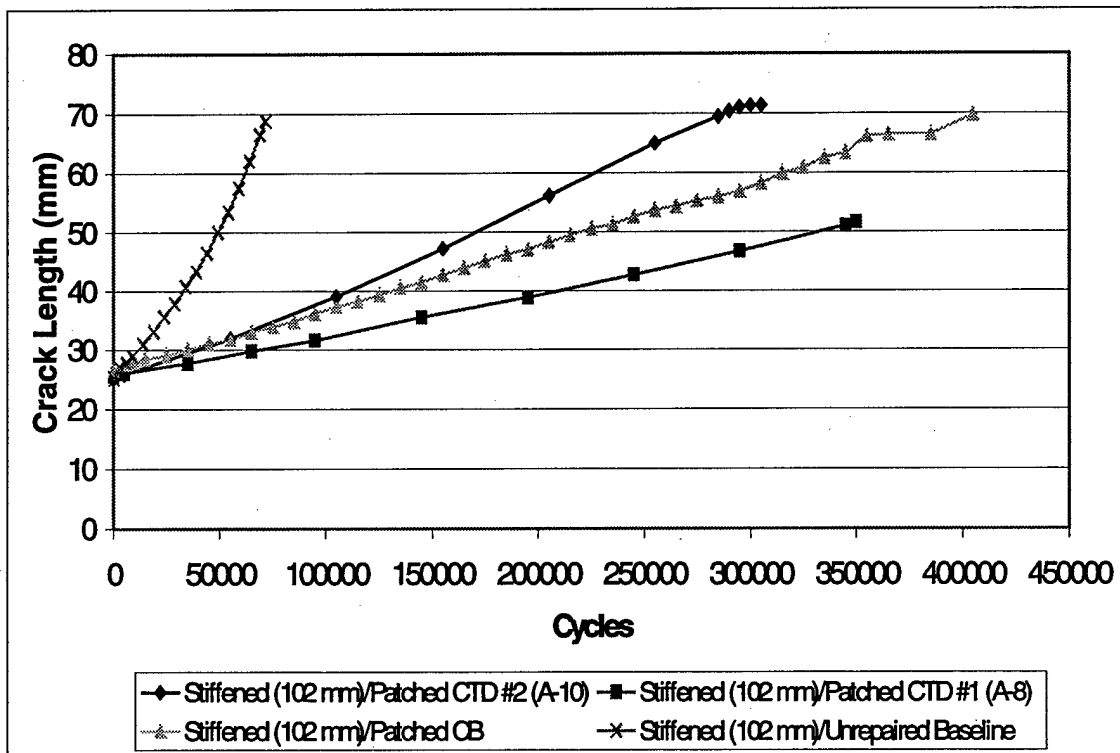
Figure 46 Effects of CTD on 102 mm Spaced Stiffened Panels

The only difference between the two CTD panels was in the way the patches were bonded on. In panel A-10, like in the preceding panels, the patch was first bonded on, followed by a separate cure cycle for the stiffeners. In order to save time, since the cure cycle was the same, the patch and stiffeners for panel A-8 were bonded at the same time in a vacuum bag. Because of the close proximity of the stiffeners to the patch, the adhesive pooled together and hardened, causing an increase in stiffness, as seen in Figure 47. This is the reason for the increased fatigue life of panel A-8. This argument is strengthened by the fact that the same experiment was done in the case of panels A-11 and A-12. A-11 was manufactured with two cure steps, while A-12's patch and stiffeners were cured at the same time in a vacuum bag. Because the stiffeners were positioned further from the patch, the adhesive did not pool together and there was no added stiffness in the panel. As a result, the two panels, even though they were manufactured using slightly different processes, performed almost identically, as seen in Figure 42. Therefore, performing the repair in two steps, as opposed to one step, did not change the patch properties or the material properties of the repair system in any way. Performing a one step cure simply provided a means for increased stiffness of the system in the case of the 102 mm spaced stiffeners due to the mixing of adhesive between patch and stiffener. Panel A-10 provided realistic data for the case of panels with 102 mm spaced stiffeners, while panel A-8 provided skewed data.

A-17 **A-8**
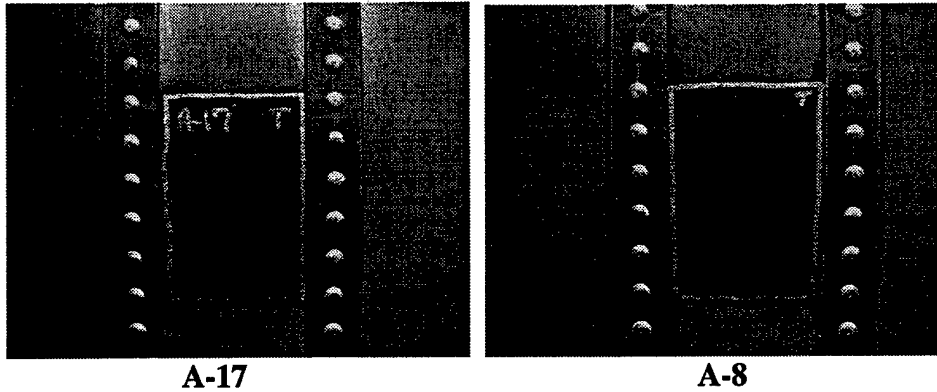
Figure 47 "Pooling" of Adhesive in Panel A-8

The overall fatigue life of panel A-10 decreased slightly when compared to the perfectly bonded case, as seen in Figure 46. By comparing the data within the two regions defined in Table 17 (2a = 45 mm and 2a = 69 mm), a better picture of the result of the disbond can be seen. Table 19 shows the crack growth per cycle (da/dN) for the two panels broken out by crack length and Figure 48 shows the same data in graphical form. From the end of the precrack out to the beginning of the disbond, the CTD panel had a 32% faster crack propagation rate than the completely bonded panel. Within the area of the disbond, the CTD panel had a 62% faster crack propagation rate than the completely bonded panel. The difference in crack propagation rates between the two cases is almost twice as much within the disbond, further supporting Baker's (32) observations. Figure 48 shows that panel A-10 had a consistently higher crack propagation rate than the completely bonded case. Crack propagation rate versus crack length is also provided for the unrepaired baseline panel with 102 mm spaced stiffeners for comparison in Figure 48. The oscillation in the curve is due to the extremely small

94

scale associated with da/dN and the fact that all crack length measurements were taken by

human eye through a microscope.

Table 19 Average Crack Growth per Cycle for 102 mm Spaced Stiffener Panel with CTD

Specimen Number	Configuration	da/dN Section I (mm/cycle)*	da/dN Section II (mm/cycle)*
A-5	102 mm stiff/CB	0.000053	0.000053
A-10	102 mm stiff/CTD	0.000070	0.000086

Section 1 – crack growth between end of precrack and start of disbond
Section 2 – crack growth within the disbond area
* Interpolated data
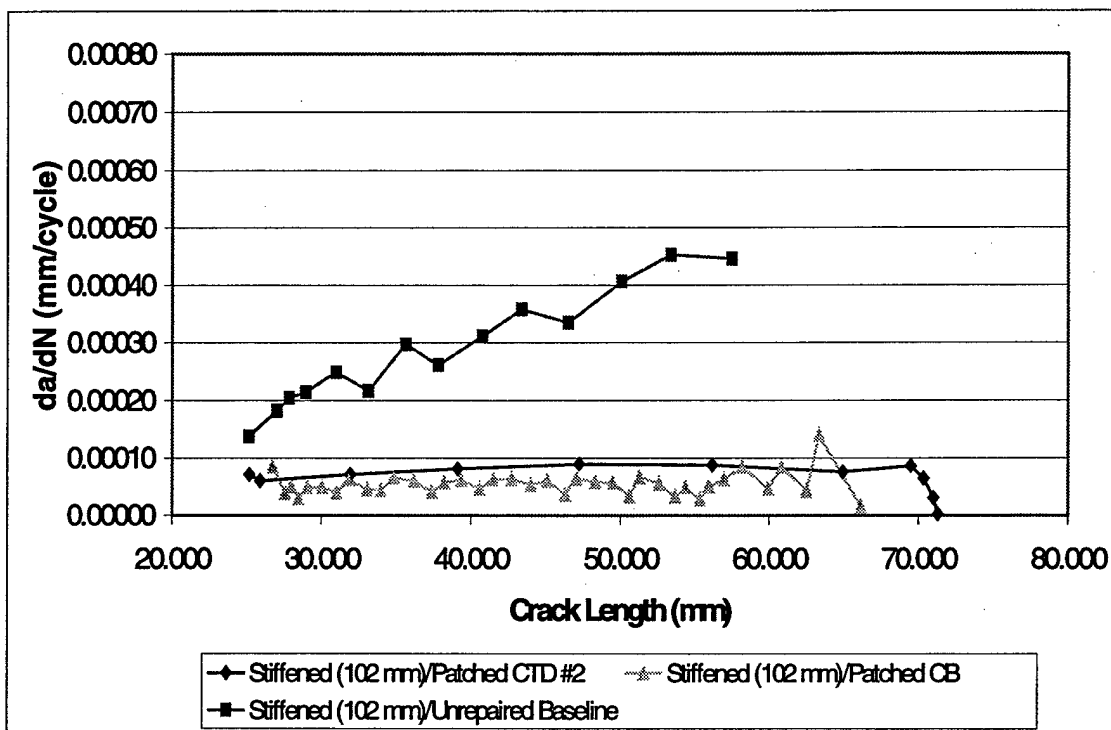
Figure 48 Crack Growth per Cycle for 102 mm Spaced Stiffener Panel

While there was a decrease in fatigue life with the CTD as compared with the

perfectly bonded patch, panel A-10 still had a life over 400% longer than the

95

unrepaired/102 mm stiffened panel. IR pictures of the repair taken during testing, when compared to a C-scan of the repair taken after testing was completed, show no substantial disbond growth during the life of the patch. The IR pictures of panel A-10 are shown in Figure 49 and the C-SCAN is shown in Figure 50. The three IR pictures were taken at 5,007, 105,010, and 290,006 cycles and corresponded to 25.883 mm (1.019 inches), 39.091 mm (1.539 inches), and 70.358 mm (2.77 inches). The C-SCAN was taken after 305,007 cycles, corresponding to a crack length of 71.336 mm (2.809 inches).

5007 Cycles

105,010 Cycles

290,006 Cycles
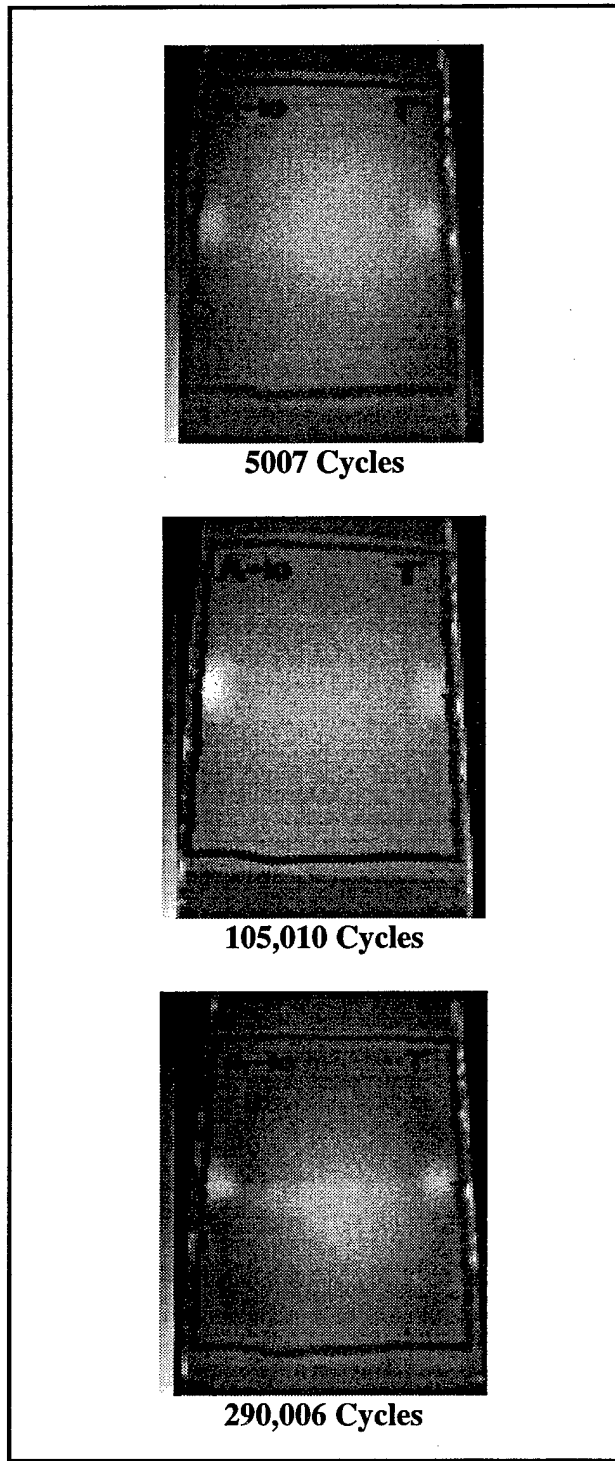
Figure 49 Infrared Pictures of Panel A-10 with CTD
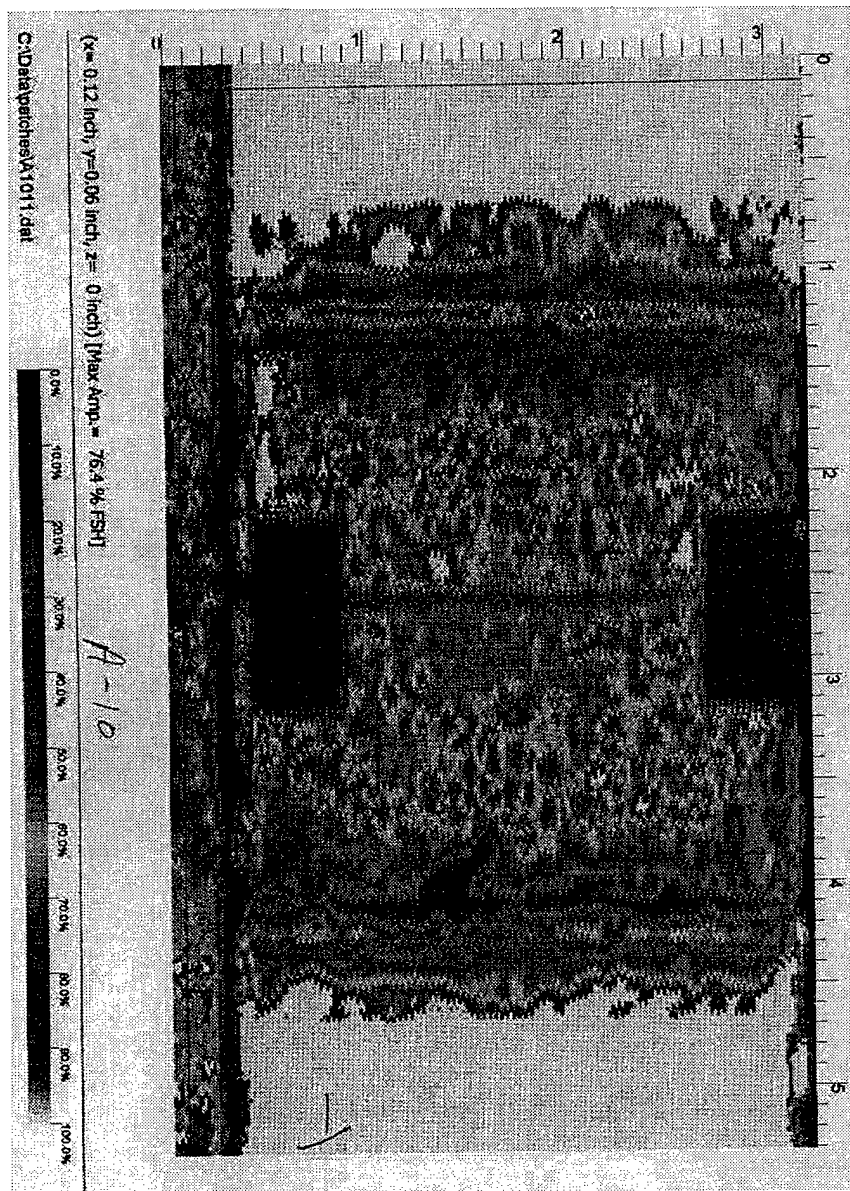
Figure 50 End-Of-Life C-Scan of Panel A-10 with CTD

98

4.2.1.3 CTD Effects in panels with 152 mm Spaced Stiffeners versus CTD Effects in panels with 102 mm Spaced Stiffener Panels

Both configurations of stiffened panels, the 152 mm spaced stiffeners and the 102 mm spaced stiffeners, behaved approximately the same with the CTD's present. Both showed slight decreases in fatigue life when compared to the perfectly bonded panels utilizing the same stiffener configuration. Figure 51 provides a direct comparison between fatigue life trends of the two different stiffener configurations when CTD's were present. From the figure, it appears that the CTD affects the panel with 102 mm spaced stiffeners more severely. Table 20 lists the effect the CTD had on the two different panel stiffener configurations. It shows the percentage of crack propagation rate increase by section when compared to the baseline panels. Looking at the data, it does appear that the disbonds affected the panel with 102 mm spaced stiffeners more severely. While this may be true to a certain extent, the fact that the crack length vs. cycles curve (a vs. N) for the 102 mm spaced stiffeners is not as severely sloped as that of the 152 mm spaced stiffeners makes any crack propagation increases appear worse for this case. For instance, when dealing with crack length versus cycles in the case of 102 mm spaced stiffeners, it took the completely bonded baseline panel approximately 11,188 cycles (interpolated) to grow from a total crack length of 50 mm to one of 51 mm. It took the baseline panel with 152 mm spaced stiffeners only 5, 249 cycles to grow the same distance, or less than half the time. This phenomenon "harshens" the affect of the CTD on panels with 102 mm spaced stiffeners, when in fact the effect on both types of stiffener configurations is very comparable.

99
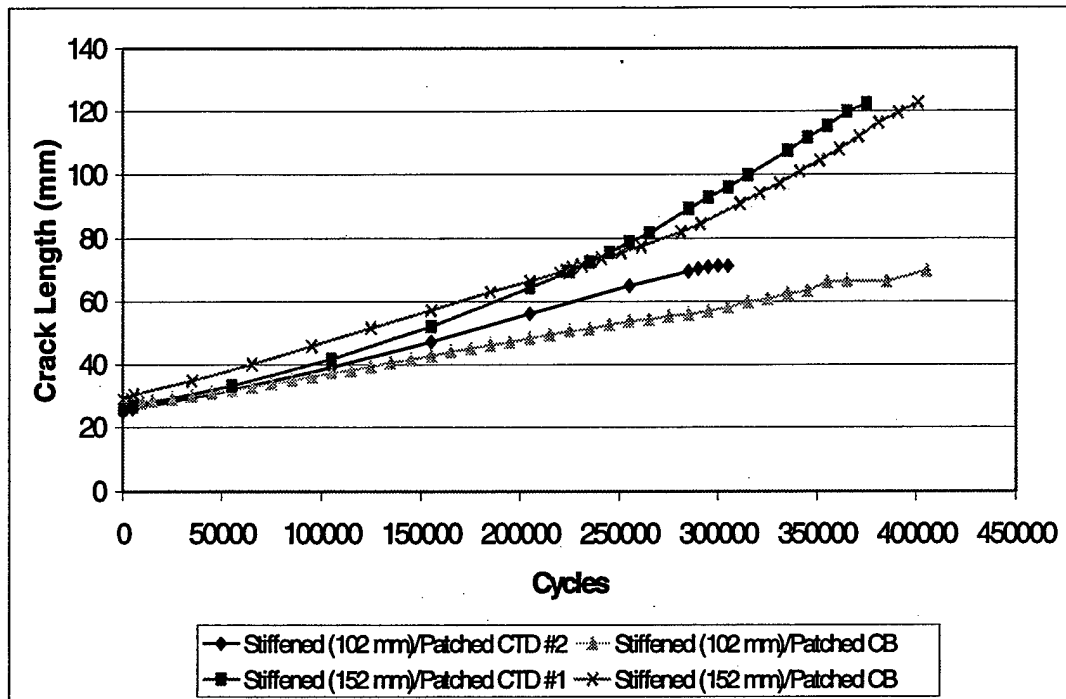
Figure 51 Fatigue Life Trend of Stiffened Panels with CTD

Table 20 Comparison of CTD Effect Between Stiffener Configurations

Specimen Number	Configuration	Section I Increase in da/dN vs. Baseline (%)	Section II Increase in da/dN vs. Baseline (%)	Section III Increase in da/dN vs. Baseline (%)
A-11	152 mm stiff/CTD	-10.1% (slower)	24.5%	18.9%
A-12	152 mm stiff/CTD	-11.2% (slower)	33.0%	17.6%
A-10	102 mm stiff/CTD	32.1%	62.3%	NA

Section 1 – crack growth between end of precrack and start of disbond
Section 2 – crack growth within disbond
Section 3 – crack growth between edge of patch and beginning of stiffener

The data from both stiffener configurations supports Baker's (32) previous

findings that disbonds in the wake of crack tips have more of an effect on crack tip

propagation than disbonds in front of the tip. Also, Figure 44, Figure 45, Figure 49, and

Figure 50 support Hart-Smith's (33) observations that adhesive bondlines are relatively

damage tolerant and pre-existing intentional disbonds will not grow.

4.2.2 Effect of Full-Width Disbond (FWD) on Fatigue Life of the Repair

Three fatigue panels with FWD's were tested—one with 152 mm spaced

stiffeners (panel A-13) and two with 102 mm spaced stiffeners (panels A-14 and A-17).

Since good correlation was already found between fatigue tests with the same

configuration, such as panels A-11 and A-12 with CTD's (Figure 42), two specimens

were not tested for every test case. This was done to preserve the number of specimens

used so that more disbond configurations could be tested. The full-width disbond took up

approximately 12% of the bondline area and is shown in Figure 52. The fatigue life data

of the FWD specimens, along with the fatigue life data of different baseline panels used

for comparison, is shown in Table 21. The data is broken up into two sections—crack

growth between the end of the precrack and the edge of the patch and crack growth

between the edge of the patch and the edge of the stiffener. Initial crack propagation was

under a completely disbonded patch, which had a width of 69 mm. Once the crack

extended beyond the width of the patch, the crack propagation rate changed as the crack

tips approached the stiffener edges, which were approximately 122.3 mm apart in the

case of 152 mm spaced stiffeners. The data is separated to make comparisons of the data

involving panels with 152 mm spaced stiffeners easier. Panels with 102 mm spaced

stiffeners do not have substantial crack growth between the edge of the patch and the

stiffener, since the stiffeners are located in close proximity to the patch edges. By

comparing the data separately, the effect of the disbond can be better understood.

Results of the testing are shown schematically in Figure 53, Figure 57, and Figure

62. Figure 53 shows the effect of the FWD on panels with 152 mm spaced stiffeners and

how the fatigue life of those panels compared to the baseline data. Figure 57 shows the

same for panels with 102 mm spaced stiffeners. Figure 62 shows a direct comparison

between FWD effects when dealing with 152 mm spaced stiffeners and 102 mm spaced

stiffeners.
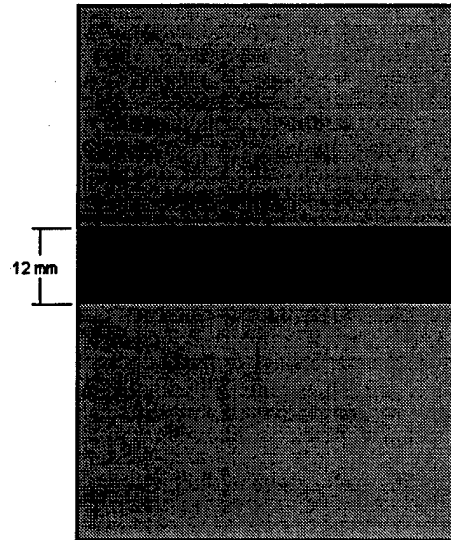
Figure 52 Schematic of FWD

Table 21 Effect of FWD on Fatigue Life

Spec. #	Configuration	Crack Length (mm/inch)	Cycles*	Crack Length (mm/inch)	Additional Cycles*
A-1	Baseline (unstiff/unrep.)	69/2.71	8,077	NA	NA
A-2	Baseline (unstiff/CB patch)	69/2.71	83,445	122.3/4.815	45,580
A-3	152 mm stiff/unrep.	69/2.71	42,238	122.3/4.815	12,293
A-18	102 mm stiff/unrep.	69/2.71	71,664	NA	NA
A-5	102 mm stiff/CB patch	69/2.71	400,580	NA	NA
A-9	152 mm stiff/CB patch	69/2.71	218,880	122.3/4.815	180,979
A-14	102 mm stiff/FWD	69/2.71	322,100	NA	NA
A-17	102 mm stiff/FWD	69/2.71	200,456	NA	NA
A-13	152 mm stiff/FWD	69/2.71	140,908	122.3/4.815	135,870

*Interpolated results
NA – panel never reached the specified crack length

4.2.2.1 FWD Effects in the 152 mm Spaced Stiffener Panel

The overall fatigue life of the repaired panel with 152 mm spaced stiffeners and an intentional FWD defect decreased substantially when compared to the perfectly bonded case, as seen in Figure 53. By comparing the data within the two regions of the panel defined in Table 21 (2a = 69 mm and 2a = 122.3 mm), it can be seen that the FWD panel did far worse than the perfectly bonded panel *and* the CTD panels. Table 22 lists da/dN data for the set of panels with 152 mm spaced stiffeners including the completely bonded baseline repair, two CTD repairs, and the FWD repair. Looking only at the area under the patch, the FWD panel had a crack tip propagation rate over 70% faster than the baseline panel and over 56% faster than either of the CTD panels. Under the patch is where the most difference should be seen, but even outside of the patch, the FWD panel did worse than the other two repair cases, with crack growth rates 32% greater than the baseline panel and over 12% greater than the CTD panels. This data supports Dennys

103

(11) earlier observations that larger disbonds in more intimate contact with the crack will cause more adverse affects to fatigue life. Figure 54 shows the crack growth rate comparison between the perfectly bonded, CTD, and FWD panels with 152 mm spaced stiffeners. The FWD panel has the highest consistent crack propagation rate of the three disbond configurations and has a very constant da/dN with respect to crack length. The CTD panel, on the other hand, has a da/dN versus crack length curve that increases once the tips reach the disbond. Figure 54 also shows the crack propagation rate versus crack length curve for the unrepaired baseline panel with 152 mm spaced stiffeners for comparison.
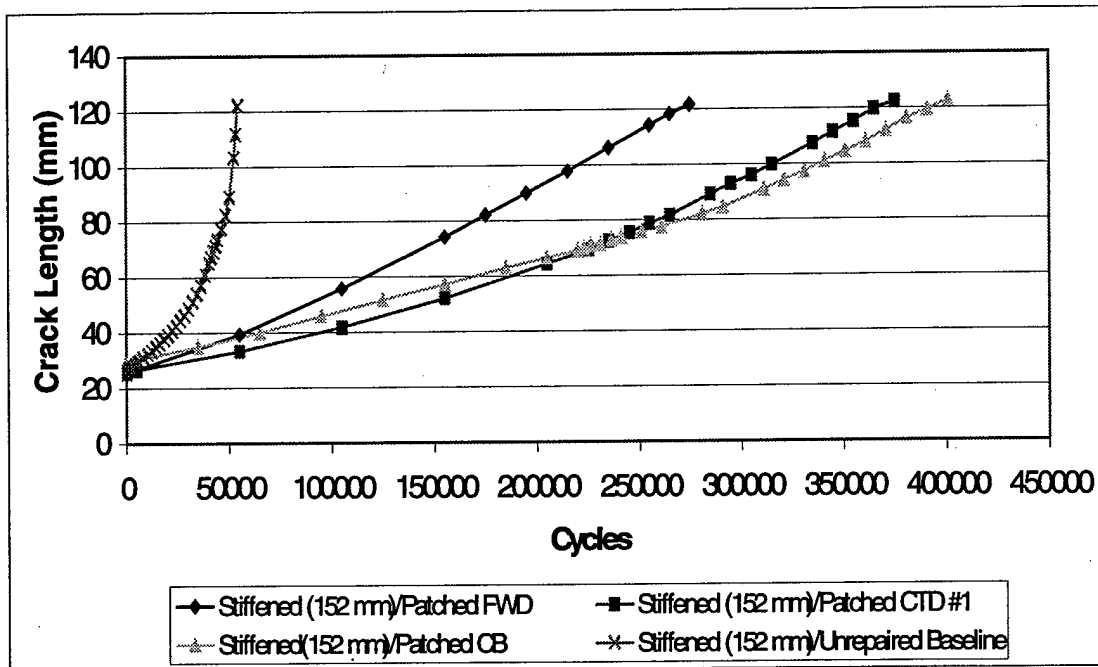
Figure 53 Effects of FWD on 152 mm Spaced Stiffened Panels

Table 22 Average Crack Growth per Cycle for 152 mm Spaced Stiffener Panels with FWD

Spec. #	Configuration	da/dN Section I (mm/cycle) *	da/dN Increase from Baseline (%)	da/dN Section II (mm/cycle) *	da/dN Increase from Baseline (%)
A-9	152 mm stiff/CB	0.000089	0.00%	0.000148	0.00%
A-11	152 mm stiff/CTD	0.000080	10.1% slower	0.000176	18.9%
A-12	152 mm stiff/CTD	0.000079	11.2% slower	0.000174	17.6%
A-13	152 mm stiff/FWD	0.000155	74.2%	0.000196	32.4%

Section 1 – crack growth between end of precrack and start of CTD (2a = 45 mm)
Section 2 – crack growth within CTD (45 mm < 2a < 69 mm)
* Interpolated data
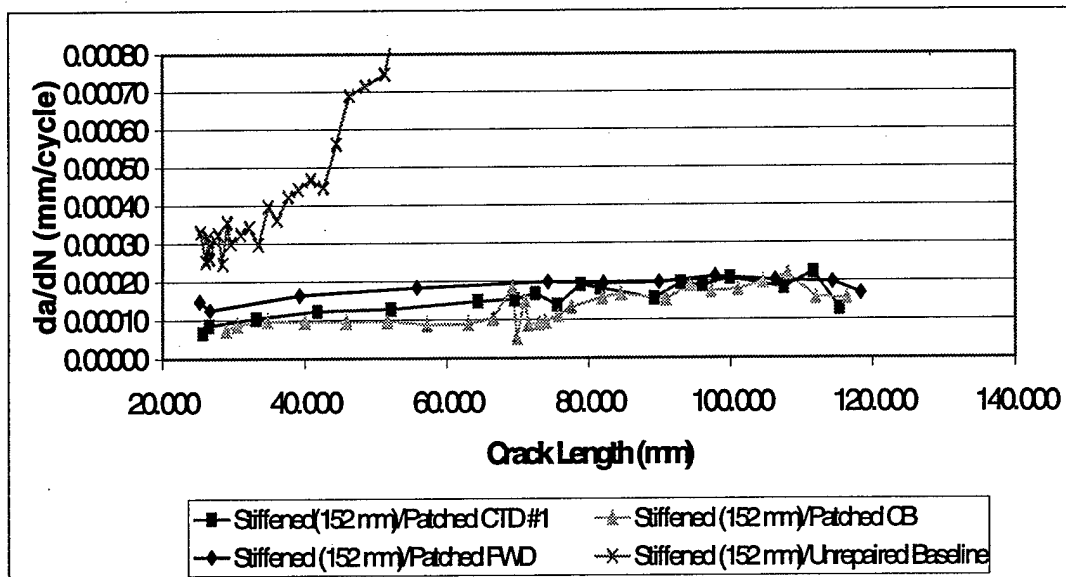
Figure 54 Comparison of Crack Growth Rates for 152 mm Spaced Stiffener Panels

While the FWD panel, A-13, experienced a significant reduction in fatigue life

compared to the CB panel and the CTD panels, it still had a significantly longer fatigue

life than the unrepaired panel with the same stiffener configuration. A-13, the worst

disbond configuration included in this study, required 333.6% more cycles to grow a

crack to 69 mm (the width of the repair patch) than the unrepaired baseline panel. Also,

105

by comparing IR pictures of the repair (Figure 55) taken at different cycle counts during testing with a C-SCAN of the repair (Figure 56) performed after failure, no substantial disbond growth occurred over the life of the repair. The two IR pictures were taken at 5,007 and 155,007 cycles and corresponded to 26.746 mm (1.053 inches) and 74.193 mm (2.921 inches). The C-SCAN was taken after 275,007 cycles and corresponded to a crack length of 121.704 mm (4.791 inches).
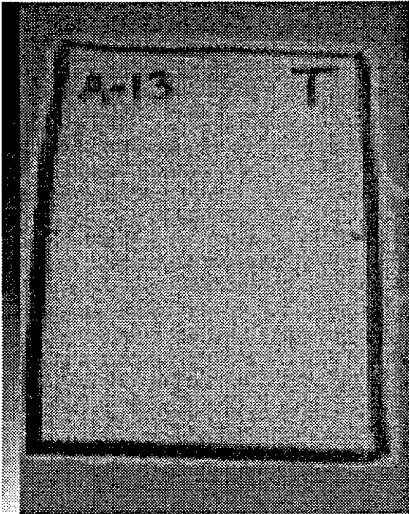
5,007 cycles
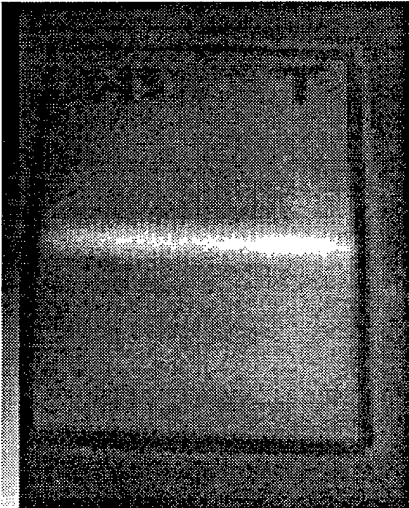
155,007 cycles

Figure 55 Infrared Pictures of Panel A-13 with FWD

107
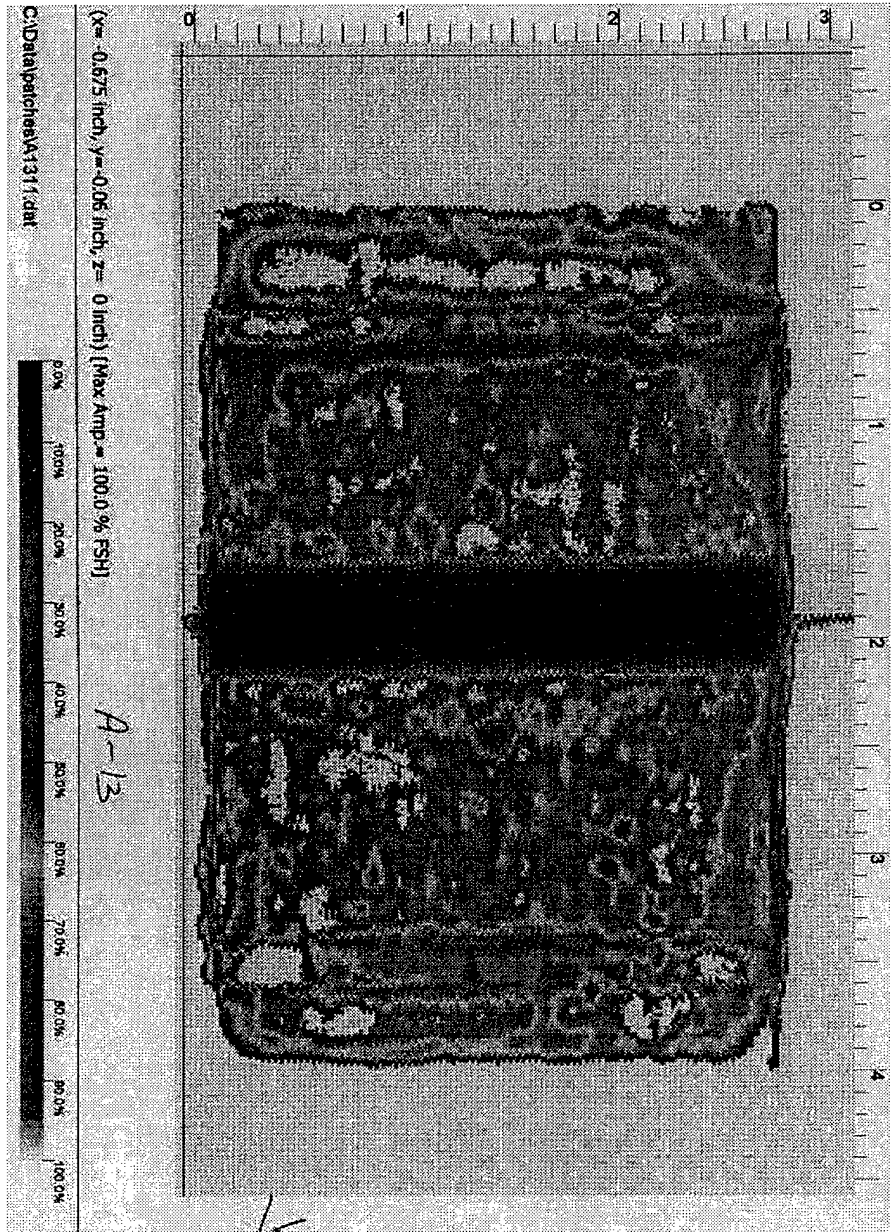
Figure 56 End-of-Life C-SCAN of Panel A-13 with FWD

108

4.2.2.2 FWD Effects in the 102 mm Spaced Stiffener Panels

Data from the testing of FWD panels with 102 mm spaced stiffeners (panels A-14 and A-17) showed identical trends as data from the FWD panel with 152 mm spaced stiffeners, but the data from the two FWD panels did not correlate very well with each other. Figure 57 shows fatigue life data for the completely bonded, CTD, and both FWD repair configurations for panels with 102 mm spaced stiffeners. Both panels had substantial fatigue life reduction when compared to the completely bonded panel, A-5, and both FWD panels also had fairly linear a vs. N curves. However, while panel A-17 had an overall fatigue life reduction of 50% compared to the completely bonded panel, A-14 only had a reduction of 20%. Table 23 lists da/dN data for all four panels in different areas under the patch. Both FWD panels had very linear crack growth rates at all areas under the patch. This differed from panels with the CTD repair configuration. As the crack grew through the CTD repair configuration, it first encountered a perfectly bonded repair, followed by complete disbonding of the repair. With both the FWD and completely bonded repair configurations, the propagation environment did not change as the crack grew—it was always either completely bonded or completely disbonded. For this reason, panels with either completely bonded repairs or with FWD's present should always have linear crack propagation curves. Figure 58 shows the crack growth rate comparison between the perfectly bonded, CTD, and FWD panels with 102 mm spaced stiffeners. The FWD panel has the highest consistent crack propagation rate of the three disbond configurations and has a very constant da/dN with respect to crack length. The CTD panel has the next highest da/dN in comparison to the completely bonded panel.

Figure 58 also shows the crack propagation rate versus crack length curve for the

unrepaired baseline panel with 102 mm spaced stiffeners for comparison.

When trying to understand why the two FWD panels, A-14 and A-17, performed

differently under cyclic fatigue, no one thing stands out. The panels were manufactured

exactly the same, with the same material, the same boron patch dimensions, and the same

bonding processes and temperatures. The stiffeners also were manufactured and applied

in the same way. Ideally, they should have had approximately the same fatigue
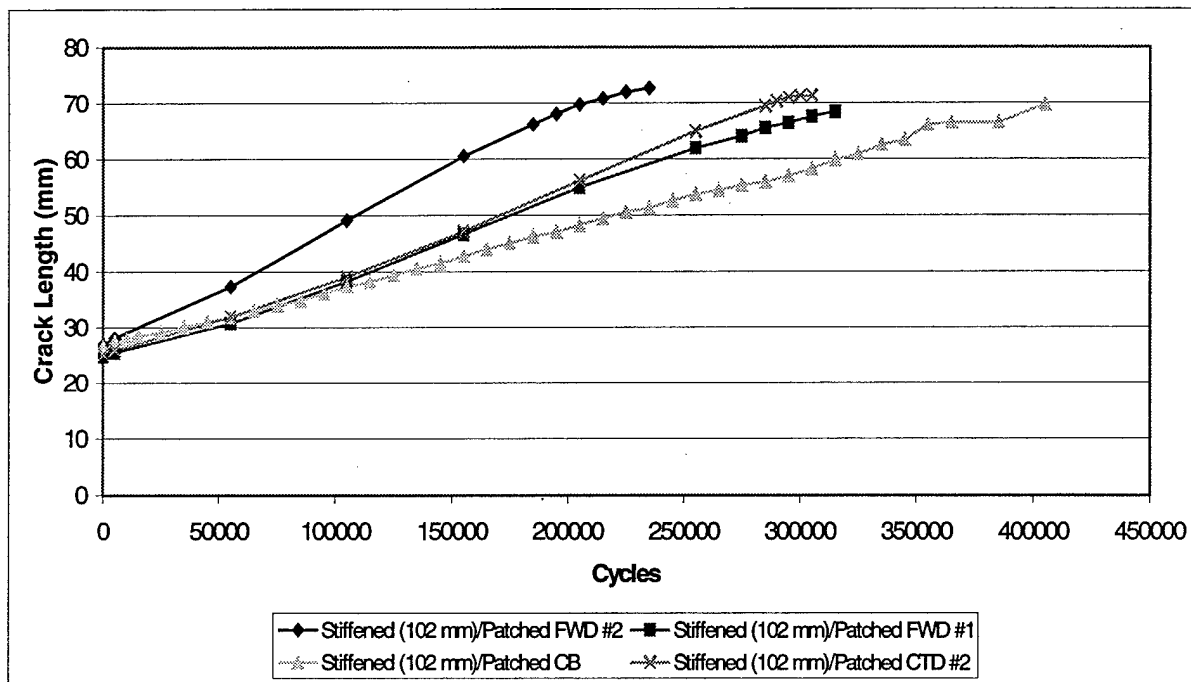
Figure 57 Effects of FWD on 102 mm Spaced Stiffened Panels

Specimen Number	Configuration	da/dN Section I (mm/cycle)	da/dN Increase from Baseline (%)	da/dN Section II (mm/cycle)	da/dN Increase from Baseline (%)
A-5	102 mm stiff/CB	0.000053	0.00%	0.000053	0.00%
A-10	102 mm stiff/CTD	0.000070	32.1%	0.000086	62.3%
A-14	102 mm stiff/FWD	0.000070	32.1%	0.000068	28.3%
A-17	102 mm stiff/FWD	0.000104	96.2%	0.000106	100%

Section 1 – crack growth between end of precrack and start of CTD (2a = 45 mm)
Section 2 – crack growth with CTD (45 mm < 2a < 69 mm)
* Interpolated data
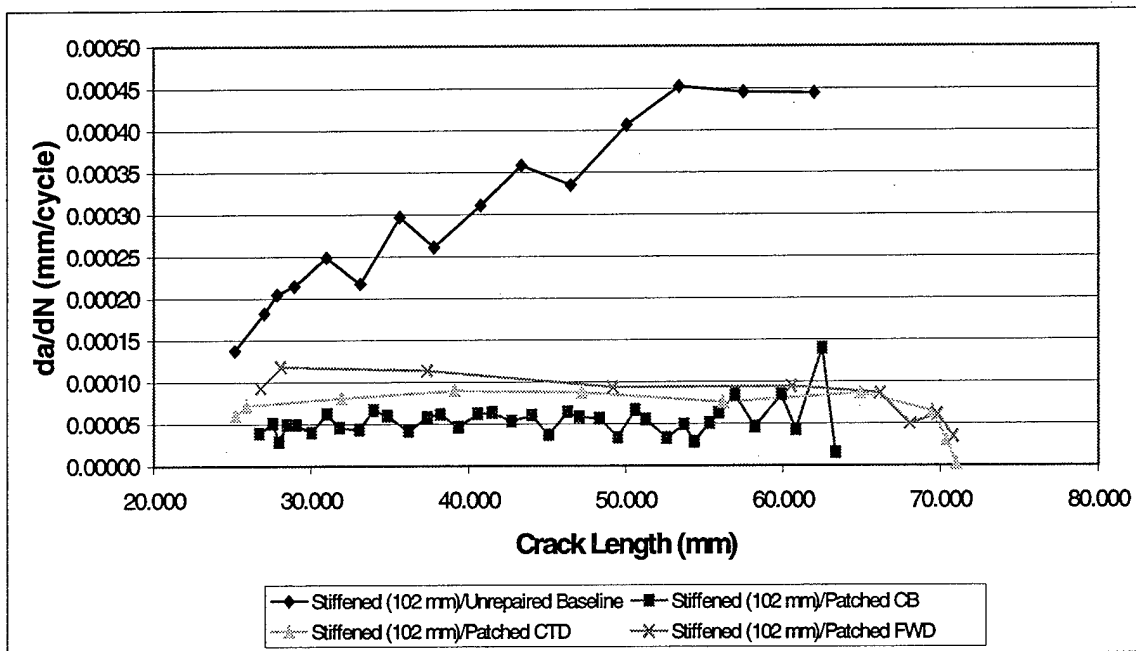
Figure 58 Comparison of Crack Growth Rates for 102 mm Spaced Stiffener Panels

111

life data. There are a few reasons, however, that, when combined together, could account for the approximately 53% difference in fatigue lives between the two panels. Firstly, all crack lengths were measured with a microscope and human eye, so operator error plays some role. Secondly, the hand-riveting process is not scientific. The pressure on the aluminum panel is not necessarily exactly the same from rivet to rivet and panel to panel. This can lead to different residual stresses between panels, possibly contributing to differences in the fatigue life data. Lastly, panel A-14 visibly had more curvature, and hence residual stresses, than panel A-17, as seen in Figure 59. It makes sense that A-14 performed better in tensile fatigue, since the panel had more residual compressive stresses than panel A-17. This is due in part to possible differences in stresses due to riveting. Also, during the riveting process, the pneumatic rivet gun head slipped off the rivet and slammed into the panel, leaving a large dent that had to be worked out. Because of a lack of panels, A-14 was still used. This was most likely the main cause for the difference in fatigue life of the two panels, so panel A-17 produced the most accurate data.
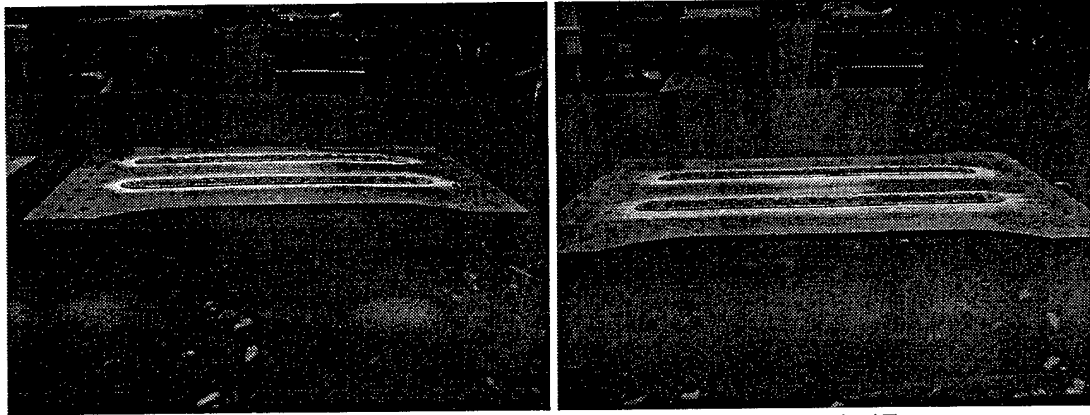
Panel A-14   **Panel A-17**

Figure 59 Panel Curvature Differences Between A-14 and A-17

While there was a decrease in fatigue life of FWD panels when compared to the baseline completely bonded repair, A-17 still performed much better than the unrepaired specimen, with a 280% longer fatigue life. Also, comparing IR pictures of the repair taken at different stages during cycling with a C-SCAN of the repair taken after cycling was completed, the bonded repair proved very durable as the intentional FWD did not grow. The infrared pictures are shown in Figure 60, and the C-SCAN is shown in Figure 61. The three IR pictures were taken at 5,006, 155,007, and 235,011 cycles corresponding to crack lengths of 28.08 mm (1.106 inches), 60.528 mm (2.383 inches), and 72.708 mm (2.863 inches). The C-SCAN was taken after 235,011 cycles corresponding to a crack length of 72.707 mm (2.863 inches).

5,006 cycles

155,007 cycles

235,011 cycles
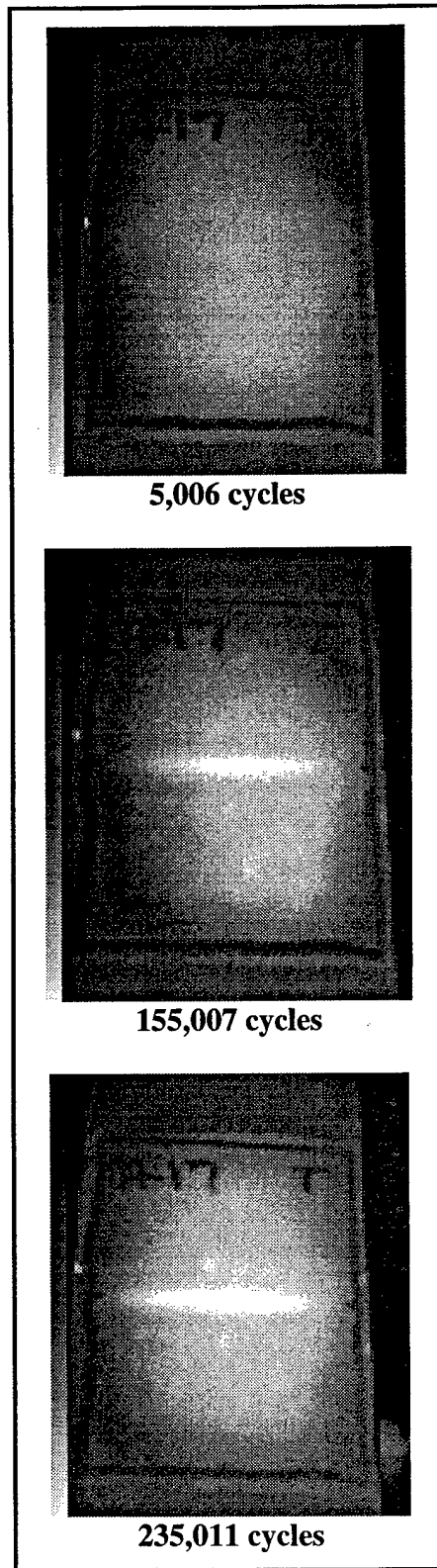
Figure 60 Infrared Pictures of Panel A-17 with FWD

114
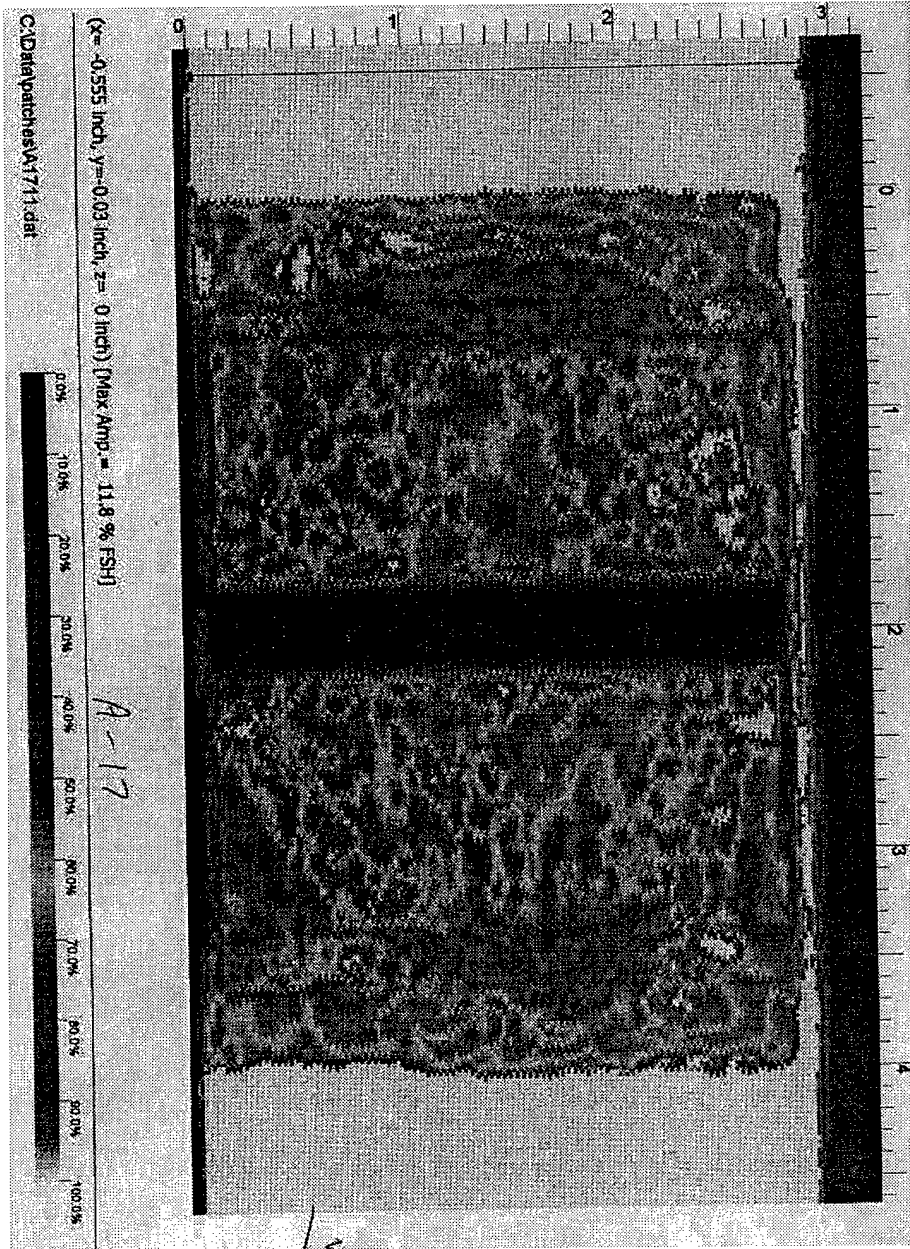
Figure 61 End-Of-Life C-SCAN of Panel A-17 with FWD

115

4.2.2.3 FWD Effects in the 152 mm Spaced Stiffener Panel versus FWD Effects in the 102 mm Spaced Stiffener Panel

Both configurations of stiffened panels, the 152 mm spaced stiffeners and 102 mm spaced stiffeners, behaved approximately the same with FWD's present. For simplicity, since possible problems with panel A-14 were already brought to light, panel A-17 will be the only FWD panel with 102 mm spaced stiffeners discussed and compared to the 152 mm spaced stiffener configuration in this section. Both configurations showed considerable decreases in fatigue life, more than the CTD configuration, when compared to the perfectly bonded panels, which was expected. Figure 62 provides a direct comparison between fatigue life trends of the two different stiffener configurations. From the figure, both stiffener configurations appear to have been affected approximately the same with the disbonds present. Table 24 lists the effect the FWD had on the two different panel stiffener configurations. It shows the percentage of crack propagation increase for both stiffener configurations when compared to the completely bonded panels. Both configurations experienced a large impact on fatigue life due to the disbond, but, as with the CTD panels, the 102 mm spaced stiffener panel experienced a larger effect. As explained before, while this may be the case to some extent, panels with 152 mm spaced stiffeners have crack propagation rate curves more severely sloped than panels with 102 mm spaced stiffeners. This causes the detrimental effects of the disbonds to seem less severe for that configuration.
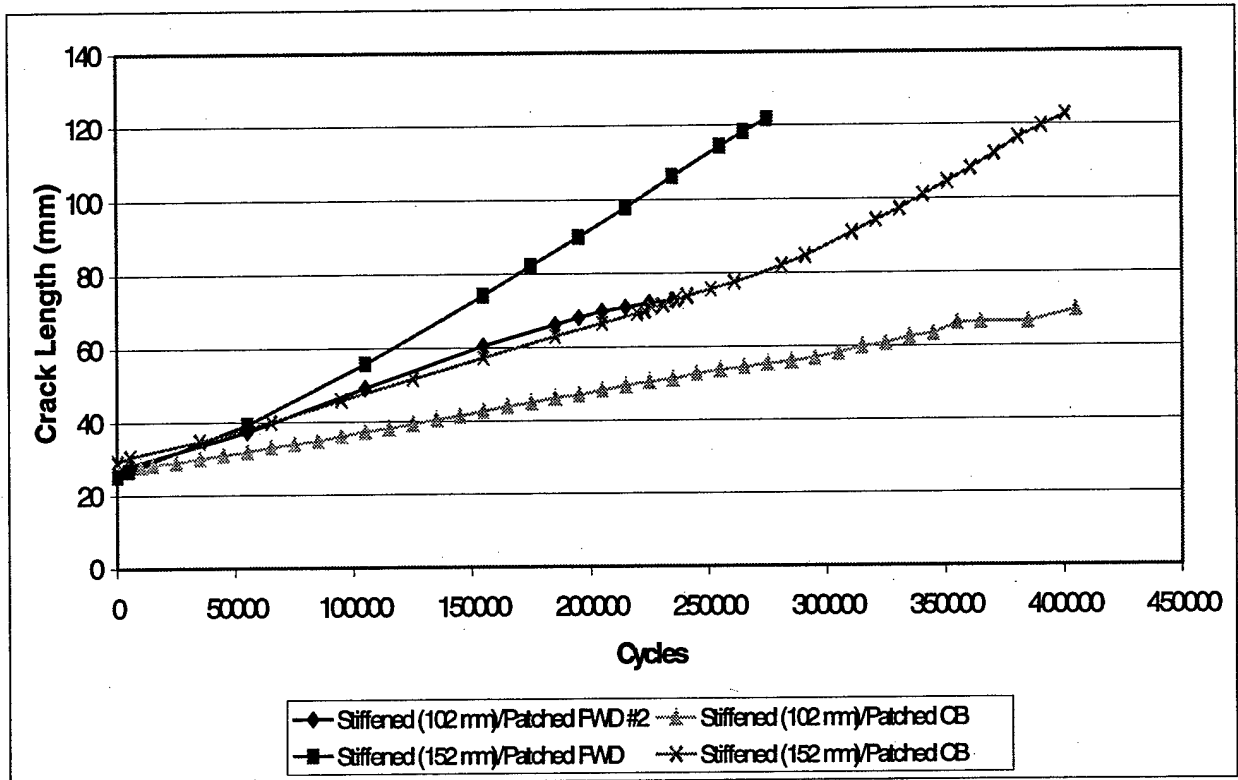
Figure 62 Fatigue Life Trend of Stiffened Panels with FWD

Table 24 Comparison of FWD Effect Between Stiffener Configurations

Specimen Number	Configuration	Increase in da/dN vs. Baseline Panel (%)*
A-13	152 mm stiff/FWD	69.4%
A-17	102 mm stiff/FWD	98.1%

* Interpolated Results

The data from both stiffener configurations, especially when compared to data from panels with CTD's present, supports Baker's (32) previous findings that disbonds in the wake of crack tips have more of an effect on crack tip propagation than disbonds in front of the tip. Table 25 provides a comparison in crack propagation rates between panels with CTD's present and those with FWD's present. The data shows a much higher crack propagation rate in section 1 for FWD's than for CTD's. Once the cracks

117

reached 45 mm in length, however, panels with CTD's present experienced a severe

increase in crack propagation rate, where as panels with FWD's maintained constant

crack growth rates, or less severe increases in crack growth rate for the case of panel A-

13. Also, comparisons between Figure 55, Figure 56, Figure 60, and Figure 61 support

Hart-Smith's (33) observations that adhesive bondlines are relatively damage tolerant and

pre-existing intentional disbonds will not grow.

Table 25 Average Crack Tip Propagation Rate Comparison Between FWD and CTD Panels

Specimen Number	Configuration	da/dN in Section I (mm/cycle)*	da/dN in Section II (mm/cycle)*
A-12	152 mm stiff/CTD	0.000079	0.000125
A-13	152 mm stiff/FWD	0.000137	0.000175
A-10	102 mm stiff/CTD	0.000070	0.000086
A-17	102 mm stiff/FWD	0.000104	0.000106

Section 1 – crack propagation between end of pre-crack and beginning of CTD ($\cong$ 25.4 mm – 45 mm)
Section 2 – crack propagation within region of CTD (45 mm – 69 mm)
* Interpolated data

4.2.3 Effect of Patch End Disbond (ED) on Fatigue Life of the Repair

Two fatigue panels with ED's were tested—one with 152 mm spaced stiffeners

(panel A-16) and one with 102 mm spaced stiffeners (panel A-15). Disbonds accounted

for approximately 18% of the bondline area of the patch and are shown schematically in

Figure 63. The fatigue life data of the disbonded panels, along with fatigue life data of

different baseline panels used for comparison, are shown in Table 26. The data is shown

only for crack growth underneath the patch. Crack growth data for the area between the

patch and stiffener would have been shown for the case of 152 mm spaced stiffeners, but

the ED panel with 152 mm spaced stiffeners failed early, as noted below the table. All

crack propagation occurred within the realm of a completely bonded patch, since the disbond was intentionally placed away from the crack. The results are shown schematically in Figure 65, Figure 69, and Figure 73. Figure 65 shows the effect of the ED on panels with 152 mm spaced stiffeners and how the fatigue life of those panels compared to the baseline data. Figure 69 shows the same for panels with 102 mm spaced stiffeners. Figure 73 shows a direct comparison between ED effects when dealing with 152 mm spaced stiffeners and 102 mm spaced stiffeners.
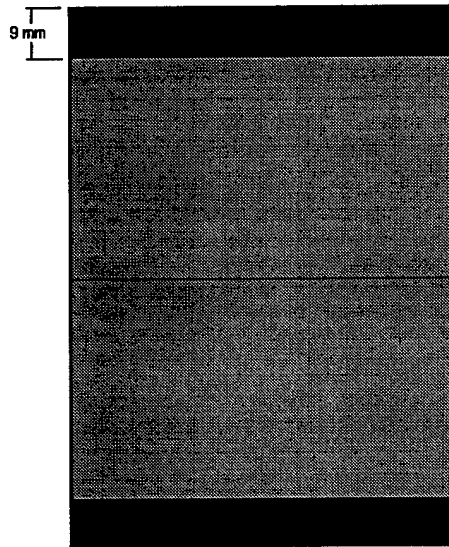
Figure 63 Schematic of ED

Table 26 Effect of ED on Fatigue Life

Specimen Number	Configuration	Crack Length (mm/inch)	Cycles*
A-1	Baseline (unstiff/unrep.)	69/2.71	8,077
A-2	Baseline (unstiff/CB patch)	69/2.71	83,445
A-3	152 mm stiff/unrep.	69/2.71	42,238
A-18	102 mm stiff/unrep.	69/2.71	71,664
A-5	102 mm stiff/CB	69/2.71	400,580
A-9	152 mm stiff/CB	69/2.71	218,880
A-15	102 mm stiff/ED	69/2.71	398,275
A-16	152 mm stiff/ED	69/2.71	316,421**

* Interpolated Results
** Panel failed early due to fatigue crack initiation at the stiffener tips

4.2.3.1 ED Effects in the 152 mm Spaced Stiffener Panel

The ED fatigue life data for the case of 152 mm spaced stiffeners was cut short due to fatigue crack initiation in the aluminum skin at the stiffener tips, leading to premature failure. Figure 64 shows an actual picture of the failure. There are a few possible reasons why fatigue cracking might have initiated at the stiffener tips, but the most probable relates back to the riveting procedure. Applying rivets by hand with a pneumatic gun is not a very complicated process, but it requires some skill. It is very easy to create stress concentrations in the panel by applying too much pressure to any individual rivet. Since this problem was not encountered in the panel with 102 mm spaced stiffeners, this is most likely what happened. Because of a lack of panels, only one ED repair (panel A-16) was made for this stiffener configuration, so all conclusions about how ED's affect the 152 mm spaced stiffener configuration were taken from panel A-16's data. While the data is limited, initial data should still be accurate. It has been shown in previous cases (Section 4.1.2, Repaired Panel Comparison: panels A-4 and A-

5; panels A-6, A-7, and A-9) that even when panels failed prematurely, the data still correlated extremely well with later data over the same range of crack propagation.
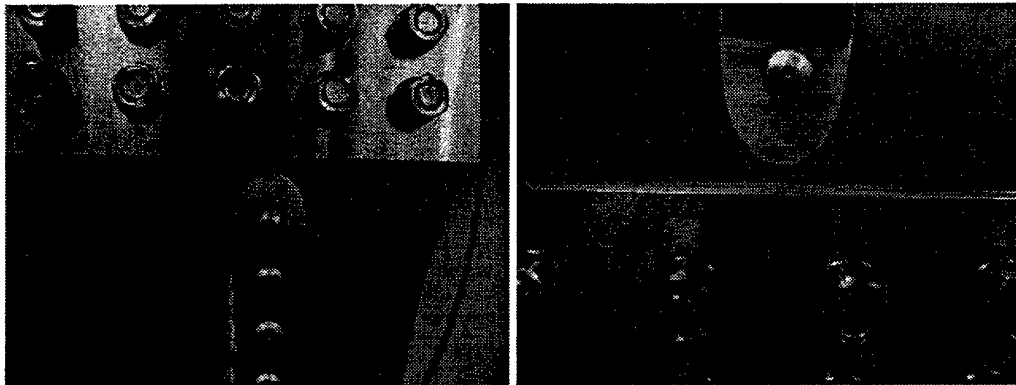
Figure 64 Pictures of Fatigue Cracks at the Stiffener Crack Tip in A-16

The overall fatigue life of the repaired panels with 152 mm spaced stiffeners showed relatively no difference between the completely bonded patch and one with ED's present, as seen in Figure 65. By comparing crack propagation data in Table 27, not only is there no increase in da/dN with an ED present, the rate decreased by approximately 30%. Figure 66 provides a graphical representation of the crack propagation rate versus crack length. According to the inclusion analogy (29; 30), the composite patch and skin act together as a region of higher stress. If the length of this higher stress region decreases, as it essentially does when ED's are present, the region attracts less load from the surrounding skin (11). This decrease in attracted load results in a reduced patch and skin stress around the crack, and hence a reduced repaired stress intensity factor, K_r. This reduced K_r results in the crack tips experiencing less stress, leading to a slightly slower crack propagation rate. ED's present in the repair appear to cause no significant reduction in repair life when compared to the completely bonded repair baseline. This is

121

in contrast to the other two disbond configurations studied, where CTD's had a slight

negative effect and FWD's had a significant negative effect on fatigue life.
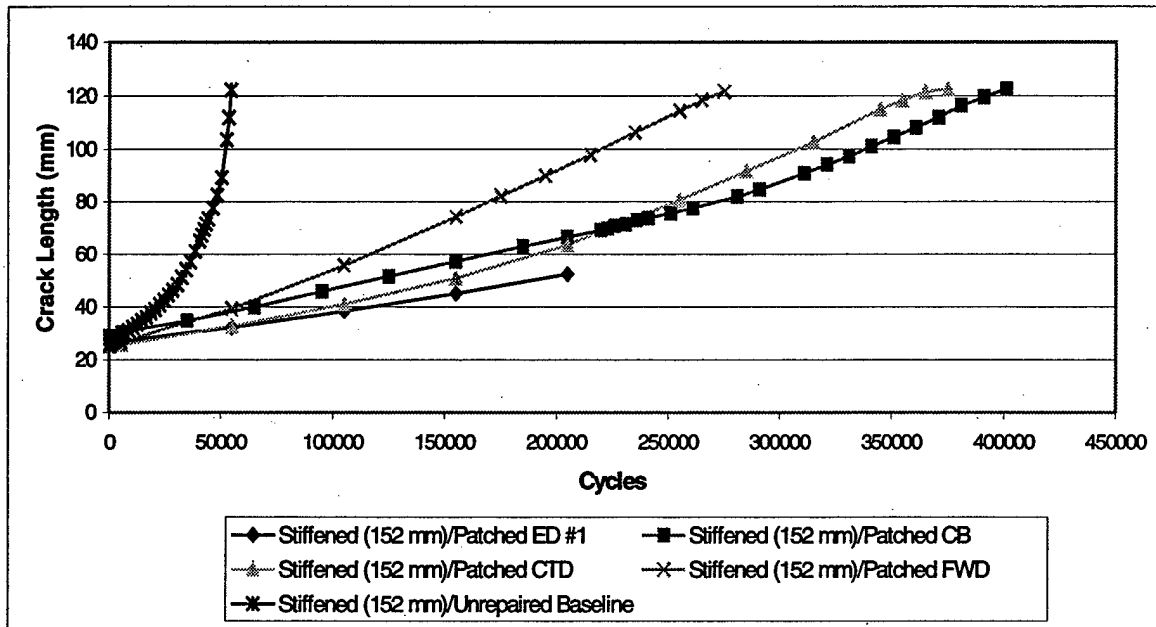
Figure 65 ED Effects on Fatigue Life of 152 mm Centered Stiffened Panels

Table 27 Crack Growth per Cycle for 152 mm Spaced Stiffener Panel

Specimen Number	Configuration	da/dN (mm/cycle)*
A-9	152 mm stiff/CB	0.000091
A-16	152 mm stiff/ED	0.000064

* Interpolated results
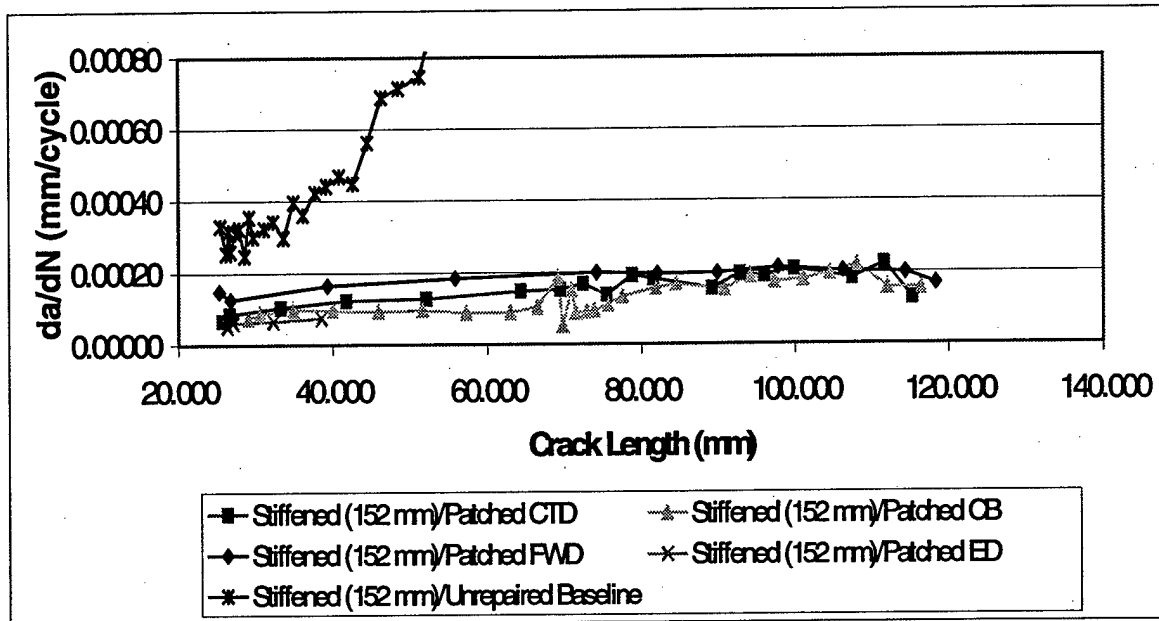
Figure 66 Comparison of Crack Growth Rates for 152 mm Spaced Stiffener Panels

Panels with ED's present proved to be just as durable under tensile fatigue as the other disbond cases. This can be seen by comparing IR pictures of the repair taken at different stages during cycling with a C-SCAN of the repair taken after cycling was completed. The infrared pictures are shown in Figure 67 and the C-SCAN is shown in Figure 68. The three IR pictures were taken at 5,011, 105,010, and 205,011 cycles corresponding to crack lengths of 27.102 mm (1.067 inches), 38.532 mm (1.517 inches), and 52.476 mm (2.066 inches). The C-SCAN was taken after 212,816 cycles corresponding to a crack length of over 52.476 mm (2.066 inches). Comparison of the pictures with the C-SCAN show that the end disbonds did not grow larger over time in the constant amplitude cyclic fatigue environment.

123

5,011 cycles

105,010 cycles

205,011 cycles
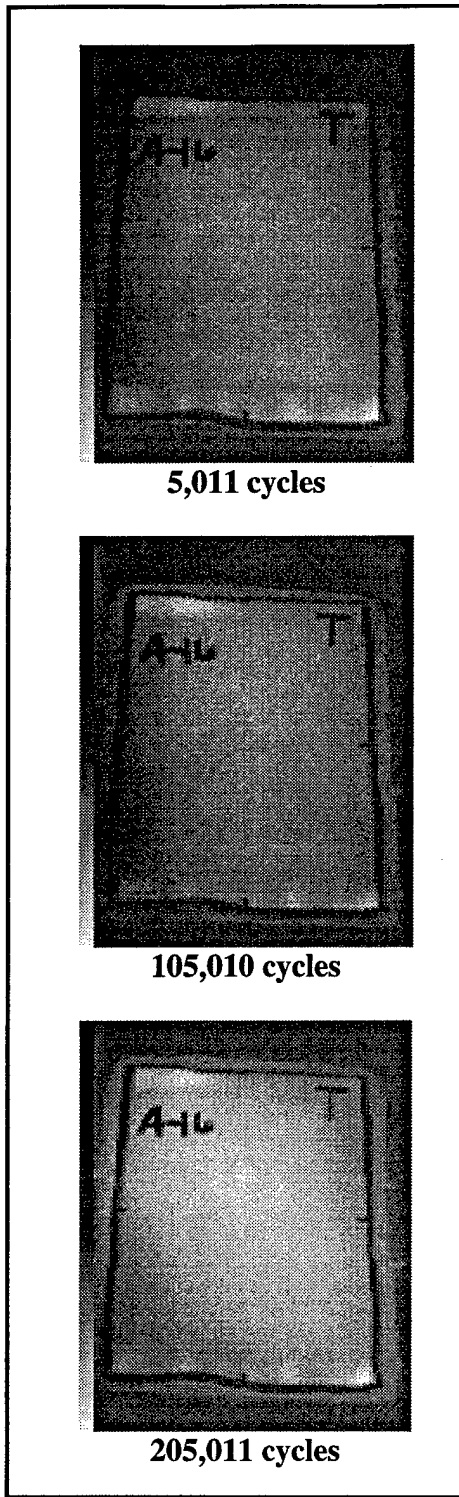
Figure 67 Infrared Pictures of Panel A-16 with ED
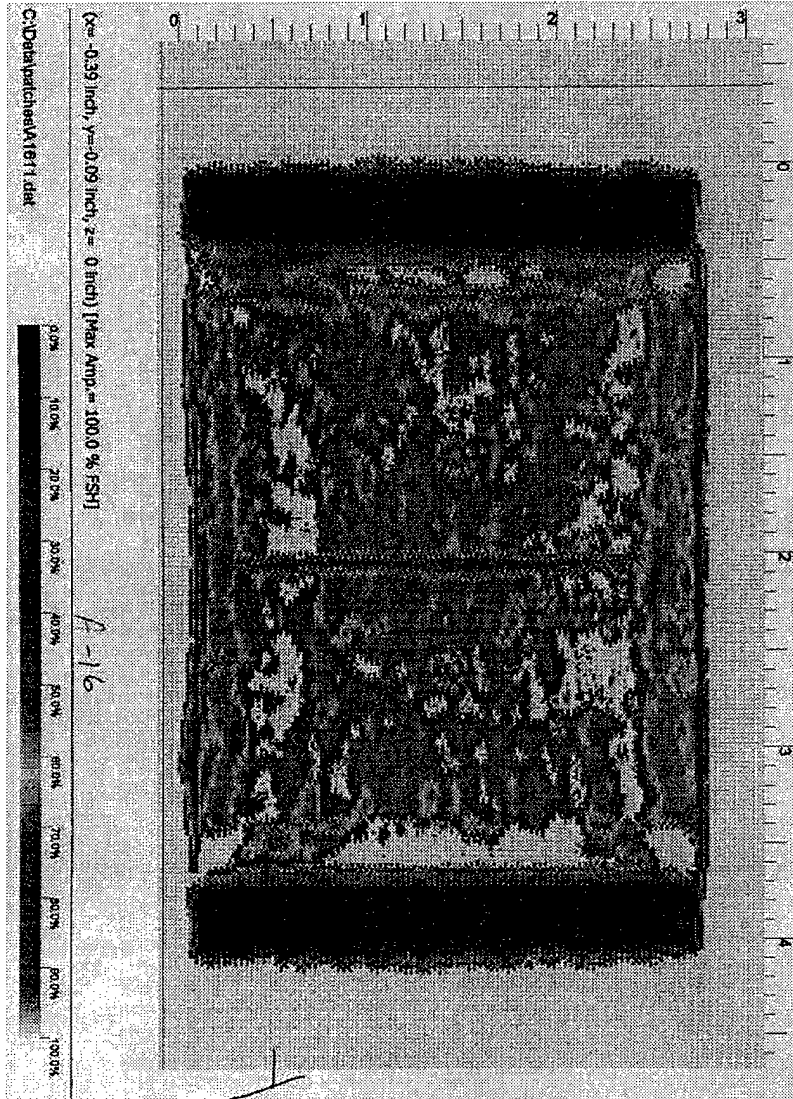
Figure 68 End-of-Life C-SCAN of Panel A-16 with ED

4.2.3.2 ED Effects in the 102 mm Spaced Stiffener Panel

Data from the testing of ED panels with 102 mm spaced stiffeners (panel A-15) showed a similar trend as did data from the ED panel with 152 mm spaced stiffeners. Figure 69 shows fatigue life data for the completely bonded, CTD, FWD, and ED repair configurations, as well as the unrepaired baseline configuration, for panels with 102 mm spaced stiffeners. The a vs. N curve for the ED configuration is almost identical to that of the completely bonded case. By comparing crack propagation data in Table 28, panel A-15 with ED's present has approximately the same crack propagation rate as panel A-5, which has a perfect bond. This end result is what was expected and reinforces Baker's (32) findings that disbonds have more of an effect on crack propagation rate and fatigue life when they have more intimate contact with the crack/damage. Figure 70 provides a graphical representation of the crack propagation rate versus crack length data.
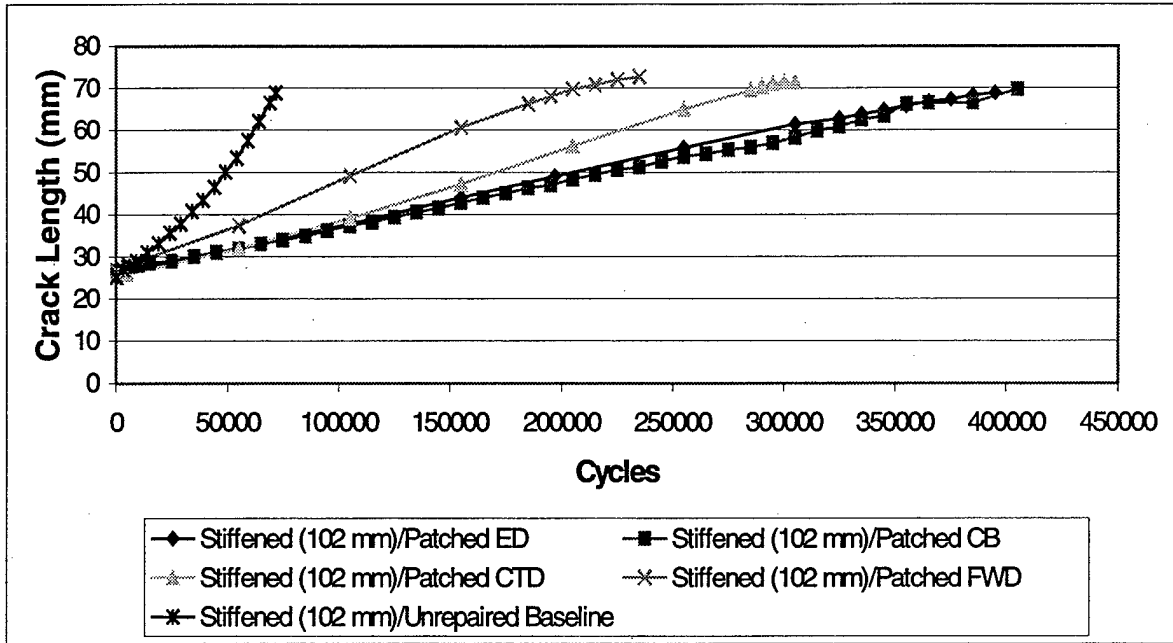
Figure 69 Effects of ED on 102 mm Spaced Stiffened Panels

*Table 28 Crack Growth per Cycle for 102 mm Spaced Stiffener Panel*

Specimen Number	Configuration	da/dN (mm/cycle)*
A-5	102 mm stiff/CB	0.000053
A-15	102 mm stiff/ED	0.000055

* Interpolated results

127
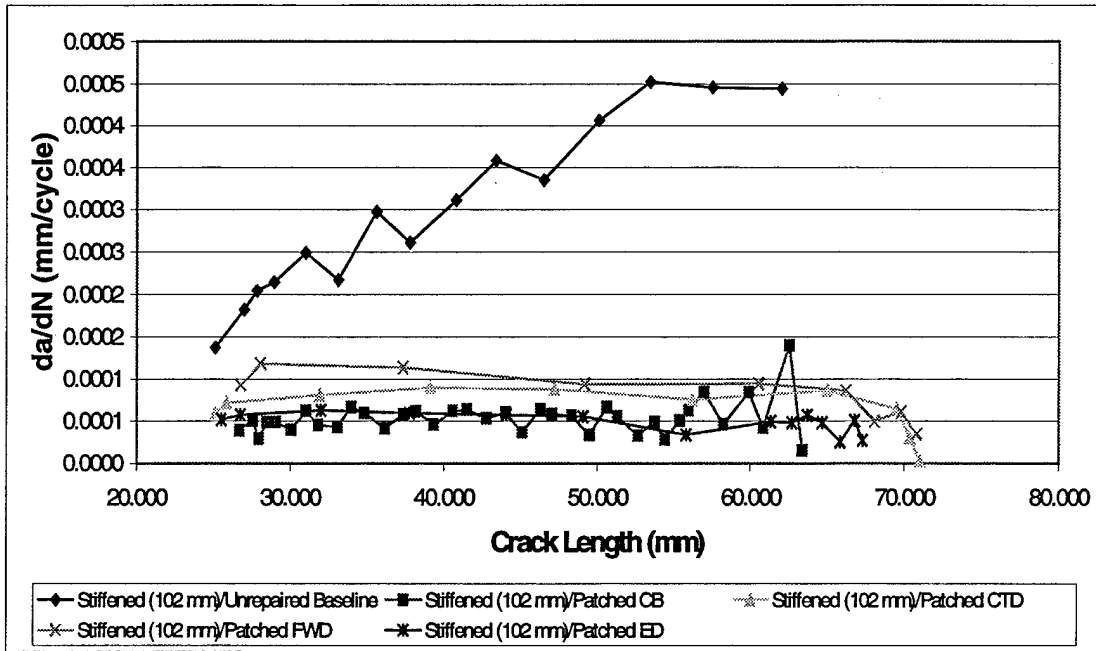
Figure 70 Comparison of Crack Growth Rates for 102 mm Spaced Stiffener Panels

Repaired panels with ED's present and 102 mm spaced stiffeners were as durable as the 152 mm spaced stiffener case. Comparing IR pictures of the repair taken at different stages during cycling with a C-SCAN of the repair taken after cycling was completed, it can be seen that no disbond growth occurred. The infrared pictures are shown in Figure 71 and the C-SCAN is shown in Figure 72. The three IR pictures were taken at 5,011, 105,010, and 375,008 cycles corresponding to crack lengths of 26.772 mm (1.054 inches), 37.757 mm (1.486 inches), and 67.259 mm (2.648 inches). The C-SCAN was taken after 395,000 cycles corresponding to a crack length of 68.821 mm (2.709 inches).

5,011 cycles

105,010 cycles

375,008 cycles
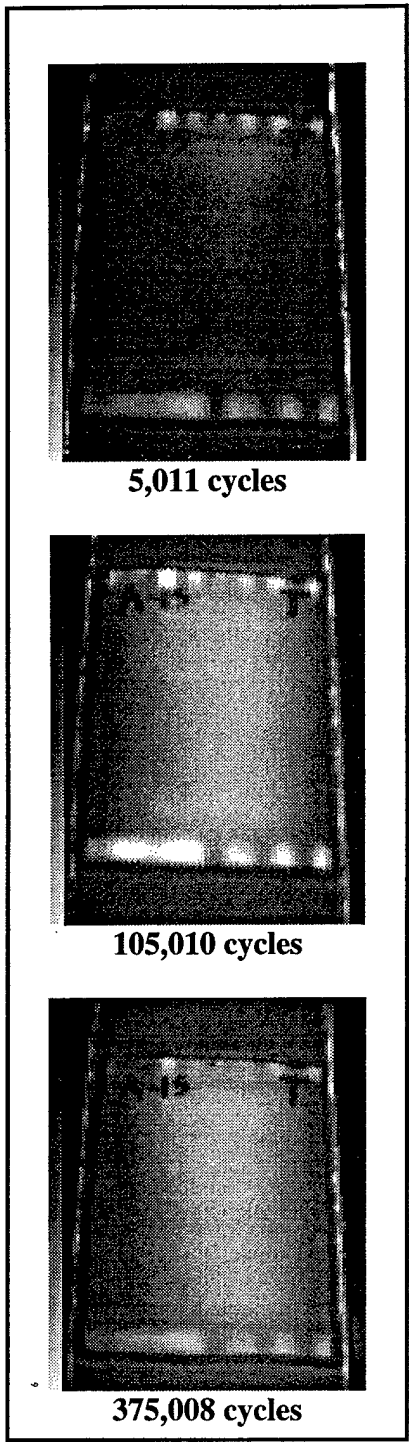
Figure 71 Infrared Pictures of Panel A-15 with ED's
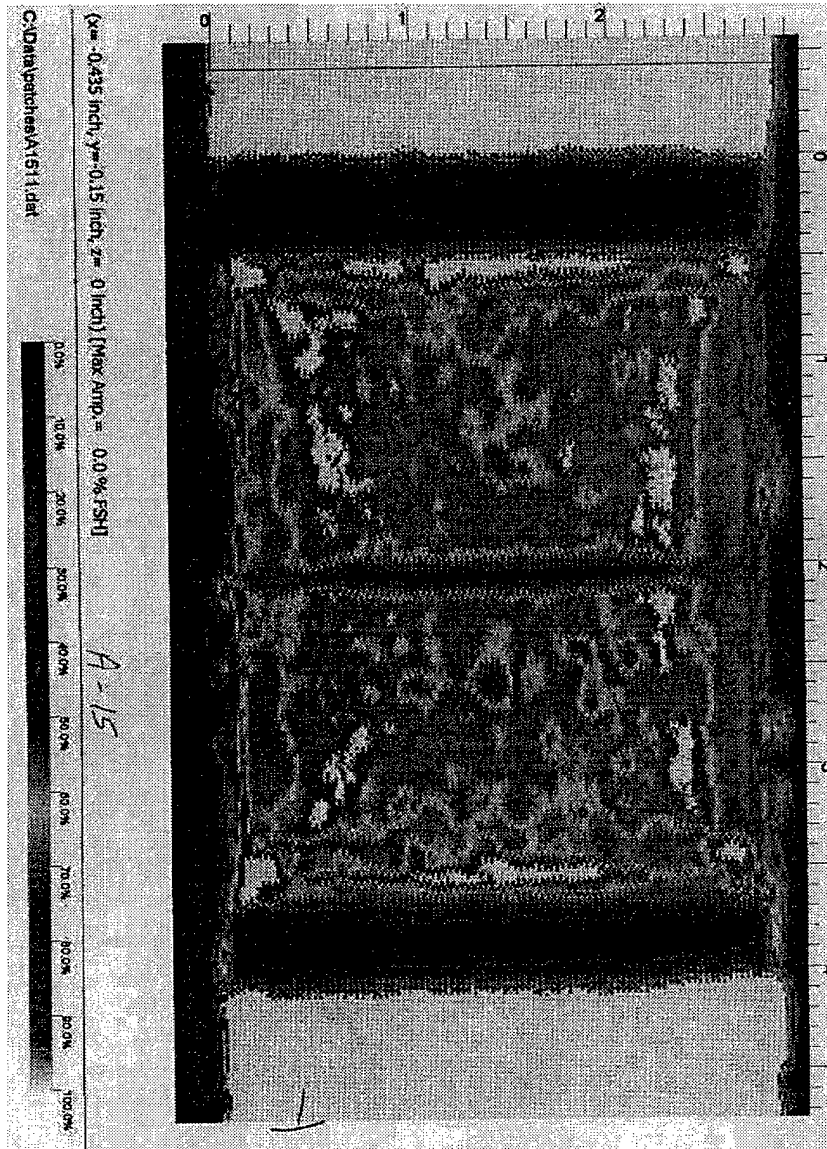
Figure 72 End-of-Life C-SCAN of Panel A-15 with ED's

130

4.2.3.3 ED Effects in the 152 mm Spaced Stiffener Panel versus ED Effects in the 102 mm Spaced Stiffener Panel

Both configurations of stiffened panels, the 152 mm spaced stiffeners and 102 mm spaced stiffeners, behaved similarly with ED's present. Both configurations showed no significant detrimental effects due to the ED's being present. The ED panel with 152 mm spaced stiffeners (panel A-16), however, showed a 30% increase in fatigue life when compared to the completely bonded panel, whereas the ED panel with 102 mm spaced stiffeners (panel A-15) showed no fatigue life increase over the CB panel. As previously explained, the increased fatigue life in panel A-16 can be attributed to a reduced K_R due to less load being attracted into the patch from the surrounding skin. This is caused by the shorter patch length with ED's present. Panel A-15 had the same end disbond configuration, so it should have experienced the same increase in fatigue life over the completely bonded panel.

The only difference between the two panels was in the stiffener configuration— 152 mm spaced stiffeners versus 102 mm spaced stiffeners. Panel A-16's stiffeners were located approximately 25.4 mm farther away from the crack tips than panel A-15's stiffeners. Therefore, panel A-15's stiffeners attracted more load away from the crack tips than did A-16's. Any patch variation, such as end disbonds, that decreased the K_R at the crack tips would have been more prominent and caused more visible effect in fatigue life data in panel A-16 than panel A-15, since the stiffeners in panel A-15 were already reducing the K_R at the crack tips more than the stiffeners in panel A-16. This is evident by noting that in every patch and disbond configuration studied, panels with 152 mm

131

spaced stiffeners had a much steeper crack length versus cycles curve than panels with

102 mm spaced stiffeners.

Table 29 contains crack propagation rate data for all disbond configurations and

both stiffener configurations. As originally hypothesized, in both stiffener

configurations, the more intimate contact disbonds had with the crack, the higher the

fatigue crack propagation rates became. End disbonds did not have much effect on the

fatigue life of the panels. Crack tip disbonds did have a significant effect on crack

propagation rates of the repair panels, but full-width disbonds had the worst effect. Data

detailing the percentage of increase in da/dN for each disbond configuration versus the

ED configuration is also shown in Table 29.
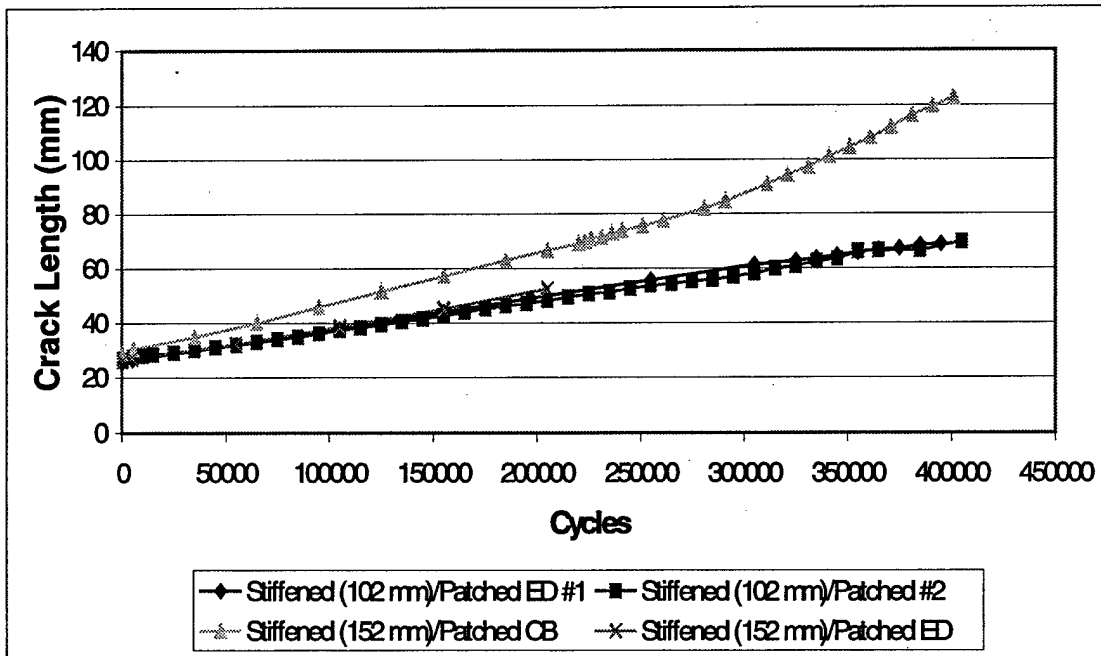
Figure 73 Fatigue Life Trend of Stiffened Panels with ED

Table 29 Crack Tip Propagation rate Comparison Between CTD, FWD, and ED Panels

Spec. #	Configuration	da/dN in Section I (mm/cycle) *	Increase in da/dN vs. ED	da/dN in Section II (mm/cycle) *	Increase in da/dN vs. ED
A-12	152 mm stiff/CTD	0.000079	29.5%	0.000125	NA
A-13	152 mm stiff/FWD	0.000137	124.6%	0.000175	NA
A-16	152 mm stiff/ED	0.000061	0%	No data	No data
A-10	102 mm stiff/CTD	0.000070	16.7%	0.000086	68.6%
A-17	102 mm stiff/FWD	0.000104	73.3%	0.000106	107.8%
A-15	102 mm stiff/ED	0.000060	0%	0.000051	0%

Section 1 – crack propagation between end of pre-crack and beginning of CTD ($\cong$ 25.4 mm – 45 mm)
Section 2 – crack propagation within region of CTD (45 mm – 69 mm)
* Interpolated results

Chapter 5   Summary, Conclusions, and Recommendations

The purpose of this study was to investigate the effects of disbonds on the fatigue life of stiffened, cracked aluminum panels repaired with bonded composite patches. To accomplish this, constant amplitude fatigue loading of cracked aluminum panels repaired with partially bonded boron/epoxy patches and stiffened with aluminum plate was performed. Disbond configurations that are commonly seen in real life bonded repair applications were simulated using teflon inserts. Two stiffener configurations were chosen to simulate real life aircraft stiffeners in fuselages and wings.

The three disbond configurations that were investigated were crack tip disbonds (CTD), full-width disbonds (FWD), and end disbonds (ED). The disbonds were monitored for growth by taking infrared (IR) pictures at specific points in the cyclic fatigue process. Subsequent IR pictures were compared to each other and to an end-of-life C-SCAN taken after panel failure. Fatigue life data for panels with disbonds present was compared to baseline panel fatigue life data to determine the effect of the different disbond configurations. Baseline panels consisted of perfectly bonded patches on stiffened and unstiffened structures, and unrepaired stiffened panels.

Results of the fatigue cycling showed that disbonds were more detrimental to the fatigue life of a repaired panel when they had more intimate contact with the actual damage, i.e. the crack. End disbonds, because they had no contact with the crack and were located at the farthest point possible away from it, did not reduce the fatigue life of repaired panels in either stiffener case. Crack tip disbonds, however, were intentionally placed directly in the propagation line of the crack, so once the crack grew a certain

134

amount, it came into direct contact with the disbond. Because of this, panels with CTD's present experienced significant detrimental effects. Panels with CTD's present experienced an average fatigue life reduction of 27% as compared to a perfectly bonded patch . Data showed that the crack propagation rate was not significantly affected by the disbond until it was in the crack *wake*. This supports Baker's (32) previous observations that disbonds in front of the crack tip have little effect on fatigue crack propagation rates.

Full-width disbonds, because they had contact with the crack for the entire duration of the fatigue cycling and took up the most area of the adhesive bondline, imparted the most fatigue life reduction of any disbond case. Panels with FWD's present showed an average fatigue life reduction of 84% when compared to panels with completely bonded repairs. Panels with FWD's present experienced approximately 46% more fatigue life reduction than CTD panels with the same stiffener configuration. Since FWD's had more intimate contact with the crack than CTD's, this again supports Baker's (32) findings that crack tip propagation is more effected by disbonds that come into direct contact with the crack.

When comparing the fatigue life data of partially bonded composite repairs with that of perfectly bonded composite repairs, significant detrimental effects were seen, depending on which disbond configurations were looked at. However, since a perfectly bonded patch increased the fatigue life of a stiffened panel an average of 470%, the disbonded repair cases still performed considerably better than an unrepaired panel. Repaired panels with intentional CTD's had a fatigue life an average of 360% longer than the unrepaired panel, while repaired panels with intentional FWD's still had a fatigue life an average of 212% longer than the unrepaired panel.

135

Hart-Smith's (33) observation that intentional disbonds do not experience significant growth during cyclic fatigue was also found to be true. By comparing IR pictures taken during testing of the panels with C-SCAN images taken after completion of testing, it was shown that the intentional disbonds did not grow larger. This was the case for all three disbond cases. Hart-Smith's findings that cyclic disbonding around the crack only occurs in the wake of the crack tip was also found to be true.

While this work has made contributions to advancing the knowledge of disbond effects on fatigue life of panels repaired with bonded composite patches, much more research needs to be accomplished. Environmental effects on disbonds needs to be examined. When a disbond exists and is exposed to harsh environments (temperature, humidity, corrosion), the effect on repaired panel fatigue life will be very different. Also, this study focused only on tension/tension (R ratio of 0.05) fatigue cycling. The effects of disbonds on fatigue life could change dramatically in a tension/compression or compression/compression environment. Compression cycling can cause a buckling effect between the patch and the aluminum substrate, significantly affecting the bondline. Problems related to compression loading involving bonded composite repairs were observed during testing involving Canadian CF-116's (34). Compression loading and its effects on bonded composite repair fatigue life needs to be further investigated. Only by continuing to perform research in the area of adhesively bonded composite repairs will the technology ever be universally accepted and utilized to it's fullest potential.

Appendix A: Composite Patch Design

1. **Stiffness:** The goal is to find the desired patch thickness.

$$S = \frac{E_p t_p}{E_s t_s}$$

where

$S = 1.1$
$E_s = 72.4\ \text{GPa}$
$E_p = 210\ \text{GPa}$
$t_s = 0.00102\ \text{m}$
$t_p = ?$

$$1.1 = \frac{(210)t_p}{(72.4)(0.00102)}$$

$$t_p = 3.81e - 4$$

Since the thickness of a boron/epoxy ply is 1.27 e –4 m, three plies were needed to achieve the correct patch thickness.

2. **CTE Mismatch:** The goal is to determine the coefficient of thermal expansion (CTE) mismatch between the patch and the aluminum panel.

   In this case, the effective CTE does not need to be calculated, since more than 30% of the panel is being heated.

3. **Patch Length:** The goal is to determine the optimum patch length.

137

$$P_l = 4(l_p + l_e) + l_w$$

where

P_l = patch length
l_p = plastic transfer length in the adhesive
l_c = elastic transfer length in the adhesive
l_w = defect width (zero for a crack)

    a.   Plastic Transfer Length

$$l_p = \frac{UTS_s \cdot t_s}{N\tau_p}$$

where

t_s = 0.00102 m
τ_p = 39.3 MPa
N = number of transfer zones (2 for supported single side)
UTS_s = 479.7 MPa

$$l_p = \frac{(479.7)(0.00102)}{2(39.3)} = 6.23mm$$

    b.   Elastic Transfer Length

$$l_e = \frac{3}{\lambda} \quad \text{where} \quad \lambda = \sqrt{\frac{G}{t_a}\left[\frac{1}{E_s t_s} + \frac{1}{E_p t_p}\right]}$$

where

G = 405.8 MPa
t_a = 1.3 e –4 m

$$\lambda = \sqrt{\frac{405.8}{1.3e-4}\left[\frac{1}{(72.4)(0.00102)} + \frac{1}{(210)(3.81e-4)}\right]} = 285.1m^{-1}$$

and

$$l_e = \frac{3}{\lambda} = \frac{3}{285.1} = 11mm$$

therefore

$$P_l = 4(l_p + l_e) = 4(6.23 + 11) = 68.92mm$$

4. **Patch Width:** The goal is to determine the optimum patch width.

In order to reduce the skin stress near the patch tip, an aspect ratio (P_l/P_W) of 1 is

preferred (7).

$$\frac{P_l}{P_w} = \frac{68.92}{P_w} = 1$$

therefore

$$P_w = 68.92mm$$

5. **Tapering of the Patch:** The goal is to determine the best taper ratio to reduce

stresses outside of the patch.

$$\text{Initial Step Length} = x_1 = \frac{3}{\lambda} = \frac{3}{285.1} = 11mm$$

$$\text{Every Step Thereafter} = x_n = \frac{x_{n-1}}{n}$$

139

therefore

$$\text{Second Step Length} = x_2 = \frac{x_1}{2} = \frac{11}{2} = 5.5mm$$

$$\text{Total Taper Length} = l_t = x_1 + x_2 = 11mm + 5.5mm = 16.5mm$$

therefore

$$\text{Ply 1} = 69mm + (2 \cdot 16.5mm) = 102mm$$

$$\text{Ply 2} = 102mm - (2 \cdot 11mm) = 80mm$$

$$\text{Ply 3} = 80mm - (2 \cdot 5.5mm) = 69mm$$

Bibliography

1. USAF Aging Aircraft Program Office. "Aging Aircraft: USAF Perspective."

2. Bureau of Accident Investigation. <u>Aircraft Accident Report: Aloha Airlines Flight 243, Boeing 737-200, N73711, Near Maui, Hawaii, April 28, 1988</u>. Report No. NTSB/AAR-89/o3. Washington: National Transportation and Safety Office, 14 June 1989.

3. Conley, D. S. <u>Fatigue Response of Repaired Thick Aluminum Panels with Bondline Flaws</u>. MS Thesis, AFIT/GAE/ENY/99M-03. School of Engineering, Air Force Institute of Technology, (AU), Wright-Patterson AFB, 1999.

4. <u>Jane's</u> "All The World's Aircraft." Jane's Information Group, Inc. 1340 Braddock Place, Suite 300. Alexandria, Virginia 22314-1687. ISBN 0 7106 1890 0. 1999-2000.

5. Sutherland, Bill J. "Boron Doubler Reinforcement Modification F-111 Wing Pivot Fittings." Status Report. Sacramento Air Logistics Center. 01 January 1993.

6. Baker, A. A. "Repair of Cracked or Defective Metallic Aircraft Components with Advanced Fibre Composites—an Overview of Australian Work." <u>Composite Structures</u>. Elsevier Applied Science Publishers Ltd. Printed in Great Britain. 1984. Pgs. 153-181.

7. <u>Guidelines for Composite Repair of Metallic Structure</u>. AFRL-ML-WP-TR-1998-4113.

8. Grabovac, I., R. A. Bartholomeusz, and A. A. Baker. "Composite Reinforcement of a Ship Surperstructure-Project Overview." <u>Composites, 24</u>: 501-509, (Number 6, 1993).

9. Schubbe, Joel J. <u>Thickness Effects on Cracked Aluminum Plate With Composite Patch Repair</u>. Air Force Institute of Technology (AU), Wright-Patterson AFB OH, May 1997 (AFIT/DS/ENY/97-4)

10. Ryan, J., and T. B. Mills. "The Effects of Disbonds on Patching Efficiency Over Thicker Structure," <u>Proceedings of the 1998 USAF Structureal Integrity Program Conference</u>. San Antonio, Texas: December 1998.

11. Denney, J.J. <u>Fatigue Response of Cracked Aluminum Panel with Partially Bonded Composite Patch</u>. MS thesis, AFIT/GAE/ENY/95D-7. School of Engineering, Air Force Institute of Technology (AU), Wright-Patterson AFB OH, 1995

12. Bruhn, E.F. and others. <u>Analysis and Design of Flight Vehicle Structures</u>. Carmel IN: Jacobs Publishing, Inc. 1973.

13. Palazotto, Anthony. Class notes, MECH 605, Fracture Mechanics. School of Engineering, Air Force Institute of Technology, Wright-Patterson AFB OH, Spring Quarter 1999.

14. Broek, David. <u>Elementary Engineering Fracture Mechanics</u> (4th revised edition). Kluwer Academic Publishers. 1986.

15.   Baker, A.A. "Crack Patching; Experimental Studies, Practical Applications," in <u>Bonded Repair of Aircraft Structures</u>. 107-172. A.A. Baker and R. Jones, editors. Dordrecht: Martinus Nijhoff Publishers, 1988.

16.   United States Air Force Academy. <u>Calcurep for Windows: Beta Version</u>. Colorado Springs: USAFA Department of Engineering Mechanics, May 1995.

17.   Fredell, R.S. <u>Damage Tolerant Repair Techniques for Pressurized Aircraft Fuselages</u>. Ph.D. dissertation. Delft University of Technology, Delft, The Netherlands, June 1994 (WL-TR-93-3134).

18.   Mallick, P.K. <u>Fiber-Reinforced Composites</u> (2nd revised edition). New York: Marcel Decker, 1993.

19.   Reinhart, T.J. "Surface Treatments for Bonded Repairs of Metallic Components," in <u>Bonded Repair of Aircraft Structures</u>. 19-29. A.A. Baker and R. Jones, editiors. Dordrecht: Martinus Nijhoff, Publishers, 1988.

20.   Baker, A.A., R.J. Chester, M. J. Davis, M.A. Retchford, and J.D. Roberts. "The Development of a Boron/Epoxy Doubler System for the F-111 Wing Pivot Fitting-Materials Engineering Aspects," <u>Proceedings of the International Conference on Aircraft Damage Assessment and Repair</u>. August 1991.

21.   <u>Primary Adhesively Bonded Structure Technology (PABST) Full Scale Test Report</u>. Douglas Aircraft Company, McDonnell Douglas Corporation. November 1980. AFWAL-TR-80-3112.

22.   Fredell, R.S., David Conley, and Shane Knighton. "Design Development of a Bonded Fuselage Repair for the C-5A," <u>Proceedings of the 1995 USAF Structural Integrity Program Conference</u>. 887-902. San Antonio, Texas: December 1995.

23.   Kan, H. P., and M. M. Ratwani. <u>Composite Patch Repair of Thick Aluminum Structures – Final Repaort</u>. Airtask No. WF41-400, PE 62241. Report No. NADC-82139-60. United States Navy – Naval Air Development Center, Warminster, PA 18974, 1983.

24.   Labor, J. D., and M. M. Ratwani. <u>Development of Bonded Composite Patch Repairs for Cracked Metal Structure – Final Report</u>. Report No. NADC-79066-60 Vol. I. United States Navy – Naval Air Devleopment Center, Warminster, PA 18974, 1980.

25.   Davis, M. Royal Australian Air Force Engineering Standard C5033 RAAF.

26.   Hysol Aerospace Products. <u>Structural Adhesives: EA-9394</u>. Company Product Brochure. Pittsburgh, CA: Dexter Adhesives and Structural Materials Division, January 1991.

27.   Heinimann, M.B. <u>Analysis of Stiffened Panels with Multiple Site Damage</u>. Ph.D. dissertation. Purdue University Graduate School, IL. May 1997.

28.   Fawaz, S. A. <u>Fatigue Crack Growth in Riveted Joints</u>. Ph.D. dissertation. Delft University of Technology, Delft, The Netherlands, 1997.

29.   Rose, L.F. "A Cracked Plate Repaired by Bonded Reinforcements," International Journal of Fracture, 18: No. 2. 135-144 (February 1982).

30.   Rose, L.F. "An Application of the Inclusion Analogy for Bonded Reinforcements," International Journal of Solids and Structures, 17: 827-838 (1981).

31.   Rose, L.F. "Theoretical Analysis of Crack Patching," Bonded Repair of Aircraft Structures. 77-105. A.A. Baker and R. Jones, editors. Dordrecht: Martinus Nijhoff Publishers, 1988.

32.   Baker, A.A. "Bonded Composite Repair of Metallic Aircraft Components – Overview of Australian Activities," Proceedings of the 1994 AGARD Specialists' Meeting on Composite Repair of Military Aircraft Structures. Seville, Spain: October 1994.

33.   Hart-Smith, L.J. "Design and Analysis of Bonded Repairs for Metallic Aircraft Structures," Bonded Repair of Aircraft Structures. 31-47. A.A. Baker and R. Jones, editors. Dordrecht: Martinus Nijhoff Publishers, 1988.

34.   Gaudert, P.C., J. Heath, and M. Raizenne. "Failure Analysis of Bonded Boron Doublers," Proceedings of the 1995 International Composite Repair of Aircraft Structures Symposium. 10-1—10-30. University of British Columbia, Vancouver, Canada. August 1995.

Vita

Captain Jason B. Avram was born in Fairbanks, Alaska. He graduated from Standish-Sterling Central High School, Standish, Michigan, in 1992. He entered the United States Air Force Academy, Colorado, in June of 1992 and graduated with a Bachelor of Science in Engineering Mechanics on 29 May 1996. Also on 29 May 1996, he was commissioned a 2nd Lieutenant in the United States Air Force. Captain Avram's first assignment was as a student in Joint Undergraduate Navigator Training, Pensacola NAS, Florida. He completed his training there in the summer of 1997 and was transferred to Randolph AFB, Texas to complete training. In August of 1997, he decided to go a different route with his career and was transferred to Wright-Patterson AFB, Ohio as a Materials Supportability Engineer in the Materials Integrity Branch, Air Force Research Laboratory. Captain Avram started attending the Air Force Institute of Technology School of Engineering in August of 1998.